UNCERTAINTY ANALYSIS OF CUTTING FORCE COEFFICIENTS DURING MICROMILLING OF TITANIUM ALLOY

A THESIS SUBMITTED TO

THE GRADUATE SCHOOL OF ENGINEERING AND SCIENCE

OF BILKENT UNIVERSITY

IN PARTIAL FULFILLMENT OF THE REQUIREMENTS FOR

THE DEGREE OF

MASTER OF SCIENCE

IN

INDUSTRIAL ENGINEERING

By

Erman Gözü

September 2017

UNCERTAINTY ANALYSIS OF CUTTING FORCE COEFFICIENTS DURING MICROMILLING OF TITANIUM ALLOY
By Erman Gözü
September 2017

We certify that we have read this thesis and that in our opinion it is fully adequate, in scope and in quality, as a thesis for the degree of Master of Science.

Yiğit Karpat (Advisor)

Savaş Dayanık

Hakkı Özgür Ünver

Approved for the Graduate School of Engineering and Science:

Ezhan Karaşan
Director of the Graduate School

ABSTRACT

UNCERTAINTY ANALYSIS OF CUTTING FORCE COEFFICIENTS DURING MICROMILLING OF TITANIUM ALLOY

Erman Gözü
M.S. in Industrial Engineering
Advisor: Yiğit Karpat
September 2017

Force modeling based on process input parameters is usually considered as the first step in process modeling. Predicting process forces in micromilling is difficult due to complex interaction between the cutting edge and the work material, size effect, and process dynamics. This study describes the application of Bayesian inference to identify force coefficients in the micromilling process. The Metropolis-Hastings (MH) algorithm Markov chain Monte Carlo (MCMC) approach has been used to identify probability distributions of cutting, edge, and ploughing force coefficients based on experimental measurements and a mechanistic model of micromilling. The Bayesian inference scheme allows for predicting the upper and lower limits of micromilling forces, providing useful information about stability boundary calculations and robust process optimization. In the first part, experiments are performed to investigate the influence of micromilling process parameters on machining forces, tool edge condition, and surface texture. Built-up edge formation is observed to have a significant influence on the process outputs in micromilling of titanium alloy Ti6Al4V. In the second part, Bayesian inference is applied to model micromilling forces. The effectiveness of employing Bayesian inference in micromilling force modeling considering special machining cases is discussed. In the third part, finite element simulation of machining processes is employed and process outputs are used to update our knowledge about force coefficients. As a result of uncertainty analysis, the mean and standard deviations of the micromilling forces can be estimated. Bayesian inference can be useful since previous evidence or expertise is insufficient, or when obtaining the related information requires costly and time-consuming machining experiments.

Keywords: Micromilling, Mechanistic modeling, Bayesian inference, Markov chain Monte Carlo, Uncertainty analysis, Finite element simulation.

ÖZET

MİKRO FREZELEME KUVVETLERİNİN BELİRSİZLİK ANALİZİ VE OLASILIKSAL MODELLEMESİ

Erman Gözü
Endstri Mühendisliği, Yüksek Lisans
Tez Danışmanı: Yiğit Karpat
Eylül 2017

Mikro-frezeleme üretim sürecinin performansını öngörebilmenin ilk adımı kesme kuvvetlerinin modellenebilmesidir. Fakat kesici takım ile malzeme arasındaki karmaşık etkileşim sebebiyle mikro-frezeleme kuvvetlerinin öngörülebilmesi oldukça zordur. Bu çalışmada, Bayesci sonuç çıkarımı uygulanarak mikro-freze kuvvet katsayıları rassal olarak modellenmiştir. Deneysel ölçümler ve literatürdeki mekanik kuvvet modellerinden yola çıkarak Metropolis-Hastings algoritması ve Markov zinciri Monte Carlo benzetimi uygulanmıştır. Bu sayede kesme, kenar ve sürme kuvvet kaysayılarının olasılık yoğunluk fonksiyonları bulunmuştur. Bayesci sonuç çıkarımı sayesinde kuvvetlerin alt ve üst sınırları tahmin edilmiş olup, güvenilir kesme şartlarının hesaplanbilmesi ve eniyilenebilmesi için bilgi sağlanmıştır. Bu araştırmanın ilk bölümünde, mikro-frezeleme deneyleri yürütülerek işleme şartlarının kuvvetler, kesici takım kenarı ve yüzey hassasiyeti üzerindeki etkisi araştırılmıştır. Bu çalışmada kullanılan deneysel koşullar altında kesici kenara talaş yapışması görülmüş olup, bu durumun titanyum alaşım Ti6Al4V'nin mikro-frezeleme süreci çıktıları üzerinde önem teşkil ettiği gözlemlenmiştir. Araştırmanın ikinci kısmında, kesme kuvveti tahminlemesi yapmak üzere Bayesci sonuç çıkarımı uygulanmıştır. Öğrenilen modellerin etkinliği farklı deney şartlarında sınanmıştır ve sonuçlar tartışılmışır. Üçüncü kısımda sonlu elemanlar metodu kullanılarak talaşlı imalat süreci benzetimlenmiştir. Benzetim sonuçları Bayesci sonuç çıkarımı içerisinde kullanılmıştır. Belirsizlik analizinin sonucu olarak mikro-frezeleme kuvvetlerinin rassal dağılımları hesaplanabilmektedir. Bayesci sonuç çıkarımı, sahip olunan bilginin yeterli olmadığı veya gerekli bilgiyi elde etmenin maliyetli ve vakit alıcı olduğu durumlarda etkin bir araç olarak karşımıza çıkmaktadır.

Anahtar sözcükler: Mikro frezeleme, Kesme kuvvetleri, Bayesci sonuç çıkarımı, Markov zinciri Monte Carlo, Belirsizlik analizi, Sonlu elemanlar metodu.

Acknowledgement

First of all, I would like to express my sincere gratitude to my advisor Dr. Yiğit Karpat for his invaluable support, understanding, and guidance during my graduate study. It has always been a pleasure to work with him.

I convey my thanks to Assoc. Prof. Dr. Savaş Dayanık and Asst. Prof. Dr. Özgür Ünver for accepting to read and review this thesis, and their insightful comments and suggestions.

I would like to thank my fellow colleagues and officemates Samad Nadimi Bavil Oliaei, Barış Emre Kaya, Ümit Emre Köse, Melis Beren Özer, Elif Akkaya, Emirhan Buğday, Milad Malekipirbazari and all other members of the office EA307 for all their moral support and the good times we spent together.

I would also like to extend my sincere thanks to Şakir Duman and Mustafa Kılıç for their precious time to utilize the instruments in the lab and their contributions to my research.

Above all, I would like to thank my family; my mother Ayşe Gözü, my father Mustafa Gözü, my sister İrem Gözü and my dear Auntie Zeynep Seyrantepe for supporting me in every stage of my life. Their efforts enabled me to achieve all my accomplishments.

Finally, I would especially like to thank to İlkim Canoler for her love, endless support and understanding.

Contents

List of Figures

List of Tables

Nomenclature

α_e	Rake angle
A_p	Ploughed area
dF_{t_j}	Differential tangential force corresponding to cutting edge j
dF_{r_j}	Differential radial force corresponding to cutting edge j
dF_{tp_j}	Differential tangential ploughing force
dF_{rp_j}	Differential radial ploughing force
dF_{x_j}	Measured forces in x-direction corresponding to cutting edge j
dF_{y_j}	Measured forces in y-direction corresponding to cutting edge j
dz	Differential height element
φ	Cutting angle
$F_{measured}$	Instantaneous experimental cutting force data point
$F_{predicted}$	Predicted cutting force data point
h	Uncut chip thickness in milling
h_c	Critical chip thickness
h_j	Uncut chip thickness corresponding to cutting edge j
K_{te}	Tangential edge coefficient
K_{tc}	Tangential cutting coefficient
K_{re}	Radial edge coefficient
K_{rc}	Radial cutting coefficient
K_{tp}	Tangential ploughing coefficient
K_{rp}	Radial ploughing coefficient
r	Edge radius
Sa	Areal surface roughness
Ssk	Surface skewness
Sku	Surface kurtosis
Sq	Root mean square height
t_u	Uncut chip thickness in 2D cutting
V_p	Ploughing volume
$\bar{F}_{x,m}$	Measured average forces in x-direction
$\bar{F}_{y,m}$	Measured average forces in y-direction

Chapter 1

Introduction

Micromechanical milling is an effective technique to produce microcomponents having three-dimensional surfaces made from engineering materials [1, 2]. There is a strong demand for the production of micro scale consumer products used in a wide range of applications such as automotive, biomedical devices and micro-sensors [3, 4]. The current technological trend requires the processes of micro-hot embossing and micro-injection molding for the mass production of polymer micro-parts with high productivity and repeatability. The replication technologies including micro-dies and micro-molds should be specifically oriented to micro fabrication in terms of features, dimensional and geometrical tolerances and surface quality [5]. While lithography, micro-EDM and laser ablation can also be used to produce micro-molds, micro mechanical milling has emerged as a strong alternative since it offers, high material removal rate, process flexibility and enhanced surface quality.

Force modeling based on process input parameters is usually considered as the first step in process modeling. Mechanistic process modeling is usually preferred to model process forces in micromilling where the relationship between the work material and the cutting edge is obtained through cutting, edge, and ploughing force coefficients [6, 7, 8]. These coefficients are often calculated from either experimental measurements of process forces or finite element-based simulation models

[9]. The elasto-plastic behavior of the work material, tool cutting edge radius, tool deflections, tool runout, and tool vibrations all affect the forces, leading to uncertainties in micromilling forces especially when machining a difficult-to-cut material such as titanium alloy. Titanium alloy Ti6Al4V is a popular material in the biomedical industry due its bio-compatibility and low density.

There are uncertainties associated with cutting, edge, and ploughing force coefficients. When micromilling forces are calculated based on these coefficients, providing uncertainty information would be useful for the users. In a recent study, Karandikar et al. [10] demonstrated application of Bayesian inference to milling force modeling. They used the Markov chain Monte Carlo (MCMC) method to calculate the posterior distributions of the force coefficients. They concluded that Bayesian inference improves the predictive capability compared to linear regression-based traditional methods. Karandikar et al. [11, 12] also used Bayesian inference to model tool life in milling and turning operations. Niaki et al. [13] demonstrated the use of Bayesian inference in a mechanistic model of the tool wear while machining nickel-based alloys. Mehta et al. [14] used the Bayesian parameter inference method to model machining forces. Cao and Li [15] emphasized the importance of uncertainties in selecting stable machining conditions in micromilling. Jaffery et al. [16] studied the influence of micromachining process parameters by considering the relationship between undeformed chip thickness and tool edge radius. They found that when the feed is set above the tool edge radius, the feed rate is the most important parameter affecting tool wear, surface roughness, and burr width. When the undeformed chip thickness is set less than the tool edge radius, the influence of the feed on tool wear, surface roughness, and burr width was observed to be lower. Jaffery et al. [17] also pointed out that tool wear is driven by stochastic factors.

Built-up edge (BUE) formation is a common issue during micromachining of ductile materials affecting the process outputs. The size and stability of BUE depends on the machining conditions. In some cases, it is known to protect the cutting edge from rapid wear, but it has a detrimental effect on the surface finish, which is quite important in micromachining [18]. In this study, BUE is investigated in detail and considered as an important source of uncertainty.

1.1 Motivation of the Study

The objective of this study is to understand and model the process mechanics of micromilling. In particular, titanium alloy Ti6Al4V is selected as work material due to its popularity in the biomedical industry due its bio-compatibility and low density. First of all, the micromilling of titanium alloy and the process outputs are needed to be investigated. Controlling the dimensional tolerances and surface quality of microcomponents considering productivity issues is a challenge. The quality of micro-dies and micro-molds are dependent on the resulting surface texture of micro milling process. Therefore, the effect of machining conditions on cutting forces, cutting tool and the resulting surface texture are needed to be examined. This research aims to contribute the knowledge base of the micromilling of titanium alloy Ti6Al4V.

Predictive process models which have been successfully applied to macroscale milling, would be helpful to assist in selecting stable machining conditions, estimating surface location errors, and optimizing process parameters in micromilling [19, 20]. However, extending such predictive models to micromilling is not a straightforward task due to work material size effects, tool run-out, tool wear, built-up edge, and difficulties in identifying structural dynamic parameters. It is difficult to deal with the stochastic behavior of the micromilling process and uncertainties introduced by these factors using deterministic predictive process models.

Bayesian inference to milling force modeling provides a rational way to address the variability in micromilling and offers a number of advantages over the traditional methods. The formulation of updating the four force coefficients proposed by Karandikar et al. [10] is developed by including ploughing force coefficients which is proposed by the the work of Malekian et al. [6]. Bayesian inference to milling force modeling can be considered as one of the recent modeling techniques regarding cutting force modeling and the applications to the micromilling forces are limited in literature. This research aims to contribute to the literature by illustrating an application to micromilling force modeling. In order to assess the

generalization capability of Bayesian milling models, different test conditions are planned with a different micro end mill. As a result of the uncertainty analysis, mean and standard deviations of the micromilling forces can be estimated and reported to the literature.

Finally, this thesis aims to illustrate the application of physics-based machining models capable of predicting process outputs without conducting time-consuming and costly experiments. One of the main benefits of Bayesian inference is, it allows combining different sources information. Finite element simulations provide a cheaper method of estimating cutting forces. On the other hand, the quality of fits are expected to be poorer compared to the models established with experimental data. In this thesis, the outputs of the finite elements simulations are used to update probability distributions of the cutting coefficients. These established models are improved by fusing experimental measurements. Since performing machining experiments is an expensive method of obtaining information, the number of data points in the training data and the experimental conditions during the collection of data are two main considerations in model development phase. The effect of the size and the characteristics of training data on Bayesian learning are aimed to be examined.

1.2 Micromilling Cutting Force Models

Cutting force models are essential for planning and optimization of conventional and micro-milling processes. Quantitative predictions of cutting force components are used for determining stable (chatter free) machining conditions, designing milling cutters and machine tools, estimating machined component surface location errors, milling power and torque requirements. [21]. Moreover, the prediction of cutting forces becomes a major consideration in micro-scale, in order to avoid excessive tool deflections and tool breakage, by means of achieving the specified part accuracy, maintaining the productivity and reducing the costs.

According to the available studies, three main methods are employed for modeling milling forces, i.e. mechanistic, numerical, and analytical. According to mechanistic (empirical) models, which are commonly used to model milling forces, the cutting tool face is divided into small elements where cutting and edge forces considered to be effective. Cutting force is estimated based on several specific cutting coefficients for a given tool-workpiece pair. These coefficients are derived from the experimentally measured force data obtained from orthogonal or oblique cutting experiments. In references [21, 22, 23, 24, 25, 26, 27, 28, 29], several studies focused on mechanistic force modeling is given.

In numerical methods, the interaction between cutting tool and the material is examined [30]. The machining process is simulated by finite element method and the cutting forces are predicted. The studies shown that, 2D finite element simulations can be used to estimate cutting force coefficients of mechanistic modeling [9, 31]. This method offers a cheaper way of calculating cutting force coefficients and predicting part quality by means of simulating 3D micromilling process forces [32].

Analytical models benefit from various scientific branches and establish the mathematical relationship between the cutting forces and the mechanical aspects like friction, geometry and material behavior [33]. One of the well known models of this kind was proposed by Merchant [34]. However, in case of micro-machining, tool edge radius effect results in high negative rake angle and elastoplastic effects [2]. Therefore, the idealized assumptions of analytical models usually does not compensate the random nature of the both machining system and the workpiece.

Other recent studies [35, 36, 37] use non-linear optimization methods to estimate specific cutting force coefficients. This type of approach requires cutting force data and by minimizing the error between time domain simulations and measurements, the unknown cutting force coefficients are optimized. Unlike traditional least-squares method to the identification of force coefficients in milling, a single slot milling experiment is sufficient to determine unknown process parameters and run-out parameters. However, the estimated force coefficients are specific to the chosen machining parameters and expected to lose its predictive

performance as the machining conditions change. For instance, previous results show that the expected range of force coefficients vary for different feed per tooth values [37]. Especially for micro-milling, the effects of process dynamics are much more significant than the conventional milling. In order to obtain a representative set of specific force coefficients which is independent from the process parameters, the need of experiments with several machining conditions appear similarly to the linear regression procedure used in mechanistic modeling. Otherwise, a single measurement might be biased and lose its predictive power, given a tool-workpiece pair.

1.3 Organization of the Thesis

The rest of this thesis organized as follows: In *Chapter 2*, micromilling of titanium alloy and process outputs are investigated in detail. *Chapter 3* describes the application of MCMC method to the micromilling process to describe uncertainties in force predictions. A mechanistic micromilling model from the literature [6] is adopted, and the probability distributions of cutting, edge, and ploughing force coefficients are calculated. The effectiveness of employing Bayesian inference in micromilling force modeling considering special machining cases is discussed. In *Chapter 4*, finite element simulation of machining processes is employed and process outputs are used for updating our prior knowledge about force coefficients. As a result of uncertainty analysis, the mean and standard deviations of the micromilling forces can be estimated. Finally, *Chapter 5* offers a summary and conclusion.

Chapter 2

Investigation of Micromilling of Titanium Alloy

In this chapter, first, the experimental conditions of micromilling of Titanium alloy Ti6Al4V is given. Then, process outputs such as tool edge condition, surface texture and cutting forces are investigated.

2.1 Experimental Details

The micromachining experiments were performed on a CNC milling center DMG HSC 55 together with a NSK HES 510 high-speed spindle (max 50,000 rpm) as shown in Figure 2.1a. The work material is selected as titanium alloy Ti6AL4V due to its popularity in practice and research. The workpiece is 80 mm long and its width is 37 mm. The titanium work material has a lamellar structure consisting of 80% alpha and 20% beta phases as shown in Figure 2.1b. Slot micromilling experiments were performed under dry conditions. Machining forces were measured using a Kistler mini dynamometer (9256 C1) with its charge amplifier (5080A). The measurements were transferred to a PC using a data acquisition system (National Instruments).

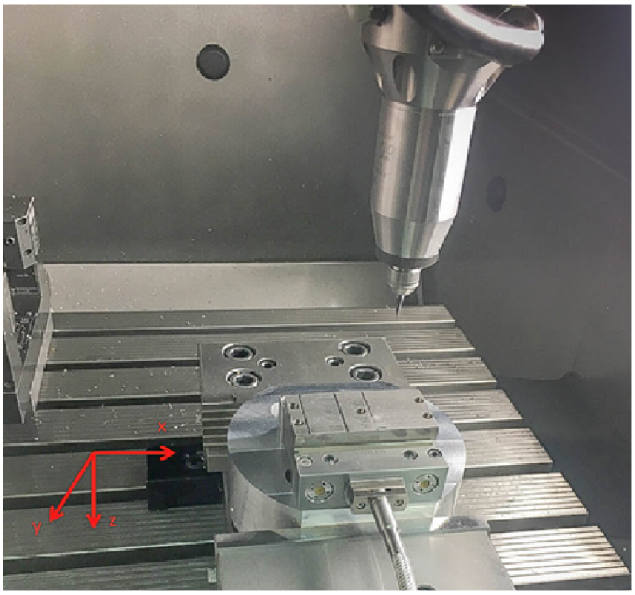

a)

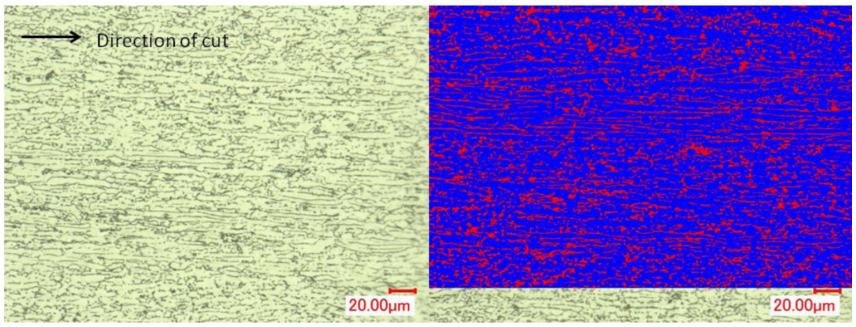

b)

Figure 2.1: *a*. Experimental setup of milling experiments. *b*. Microstructure of the material

Force signals were acquired with 10^5 data points per second during the experiments. Micro end mills (NS Tools MSE 230 0.4×0.8) having a 0.4 mm diameter and 2 µm cutting edge radius were used in the experiments. The cutting speed was kept constant at 35 m/min, which corresponds to 28,000 rpm spindle speed. As the micro end mill diameter decreases, the rotational speed of the micro-tool must be increased in order to attain an acceptable cutting speed. However, the tooth passing frequency should not exceed the bandwidth of the dynamometer [18]. A special attention was paid to the placement of the micro end mill to the tool holder; the static run-out was measured to be less than 1 µm using the Mahr

Millimar C-series indicator. The duration of cut (10 s) was kept the same in all experiments. Micromachining conditions are given in Table 2.1. The axial depth of cut was set as 10% of the nominal tool diameter. Feed per tooth values were set considering the edge radius of the endmill. Force measurements during the micromilling experiments, the condition of the tool edge after the experiments, and the resulting surface texture have been investigated in detail.

Table 2.1: Machining conditions for micromilling of Ti6AL4V

Rotational speed (rpm)	**Cutting speed (m/min)**	**Axial depth of cut (μm)**	**Feed per tooth (μm/rev)**
28 000	35	40	0.4, 0.6, 0.8, 1, 1.2, 1.5, 2, 3, 4

2.2 Micromilling Force Measurements

Figure 2.2a shows the micromilling forces in x, y, and z directions for a feed value of 0.4 µm/tooth. The variation peak forces and different directions can also be identified (as shown with "o") in this figure. Peak forces are important in micromilling since calculating the mean forces does not yield satisfactory information about the process conditions. The peak forces were counted using the data acquisition software NI DIAdem for the whole duration of the process. Peak-to-valley forces in positive and negative directions were calculated for all feed values, and the mean values are shown in Figure 2.2b. Peak-to-valley forces decrease down to 1 µm/tooth feed, and around this feed value, force instability occurs where the peak-to-valley forces slightly increase and start decreasing again around 0.6 µm/tooth. Based on these results, feed above 1 µm/tooth can be identified as the shearing dominated zone, feed between 0.6 and 1 µm/tooth can be identified as the transition zone, and feed less than 0.6 µm/tooth can be identified as the ploughing-dominated zone.

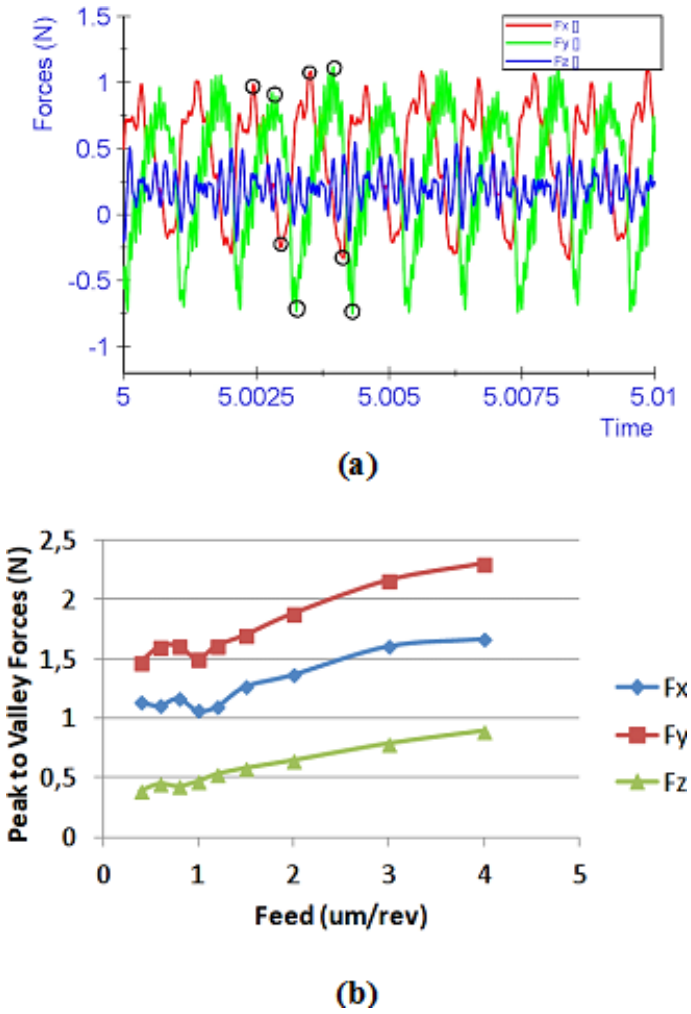

Figure 2.2: *a*. Acquired force signals from the micromilling experiments, 0.4 µm/tooth. *b*. Peak-to-valley forces for different feed values

2.3 Tool Edge Condition

Figure 2.3a shows the edge condition at the end of slot micromilling tests, which reveals that a built-up edge (BUE) at both cutting edges was formed during machining tests. The same micro end mill was used in all machining experiments in order to keep experimental conditions constant (tool overhang length, run-out, etc.). BUE is known to be detrimental to surface quality, but if it is stable and small in size, it may help to protect the cutting edge. Figure 2.3b shows the image of the cutting edge scanned with a confocal laser microscope (Keyence VHX-110). The cutting edge has a chamfered tip, which increases the strength

of the tip and also promotes work material accumulation in front of the tool which acts like the cutting edge. BUE changes the rake and clearance angles of the cutting edge, and its size depends on the machining conditions [38]. It is possible to eliminate BUE by increasing the cutting speed, but in micromilling, it is limited by the maximum spindle speed and dynamics of the process. A high cutting speed would also result in faster tool wear, especially when difficult-to-cut materials are machined. Figure 2.3c shows the edges of the micro end mill after BUE is removed by applying a cleaning procedure. The edge radii were measured to increase from initial 2 to 4 µm. A rapid increase in edge radius during the break-in period increases the possibility of material entrapment in front of the cutting edge.

In Figure 2.4, two possible cases of micromachining configurations are shown. If there is no BUE in front of the cutting edge and assuming that the uncut chip thickness t_u is smaller than the edge radius r, then the effective rake becomes negative α_e. The material underneath the cutting edge is ploughed during machining. This volume is a function of material elastic properties. It is difficult to model material behavior under such conditions, which introduce uncertainty to modeling. If there is BUE formation in front of the tool, the ploughing forces are applied to it. The resulting rake angle becomes positive, and the contact conditions between the cut material and the tool material cease. The condition of the edge directly influences the generated surface. The stability of BUE and its size and shape introduce uncertainty to modeling. Predicting BUE stability, size, and shape depending on the machining conditions is a challenging task [38].

2.4 Surface Texture Investigation

The condition of the cutting edge and feed value directly influences machined surface properties. Therefore, investigation of the surface texture would yield some useful information about the combined effect of BUE and feed on the surface texture. In this study, micromilled surfaces were investigated by considering areal surface properties. Three-dimensional topography of the micromilled surfaces

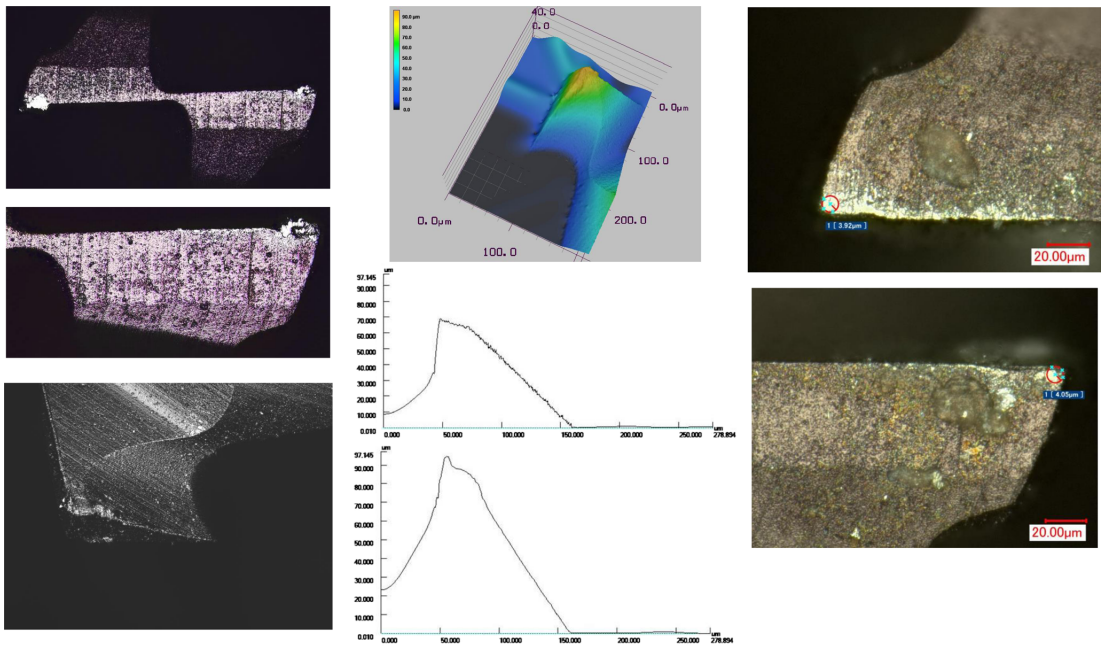

(a) (b) (c)

Figure 2.3: *a.* Edge condition of the micro end mill after machining test. *b.* Edge profile of the cutting tool with and without BUE. *c.* Edge condition of the micro end mill after BUE was removed

was obtained by using a laser scanning microscope (Keyence VK-X110). The following process steps were considered in the analysis. First, the tilt (slope) of the surface was corrected. Second, the noise in the surface height information was removed by applying a denoising algorithm. Figure 2.5 shows the raw images of the micromilled surfaces for all feed values from the smallest, 0.4 µm/tooth (a), to the largest feed, 4 µm/tooth (i), based on the experimental plan given in Table 2.1. Figure 2.6 shows extracted microscope images of the machined surfaces (with $\times$500 magnification). The influence of machining conditions is reflected on the micromilled surface. The small material particles from BUE were smeared on the surface. These appear as stochastically distributed hills over the surface. As the feed increases, feed marks become more visible.

Arithmetic mean surface roughness (Sa), surface skewness (Ssk), and surface kurtosis (Sku) parameters are investigated here. Ssk is defined as the ratio of the mean of the height values cubed and the cube of root-mean-square height (Sq) within a sampling area [39]. It describes the shape of the topography height

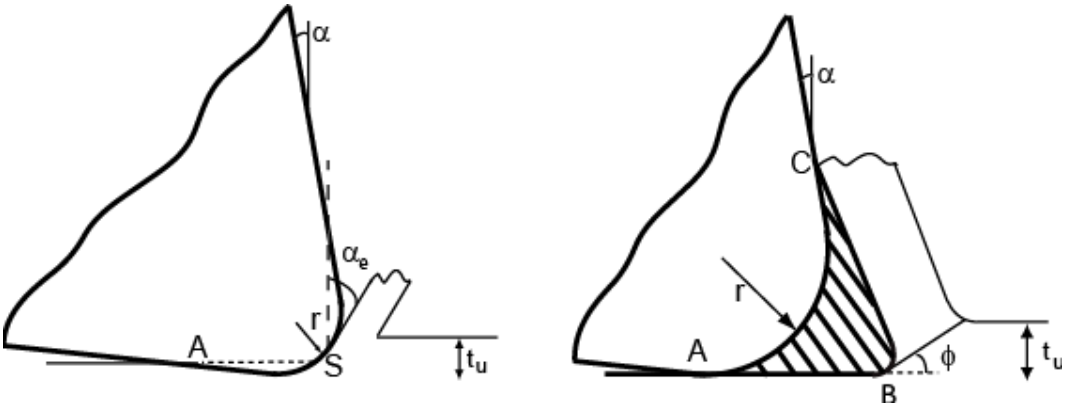

Figure 2.4: Two possible configurations of microscale cutting. Stagnation point assumption ($left$) and BUE formation ($right$).

distribution. If $Ssk > 0$, then the peaks are dominant on the surface whereas $Ssk < 0$ indicates dominance of valleys. Sku is calculated as the ratio of the mean of the fourth power of the height values and the fourth power of Sq within the sampling area [39]. It is a measure of the sharpness of the surface height distribution, and it is strictly positive. $Sku > 3.0$ indicates the existence of high peaks or deep valleys on the surface. For a surface representing normal distribution, Ssk is 0 and Sku is 3. Ssk and Sku were considered to investigate the size and distribution of the rubbed particles on the surface as they represent a histogram of heights which define the symmetry and deviation from an ideal normal distribution. The convention in areal surface texture measurements is to take one sampling area per evolution area [39]. Here, it is decided to divide the surface into nine divisions as shown in Figure 2.7, and each division was analyzed separately. This approach allows the investigation of irregular surface imperfections in isolation and observation of their variation along the machined surface. The image in Figure 2.7a represents an area of 522 × 210 µm obtained by stitching microscope images along the micromilled surface. Figure 2.7b shows the variation in Ssk and Sku at those regions indicated in Figure 2.7a. Larger particles in regions 1, 2, and 5 resulted in large values of Ssk and Sku. Large values of Ssk and Sku are due to high-order terms in their equations (Figure 2.8).

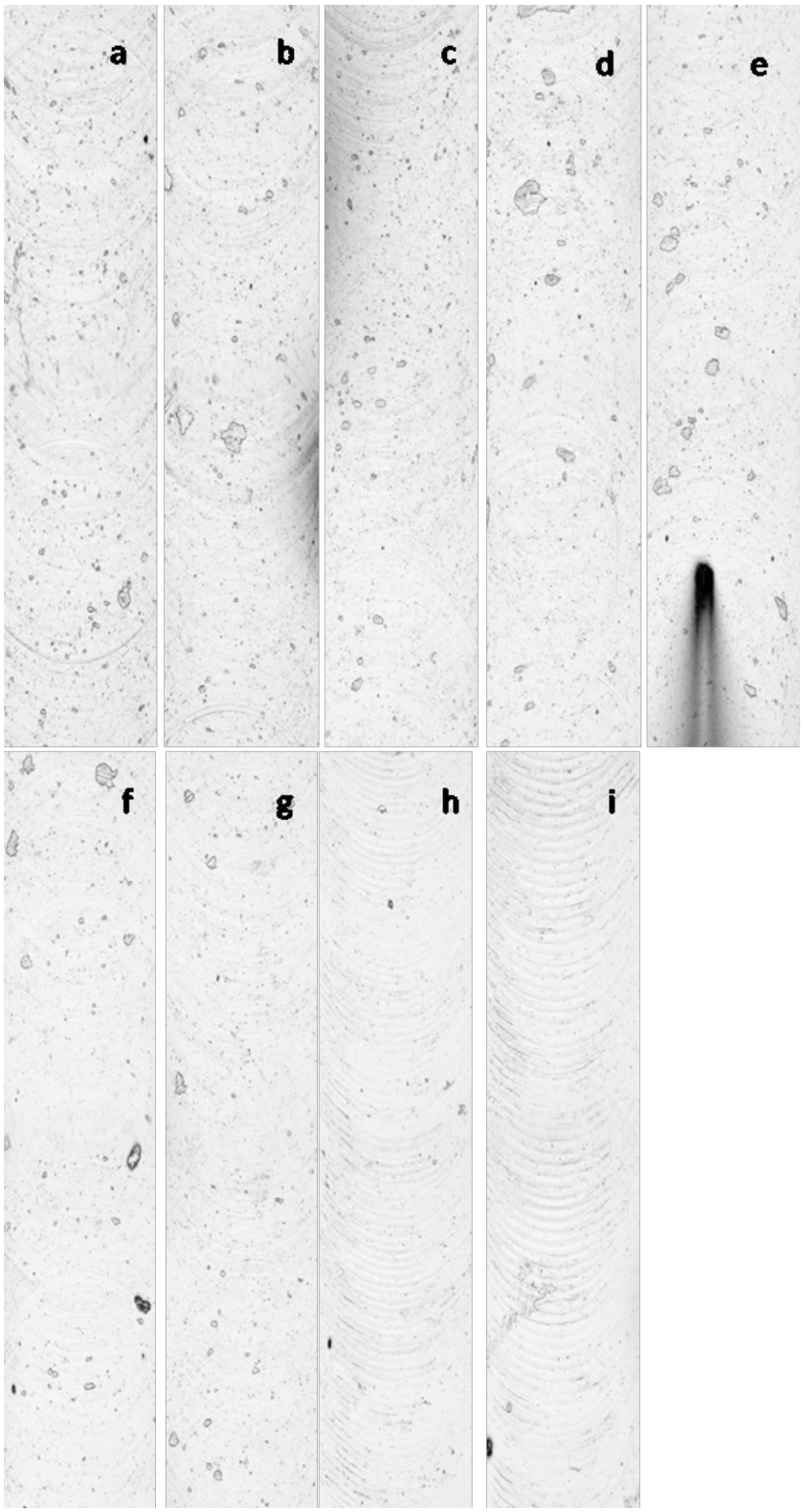

Figure 2.5: Images $(a - i)$ of the micromilled surfaces at all feed values

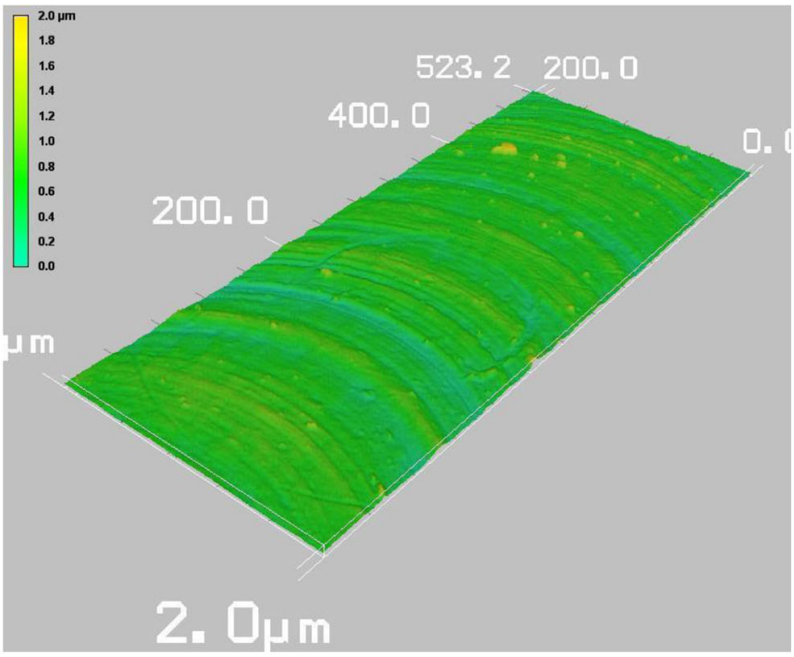

(a)

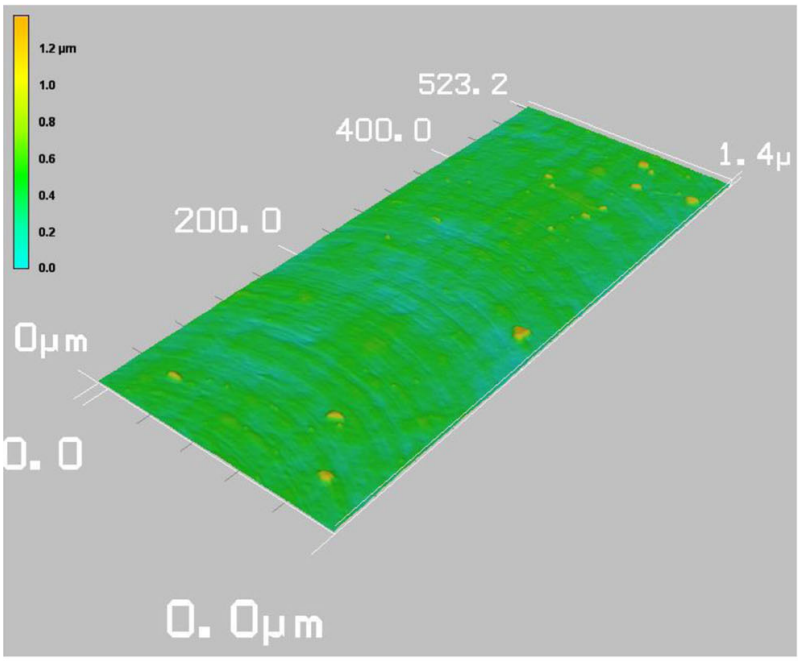

(b)

Figure 2.6: Surface topography obtained through confocal laser scanning. *a*. Feed at 0.4 µm/tooth. *b*. Feed at 2 µm/tooth

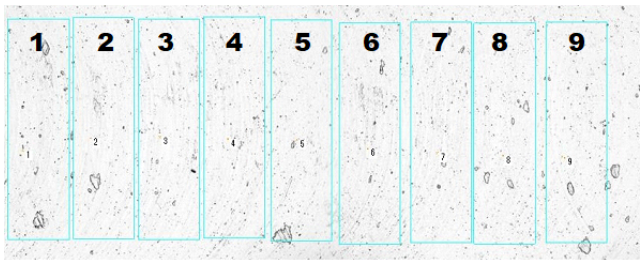

(a)

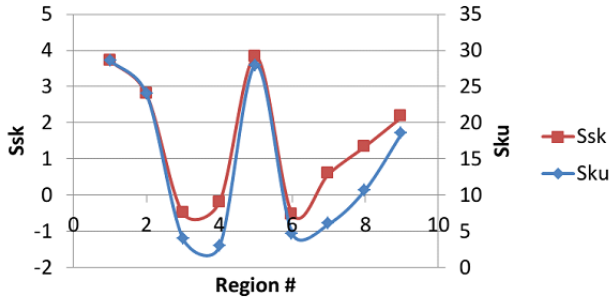

(b)

Figure 2.7: *a*. Micromilled surface for 2 µm/tooth feed divided into nine regions. *b*. Variation in skewness and kurtosis among regions

The trends of the results are in agreement with the force measurements. The lowest surface roughness value of 0.06 µm was measured around 1.52 µm/tooth, which belongs to the shearing-dominated machining region. As the feed increases further, surface roughness also increases, as expected. However, Ssk and Sku both decrease. A larger and more stable BUE with increasing feed results in less material particles smeared on the machined surface. Increasing the feed further leaves larger surface marks, which increase the areal surface roughness value as seen in Figure 2.5h-i. At feed values corresponding to the ploughing and transition regions, Ssk and Sku values increase significantly, indicating the detrimental effect of BUE on the surface texture. Results indicate the importance of feed selection in micromilling and the trade-off between surface texture parameters. With increasing feed, the process behaves like a macroscale milling process where the feed is the most influential parameter on surface roughness. The results correlate with the findings of Jaffery et al. [16]. Recently, Wang et al. [40] showed that peaks on the surface due to BUE hinder the ability to predict surface quality in micromilling.

2.5 Micromilling Mechanistic Force Modeling

In micromilling, typical feed values are in the same order of magnitude as the cutting edge radius. If the uncut chip thickness is less than a certain value (also known as the minimum uncut chip thickness), then the machining operation cannot be performed effectively. As a result, the round cutting edge ploughs the uncut material onto the work surface. Malekian et al. [6] proposed a mechanistic micromilling force model by considering shearing and ploughing phases separately. They were able to simulate dynamic machining forces for the micromilling of aluminum 6061. Ploughing forces were modeled to be proportional to the volume of the material elastically deformed underneath the cutting edge. The amount of elastic recovery, the minimum uncut chip thickness value, the edge radius of the cutting edge, and the clearance angle are the inputs to model ploughing forces. The minimum chip thickness is usually defined as the ratio of uncut chip thickness to cutting edge radius, and it is considered to be around 20% based on the assumption that a stagnation point exists on the cutting edge, which separates the work material flow into the chip and onto the workpiece. In a recent study, Oliaei and Karpat [38] showed that built-up edge formation in front of the cutting edge reduces this ratio down to 10% during microturning of titanium alloy Ti6Al4V. Figure 2.9 shows the micromilling process model proposed by Malekian et al. [6]. The forces acting on the cutting edge are defined with respect to the uncut chip thickness (h). When the uncut chip thickness is larger than a critical value ($h > hc$), shearing dominates the machining process. The tangential and radial forces acting on the cutting edge can be represented with Equation 2.1.

$$\begin{aligned} dF_{t_j} &= (K_{te} + K_{tc} h_j) dz \\ dF_{r_j} &= (K_{re} + K_{rc} h_j) dz \end{aligned} \tag{2.1}$$

Equation 2.1 represents the shearing-dominated region, where K_{rc} and K_{tc} are defined as the radial and tangential cutting coefficients, respectively. K_{re} and K_{te} are the radial and tangential edge coefficients, respectively. These coefficients represent the resistance of the material to machining and the influence

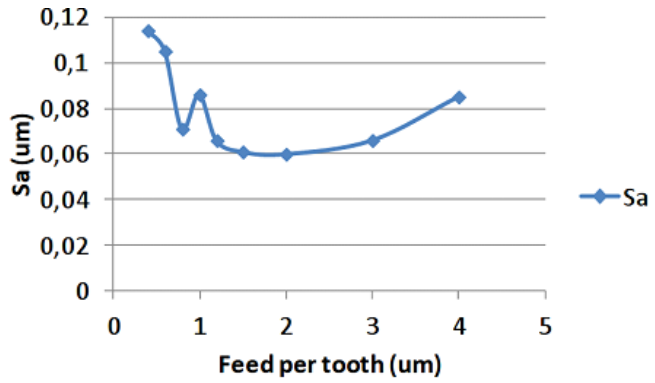

(a)

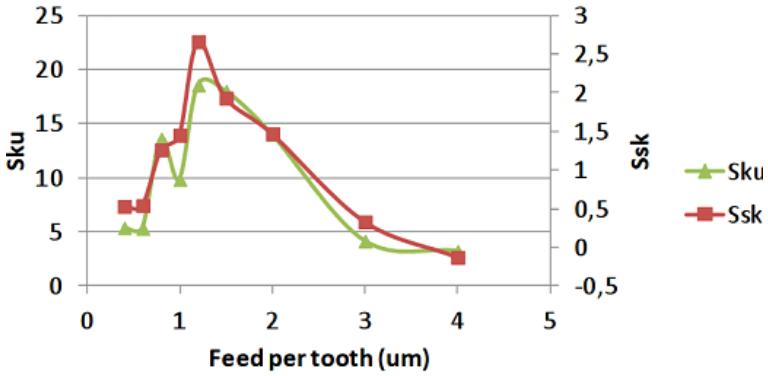

(b)

Figure 2.8: *a*. Areal surface roughness (Sa) *b*. Surface skewness (Ssk) and kurtosis (Sku) measurements as a function of feed

of the cutting edge radius. These unknown coefficients are usually calculated based on average machining forces obtained through micromilling experiments. In Equation 2.1, h_j denotes the uncut chip thickness corresponding to cutting edge j. The circular tool path assumption in which the uncut chip thickness varies from zero to the maximum value of feed per tooth is no longer acceptable in micromilling when tool run-out and feed values are close to each other. As a result, cutting edges of the micro end mills do not experience the same chip load during milling operation, which leads to fluctuations in the machining forces from one cutting edge to another. Tool run-out is directly related to the micro tool, the tool holder, and the high-speed spindle. The tool run-out model of Zhang et al. [7] has been adopted in this study. The uncut chip thickness is also a function

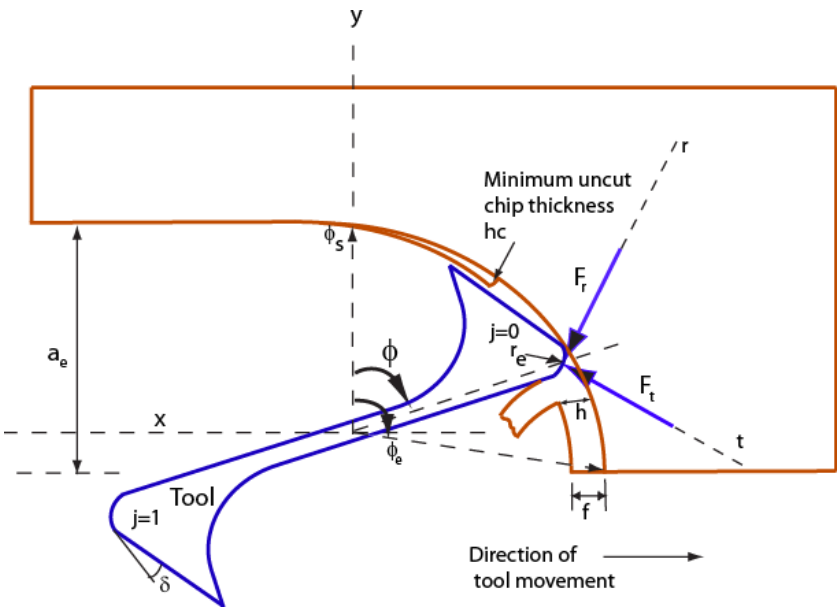

Figure 2.9: Micromilling process model

of the immersion angle and helix angle of the tool acting on a differential height element (dz) on the tool body. As for the region where $h < hc$, ploughing condition dominates the machining forces. Malekian et al. [6] modeled these forces proportional to the volume of interference between the tool and the workpiece. The ploughing volume regarding a discretized disk element of a tooth is related to the area underneath the tool as $V_p = A_p dz$. Ploughing forces in radial and tangential directions can be expressed as in Equation 2.2.

$$\begin{aligned} dF_{tp_j} &= (K_{te} + K_{tp}A_p)dz \\ dF_{rp_j} &= (K_{re} + K_{rp}A_p)dz \end{aligned} \tag{2.2}$$

F_{rp_j} and F_{tp_j} are the radial and tangential ploughing forces acting on tooth j, respectively. Edge coefficients K_{re} and K_{te} in the shearing-dominant regime are incorporated together with additional ploughing coefficients based on the ploughed area underneath the cutting edge K_{rp} and K_{tp}. The estimation procedure of the ploughed area A_p is given in [6]. Equation 2.3 summarizes the calculation of radial and tangential forces acting on a discretized disk element on tooth j as:

$$
\begin{aligned}
dF_{t_j} &= \begin{cases} (K_{te} + K_{tc} h_j) dz & \text{when } h \geq h_c \\ (K_{te} + K_{tp} A_p) dz & \text{when } h < h_c \end{cases} \\
dF_{r_j} &= \begin{cases} (K_{re} + K_{rc} h_j) dz & \text{when } h \geq h_c \\ (K_{re} + K_{rp} A_p) dz & \text{when } h < h_c \end{cases}
\end{aligned} \tag{2.3}
$$

A coordinate transformation is then required to calculate the forces in x and y directions. For measured micromilling forces in x and y directions, it is possible to identify unknown coefficients in reverse fashion.

$$
\begin{aligned}
dF_{x_j} &= dF_{t_j} \cos\varphi + dF_{r_j} \sin\varphi \\
dF_{y_j} &= dF_{t_j} \sin\varphi - dF_{r_j} \cos\varphi
\end{aligned} \tag{2.4}
$$

Cutting, edge, and ploughing force coefficients shown in Equation 2.3 together with tool run-out parameters (its magnitude and angle) can be calculated based on a methodology proposed by Malekian et al. [6]. There are a total of eight unknowns (six force coefficients and two tool run-out parameters) that need to be identified. For simplification, it can be assumed that the tool run-out magnitude and angle are the same for all feed values. The objective function can be written as Equation 2.5, which is the sum of the squared error between the data points of the measured cutting forces and the force predictions, where $F_{measured}$ is the instantaneous experimental cutting force data point and $F_{predicted}$ corresponds to the prediction, l is the number of feed values, and k is the number of data points.

$$
error = \sum_{i=1}^{k} \sum_{j=1}^{l} (F_{measured_{i,j}} - F_{predicted_{i,j}})^2 \tag{2.5}
$$

Open-source software R was used to calculate unknown coefficients using genetic algorithm. In the solution algorithm, first, cutting and edge coefficients for the shearing region were considered. Two ploughing coefficients (K_{tp} and K_{rp}) were calculated as a second step based on already calculated edge force coefficients. Table 2.2 shows the calculated force coefficients and run-out parameters which minimize Equation 2.5 for experimental condition given in Table 2.1.

Table 2.2: Identified force coefficients and run-out parameters after optimization

$\boldsymbol{K_{te}}$ **(N/mm)**	9.1
$\boldsymbol{K_{tc}}$ **(N/mm^2)**	4475
$\boldsymbol{K_{re}}$ **(N/mm)**	13.2
$\boldsymbol{K_{rc}}$ **(N/mm^2)**	2854
$\boldsymbol{K_{tp}}$ **(kN/mm^3)**	13,623
$\boldsymbol{K_{rp}}$ **(kN/mm^3)**	4300
Run-out magnitude (μm)	0.19
Run-out angle ($^\circ$)	101

The goal of this study is to calculate the distributions of force coefficients using Bayesian inference, which is explained in the next chapter.

Chapter 3

Bayesian Inference Applied to Micromilling Force Modeling

In this chapter, first, Bayes' rule and Bayesian inference formulation to the micro milling force modeling are introduced. Second, Markov chain Monte Carlo (MCMC) approach and Metropolis-Hastings (MH) algorithm to sample probability distributions is illustrated. Third, the application of Bayesian inference to milling force modeling is described and simulation results are presented. Finally, force predictions are validated with the experimental measurements and the effectiveness of established models under special machining cases is discussed.

3.1 Bayesian Inference

Bayes' rule provides a rational method for updating beliefs in light of new information (i.e., experimental measurements). It is represented with Equation 3.1 below:

$$\{A|B,\theta\} = \frac{\{A|\theta\}\{B|A,\theta\}}{\{B|\theta\}} \tag{3.1}$$

The left-hand side of the equation $\{A|B,\theta\}$ is the posterior distribution, which summarizes the state of knowledge about an event A in a statistical model, after observing the result B. The first term on the right-hand side of the equation $\{A|\theta\}$ is the prior distribution about an uncertain event A, at a state of information θ, which addresses our state of knowledge about the parameters before having an observation. The second term $\{B|A,\theta\}$ is the likelihood of obtaining an experimental result B given that the observation A has occurred. The denominator $\{B|\theta\}$ is the probability of obtaining an experimental result B without knowing that A has occurred, which behaves like a normalizing constant. Usually, the denominator is not computed explicitly, as it is known that the posterior distribution is a probability density function that integrates to one. According to Bayes rule, the posterior belief is proportional to multiplication of prior and likelihood functions. This process of learning via Bayes rule is referred to as Bayesian inference, i.e., updating prior beliefs given new data B to obtain the posterior belief

Karandikar et al. [10] proposed the formulation of updating the force coefficients, given the measured values of experimental force data. The variability of the force coefficients can be assessed by combining prior knowledge and experimental data. Bayes rule for the force coefficients, including ploughing coefficients, could be written as:

$$\begin{aligned} &f_{K_{tc},K_{rc},K_{te},K_{re},K_{tp},K_{rp}}(K_{tc},K_{rc},K_{te},K_{re},K_{tp},K_{rp}|\overline{F}_{x,m},\overline{F}_{y,m}) \propto \\ &f_{K_{tc},K_{rc},K_{te},K_{re},K_{tp},K_{rp}}\ l(\overline{F}_{x,m},\overline{F}_{y,m}|K_{tc},K_{rc},K_{te},K_{re},K_{tp},K_{rp}) \end{aligned} \tag{3.2}$$

In Equation 3.2, $\overline{F}_{x,m}$ and $\overline{F}_{y,m}$ are the measured mean forces in x and y directions, respectively. The term $f_{K_{tc},K_{rc},K_{te},K_{re},K_{tp},K_{rp}}(K_{tc},K_{rc},K_{te},K_{re},K_{tp},K_{rp}|\overline{F}_{x,m},\overline{F}_{y,m})$ is the posterior distribution of the force coefficients given measured values of the mean forces. The term $f_{K_{tc},K_{rc},K_{te},K_{re},K_{tp},K_{rp}}$ is the joint prior distribution of the force coefficients, and $l(\overline{F}_{x,m},\overline{F}_{y,m}|K_{tc},K_{rc},K_{te},K_{re},K_{tp},K_{rp})$ is the likelihood of obtaining mean forces in the x and y directions, given the six force coefficients. The multiplication of prior and likelihood is proportional to the

posterior function, which allows for updating beliefs, and then a normalization must be made as in Equation 3.1. Assuming that the force coefficients are independent, the density function of the joint force coefficients $f_{K_{tc},K_{rc},K_{te},K_{re},K_{tp},K_{rp}}$ is equal to the multiplication of the density function of each force coefficient. The mean forces in x and y directions ($\overline{F}_{x,m}$ and $\overline{F}_{y,m}$) are also assumed to be independent; thus, the likelihood of obtaining mean force measurements is multiplied for each direction in order to obtain a joint likelihood function.

In order to carry out the Bayesian updating procedure, two main inputs are required; the likelihood and prior functions. The prior function corresponds to our prior knowledge on specific force coefficients, and the likelihood function refers to the likelihood of obtaining the experimental mean force values, given specified values of the force coefficients. To select these probability distributions, a well-known bell shaped normal distribution might be an appropriate choice. In that case, it is assumed that force coefficients are distributed symmetrically around a known mean. The other option is to use non-informative, in other words, uniform priors to capture the pattern with minimal knowledge. This type of selection is favorable for situations with insufficient previous evidence or expertise, or when obtaining the related information requires tedious research. In this study, both uniform and normal prior distributions were employed. In order to define a normal distribution, mean and standard deviation are required as parameters. On the other hand, minimum and maximum values are required to define a uniform distribution.

3.2 Markov Chain Monte Carlo Method

The MCMC method is used to draw samples from a random known distribution. The Metropolis-Hastings (MH) algorithm is one of the most popular MCMC methods, and it is primarily used as a way to simulate observations from unwieldy distributions [41]. Therefore, the MH method can be used for drawing samples from a random known distribution, which, in our case, is the posterior distribution force coefficients [42]. In the MH algorithm, the proposal distribution

denoted by $q(x)$ is used to draw candidate samples that mimic samples drawn from the target distribution denoted by $p(x)$. The candidate samples from the proposal distribution are either accepted or rejected depending on an acceptance probability given below:

$$A(x, x^*) = \min\left\{1, \frac{p(x^*)q(x|x^*)}{p(x)q(x^*|x)}\right\} \tag{3.3}$$

where x^* is the candidate sample drawn from a proposal distribution $q(x)$ and x is the current state of the Markov chain. For each iteration, the Markov chain moves to x^* if the sample is accepted; otherwise, the chain stays on the current value of x. The pseudo-code of the MH algorithm is shown below:

1. Initialize the starting point x^0
2. For $i = 0$ to $i = N - 1$ iterations, do the following:
   (a) Sample $x^0 \sim q(x^*|x)$
   (b) Sample $u \sim U_{[0,1]}$
   (c) If $u < A(x, x^*) = \min\left\{1, \frac{p(x^*)q(x|x^*)}{p(x)q(x^*|x)}\right\}$
   $x^{(i+1)} = x^*$
   $else$
   $x^{(i+1)} = x^{(i)}$

The MH algorithm has been carried out to approximate posterior distribution of force coefficients. Since the posterior distribution we want to approximate is a joint density function of force coefficients, sampling for each variable is carried out using univariate proposal distributions. One variable at a time is sampled, and then sequentially, the algorithm proceeds to the remaining variables. Flowchart representing the application of MH algorithm is given in Appendix A. To illustrate the application of MH algorithm:

1. The initial values for all force coefficients are conducted as the first step.

2. The proposal distributions for each force coefficient are defined. Proposal distributions have a significant effect on the convergence process.

If we sample a wider range of K's, the proportion of the rejection will probably increase, and therefore, convergence could not be done, or requires significant numbers of iteration. On the other hand, if we select them too narrow, most of the samples will be accepted and the space could not be explored. The key point for selecting proposal distributions is that the range of samples obtained from proposal distributions should include the range of target distributions. It is highlighted that a 25 - 35% acceptance rate is appropriate for the convergence of the Markov chain [43].

3. A function needs to be defined in order to estimate force averages given a set of K's. Since experimental forces are close to zero and tool run-out is dominant in micromilling, using analytic formulas to estimate average forces results in additional errors as they underestimate, or overestimate, the effect of tool run-out on the mean forces. In this research, instead of employing analytic formulas to estimate average force equations, time-domain simulations with tool run-out extension were conducted and their averages were taken into account.

4. The acceptance ratio defined in Equation 3.3 should be estimated by an operator which needs to be defined. This operator takes the candidate and current values of the chain as input, evaluates the probabilities according to the prior and likelihood functions, and finally outputs the acceptance probability.

5. For each iteration, one variable at a time is sampled. So for every variable, basically, we have two sets of K values, first is the current set of K's in state i which is $[K_1^i, K_2^i, K_3^i, ..., K_n^i]$ and the candidate set, $[K_1^*, K_2^i, K_3^i, ..., K_n^i]$. Besides these sets, force averages are estimated using both sets and taken as inputs to the acceptance ratio operator. Then, acceptance ratio is estimated and compared with u, which is a random number generated from a uniform distribution with a range from 0 to 1. According to the comparison, K_1^* is either accepted or rejected. If it is accepted, K_1^i is updated to K_1^*. The same procedure is repeated continually for the next variable until the sample from K_n^i is drawn and evaluated. Finally, iteration ends the next iteration $i + 1$ takes place.

6. When the iterations end, we obtain samples from the distributions of K's and the traces of them. The burn-in process is applied, which refers to discarding an initial portion of the simulation in order to ensure steady-state conditions. Finally, normal distributions are fit to the samples. The maximum-likelihood values for the mean and standard deviation of the normal distribution correspond to sample statistics for the data.

3.3 Bayesian Inference Applied to Milling Force Modeling

Ploughing forces are modeled to be proportional to the volume of the elastically deformed material underneath the cutting edge which is defined by those variables. Several variables such as clearance angle, edge radius, elastic recovery, and critical chip thickness must be known to calculate ploughing forces. Identified ploughing force coefficients K_{tp} and K_{rp} depend on the condition of the tool edge as described in Figure 2.4. Assuming that BUE acts as a cutting edge, the radius of the cutting edge with BUE was measured as 5 µm, the clearance angle was measured as 7°, and the elastic recovery percentage is assumed to be 10%. However, considering the dynamic nature of BUE, these variables cannot be identified easily. A larger ploughing area at the tool-work interface would result in lower ploughing force coefficients. It is important to note that uncertainties about these variables are the reason for using the simple force models described in Section 2.5. The development of detailed models is constrained by the uncertainties of the input parameters.

Table 2.2 shows the calculated force coefficients and run-out parameters which minimize Equation 2.5 for experimental condition given in Table 2.1. Deterministic point estimates of force coefficients obtained from the genetic algorithm approach are selected as means for normal prior distributions. Since many experiments were performed and force measurements were taken, there is enough

information about the process. On the other hand, if prior knowledge or experimental data is not available, a uniform prior can also be chosen. Both approaches are used in this study to compare the results. Table 3.1 shows the selected mean and standard deviation parameters for normal prior distribution and lower and upper values of uniform prior distributions. In uniform distribution, any value is equally likely within the given range.

The likelihood function needs to be addressed in order to employ Bayesian updating. It is assumed that experimental mean force values distributed normally with a standard deviation of 0.1 N. The mean of the likelihood corresponds to the average experimental force data obtained, as it is an estimate obtained from the slot milling experiments. The likelihood function used in Bayesian learning behaves like an error correcting mechanism, providing a way to overcome problems caused by linear regression. For instance, after experimental force averages are used to update our prior knowledge, the non-linearity of the force averages at small feed values is compensated and the large confidence intervals narrowed for higher feed values. The Metropolis-Hastings algorithm was applied for 10^4 iterations to obtain samples from the joint target densities of force coefficients, and the first 1000 samples were discarded. Figure 3.1 shows the traces and Figure 3.2 shows the sampled force coefficients for normal prior. Table 3.2 shows the calculated posterior distribution parameters.

The results shown in Table 3.2 are close to each other in terms of mean values and close to those shown in Table 2.2. The edge forces in normal prior distribution are affected by the MCMC algorithm more than the cutting force coefficients as seen in Figure 3.2a. The variation in uniform posterior distribution parameters is larger than normal distribution. The posterior distribution is sensitive to the selection of prior distribution. In order to test the predictive ability of these distributions, two cases are considered such as 0.5 and 2 µm/tooth feed slot micromilling. The cutting speed and axial depth of cut was kept the same. The upper and lower limits (blue dashed lines) of the force predictions are plotted together according to 95% confidence interval ($\pm$ 2 standard deviations) with experimental measurements in Figure 3.3. The experimental measurements are observed to be within the predictions. The range of the predictions with uniform

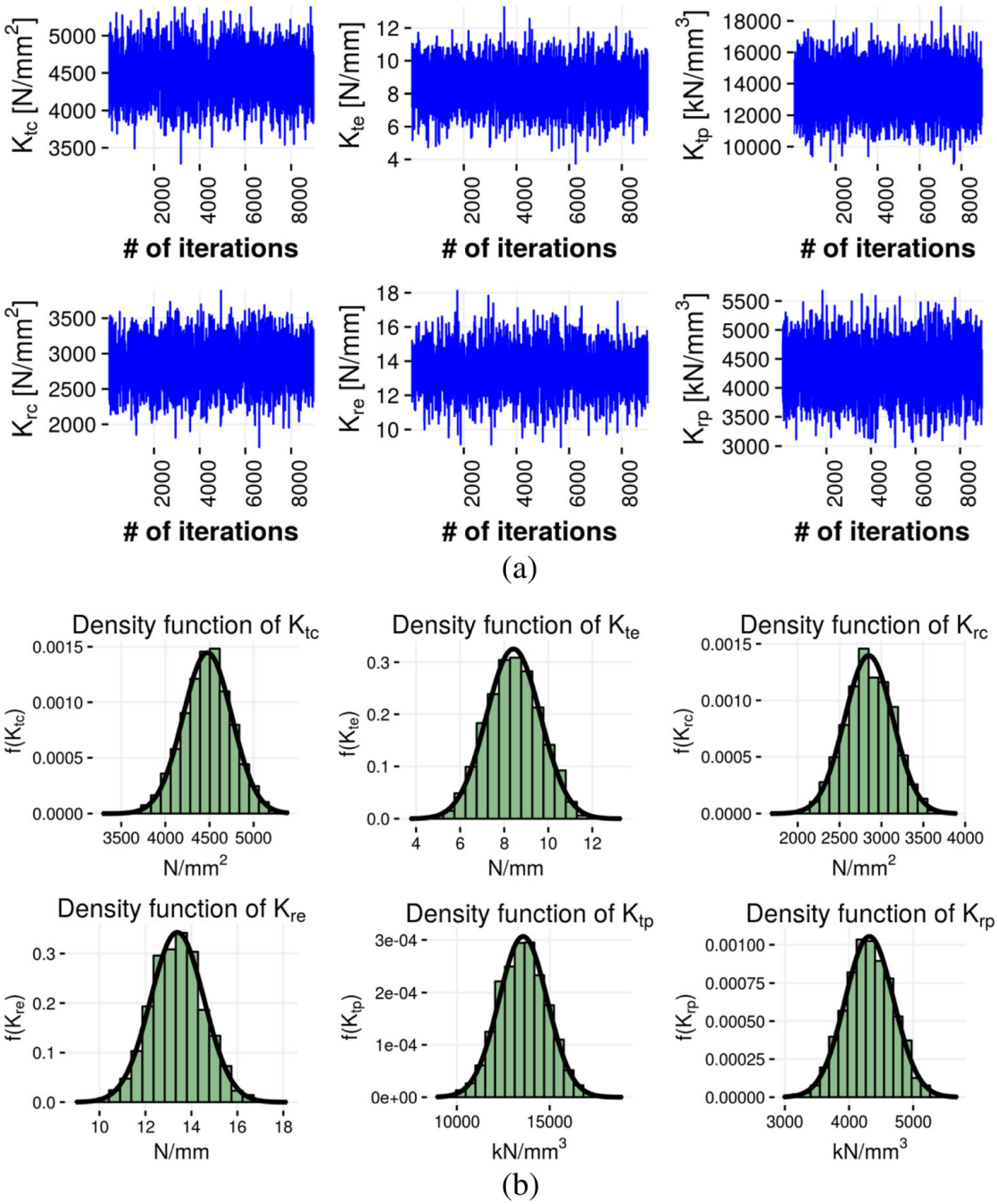

Figure 3.1: Traces *(a)* and sampled force coefficients *(b)* of force coefficients for normal prior setting

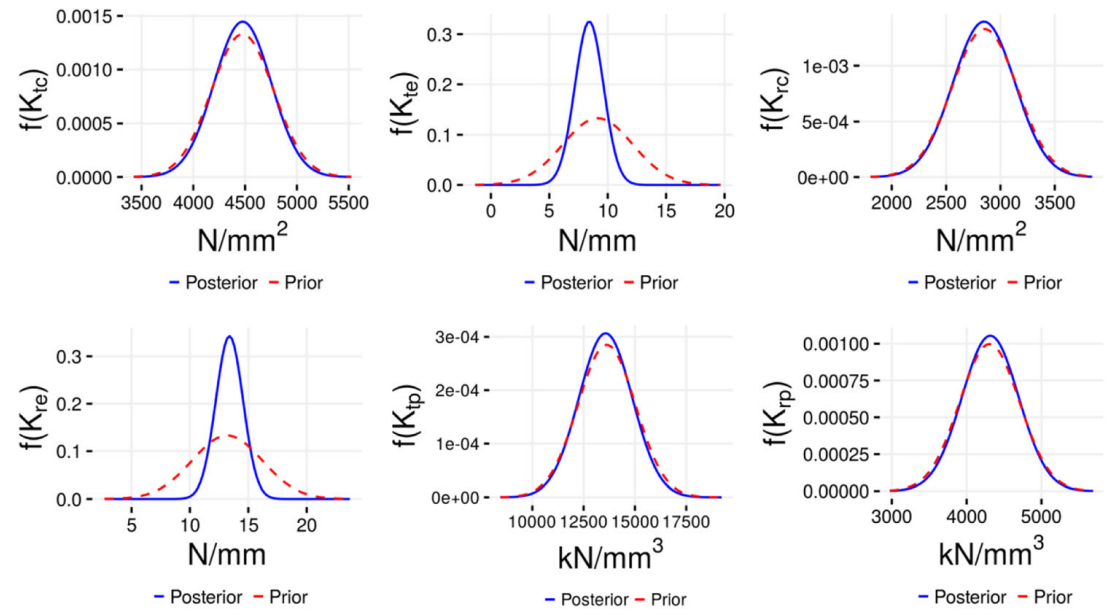

(a)

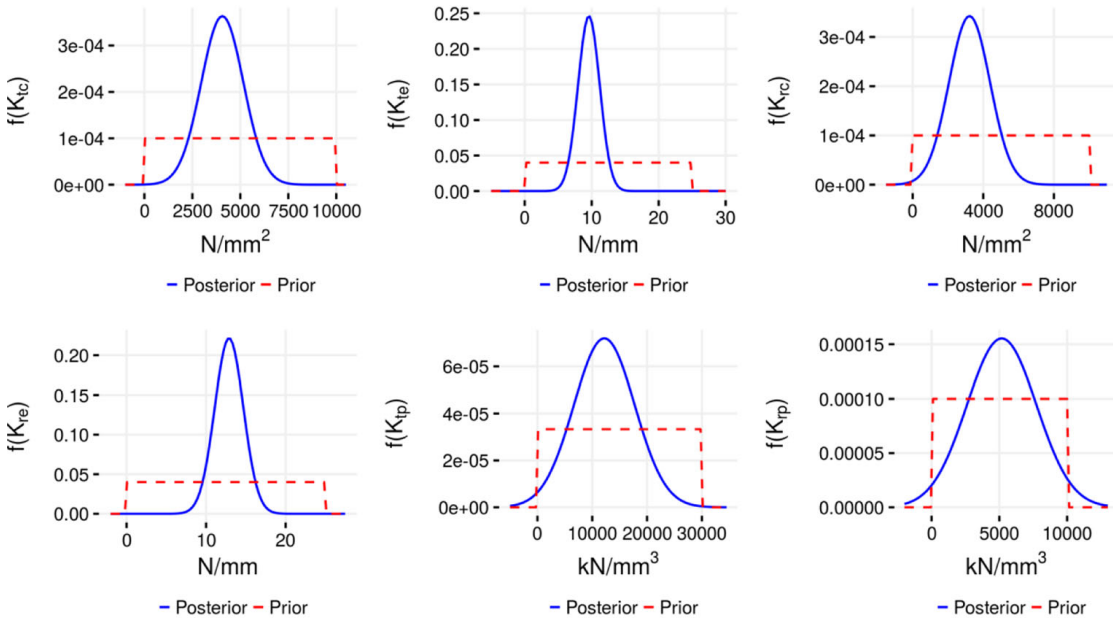

(b)

Figure 3.2: Posterior *(blue lines)* and prior *(red dashed lines)* distributions of the force coefficients. *a.* Normal *b.* Uniform

distribution is larger. Such predictions can be useful to calculate milling stability boundary calculations including force coefficient uncertainties [44].

Table 3.1: Parameters of prior distributions for uniform and normal settings.

	Normal distribution		**Uniform distribution**	
	Mean	**Standard D.**	**Lower**	**Upper**
$\boldsymbol{K_{te}}$ **(N/mm)**	9.1	3	0	25
$\boldsymbol{K_{tc}}$ **(N/mm^2)**	4475	300	0	10,000
$\boldsymbol{K_{re}}$ **(N/mm)**	13.2	3	0	25
$\boldsymbol{K_{rc}}$ **(N/mm^2)**	2854	300	0	10,000
$\boldsymbol{K_{tp}}$ **(kN/mm^3)**	13,623	1400	0	30,000
$\boldsymbol{K_{rp}}$ **(kN/mm^3)**	4300	400	0	10,000

Table 3.2: Parameters of posterior distributions for uniformand normal settings

	Normal distribution		**Uniform distribution**	
	Mean	**Standard D.**	**Mean**	**Standard D.**
$\boldsymbol{K_{te}}$ **(N/mm)**	8.4	1.2	9.6	1.6
$\boldsymbol{K_{tc}}$ **(N/mm^2)**	4477	276	4062	1098
$\boldsymbol{K_{re}}$ **(N/mm)**	13.4	1.2	12.9	1.8
$\boldsymbol{K_{rc}}$ **(N/mm^2)**	2849	286	3222	1165
$\boldsymbol{K_{tp}}$ **(kN/mm^3)**	13,571	1300	12,195	5545
$\boldsymbol{K_{rp}}$ **(kN/mm^3)**	4316	378	5175	2566

3.4 Validation of the Bayesian Inference Model

In order to test the generalization capability of the developed Bayesian milling model, additional test cases were considered. In the second set of experiments, different test conditions were conducted with a different micro end mill. Table 3.3 shows the experimental cases where various radial immersion (RI) tests were conducted. Figure 3.4 shows the model prediction for the 2 µm/tooth feed case with both posterior distributions. Both predictions are acceptable in terms of F_y forces. F_x forces are predicted on the lower limit, indicating a difference in tool edge conditions.

Figure 3.5 shows the experimental measurement of forces with different RI test cases. RI cases of 25 and 60% are considered in both upmilling and downmilling

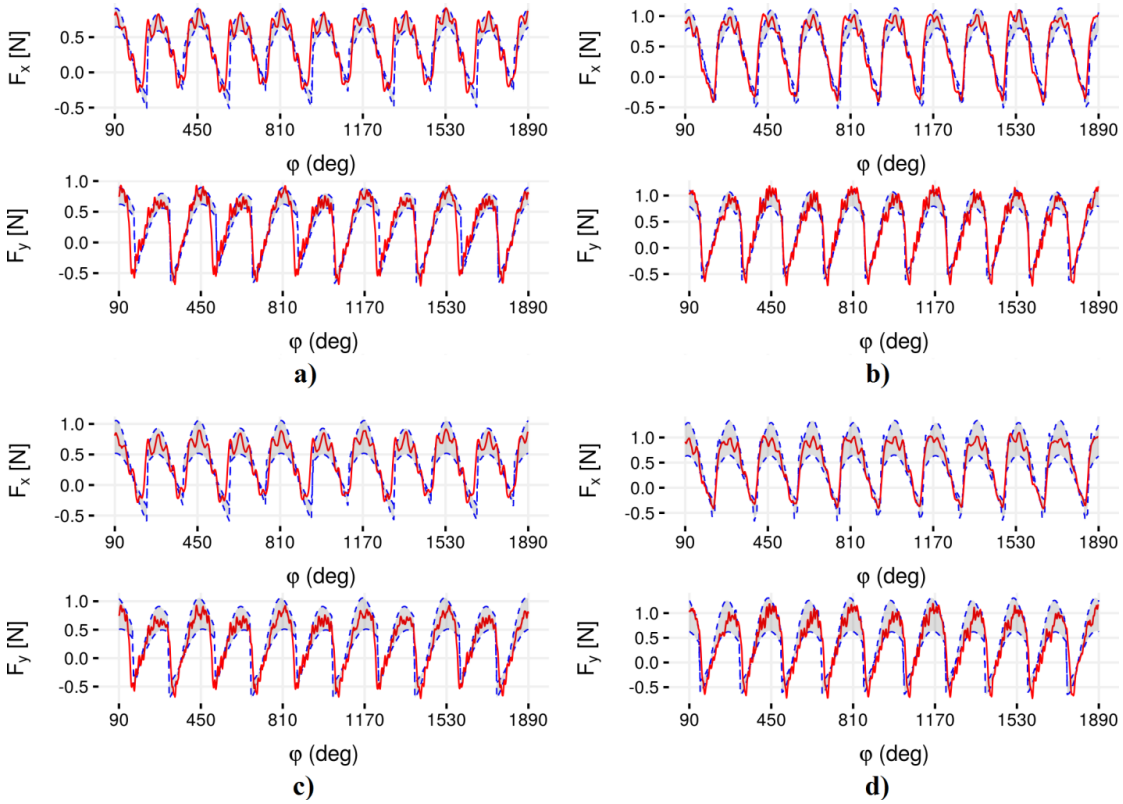

Figure 3.3: Simulated (blue dashed lines) and measured (red solid lines) force predictions for *a.* 0.4 µm/tooth-normal distribution *b.* 2 µm/tooth-normal distribution *c.* 0.4 µm/tooth-uniform distribution *d.* 2 µm/tooth-uniform distribution

Table 3.3: Summary of second set of experiments

Tool diameter (mm)	**Rotational speed (rpm)**	**Axial depth of cut (μm)**	**Feed per tooth (μm/rev)**	**Radial immersion (%)**	**Type**
0.4	28 000	40	2	100,60,25	Upmilling, downmilling

conditions. With decreasing RI percentage, F_y forces increase while F_x forces decrease in downmilling. In upmilling, forces are lower in magnitude and with decreasing RI, F_x forces increase and F_y forces decrease.

Figure 3.6 shows the model predictions. While 60% RI results are acceptable, as the predictions are within the limits, model predictions at 25% RI are poor especially for the F_y forces in both upmilling and downmilling tests.

In order to investigate the possible reasons which may cause this difference, cutting edges of the tools after the 25% immersion tests were investigated as shown in Figure 3.7. No significant BUE was observed after the micromilling tests. Altered tool-material interaction possibly resulted in a different set of force coefficients.

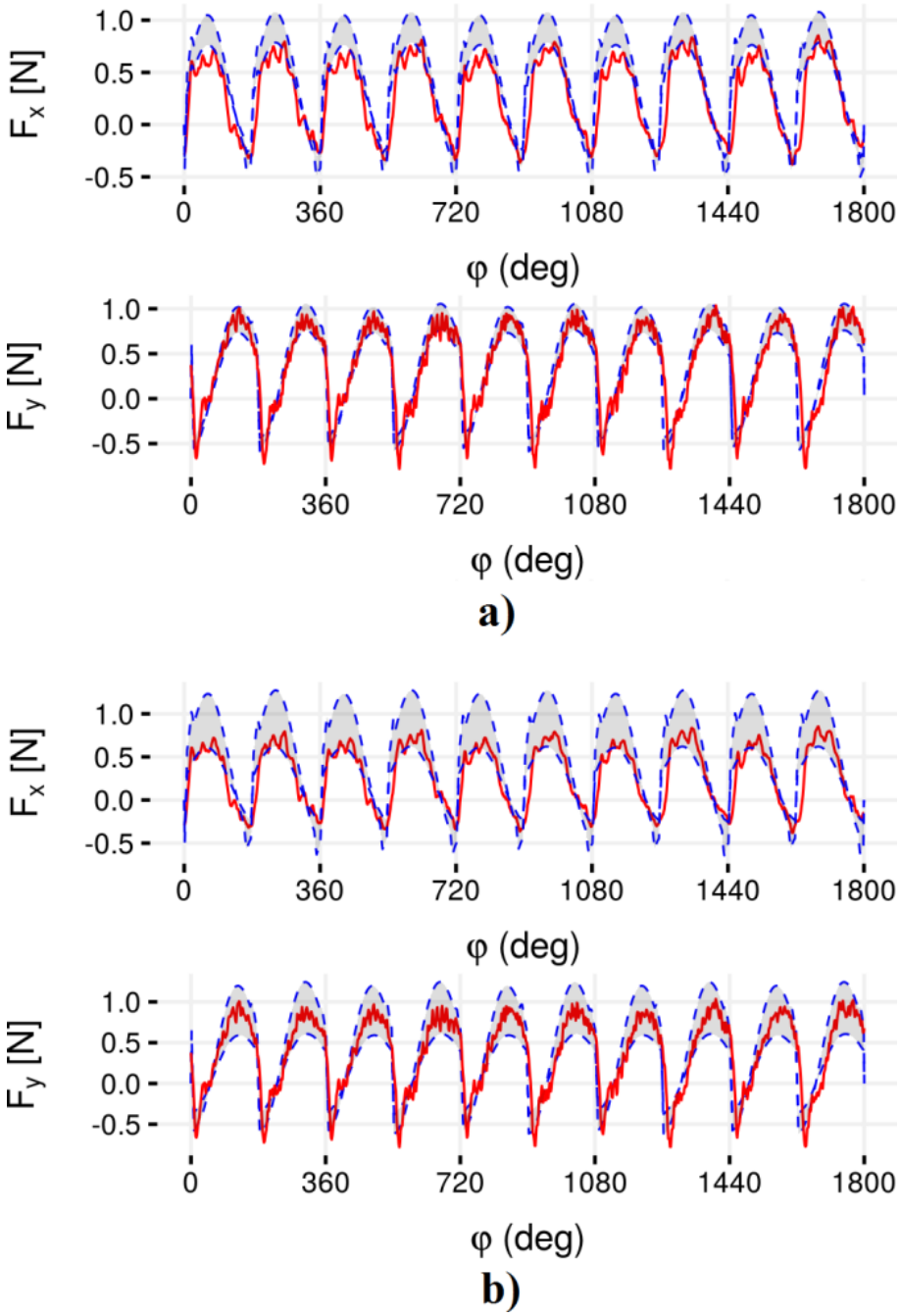

Figure 3.4: Simulated and measured force predictions for 2 µm/tooth feed slot milling with *a.* normal distribution *b.* uniform prior distribution

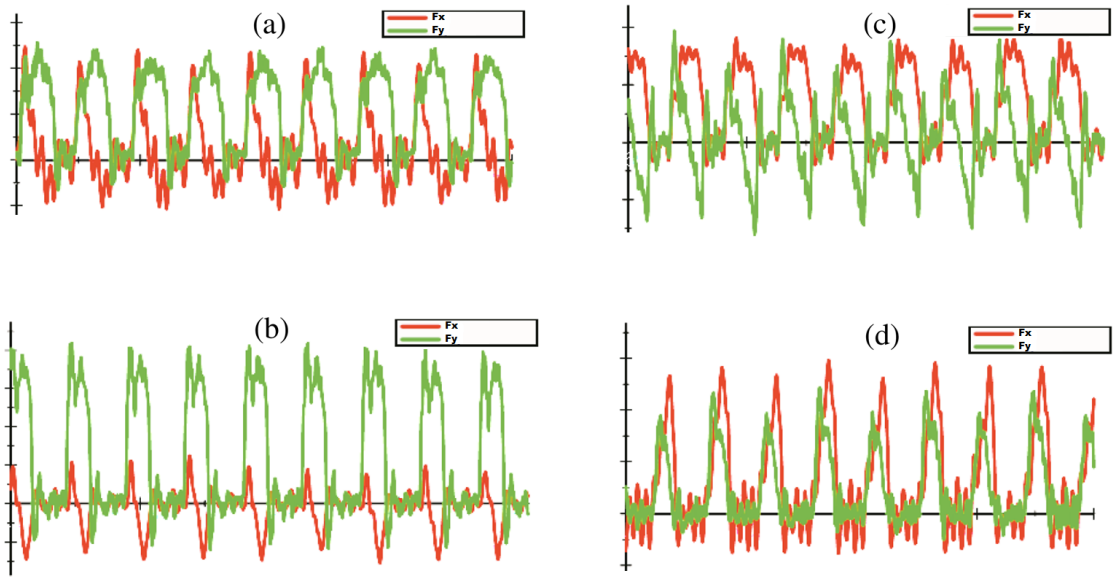

Figure 3.5: Measured micromilling forces at 2 µm/tooth and axial depth of cut 40 µm. *a.* 60% RI-downmilling. *b.* 25% RI-downmilling. *c.* 60% RI-upmilling. *d.* 25% RI-upmilling

It must be noted that cases of low-immersion milling with micro end mills are considered as special milling cases where the process dynamics are known to be significantly different than slot milling [45]. Process modeling of micromilling, including tool deflections and process dynamics, are necessary for improved predictions in cases of low-immersion machining. Uncertainty of force predictions as input to those models would be useful. In order to improve low-radial-immersion predictions, additional tests at different feed levels can be conducted and force coefficients can be recalculated based on the new experimental measurements.

With decreasing axial depth of cut, due to inhomogeneities in the work material microstructure, uncertainties are expected to increase. Similarly, during long-term machining cases, tool wear starts to influence the process forces, thereby introducing additional uncertainties. By considering existing data as prior information, the number of experimental studies in the above mentioned cases may be decreased, and their influence on the force coefficients can be easily observed within the Bayesian inference scheme.

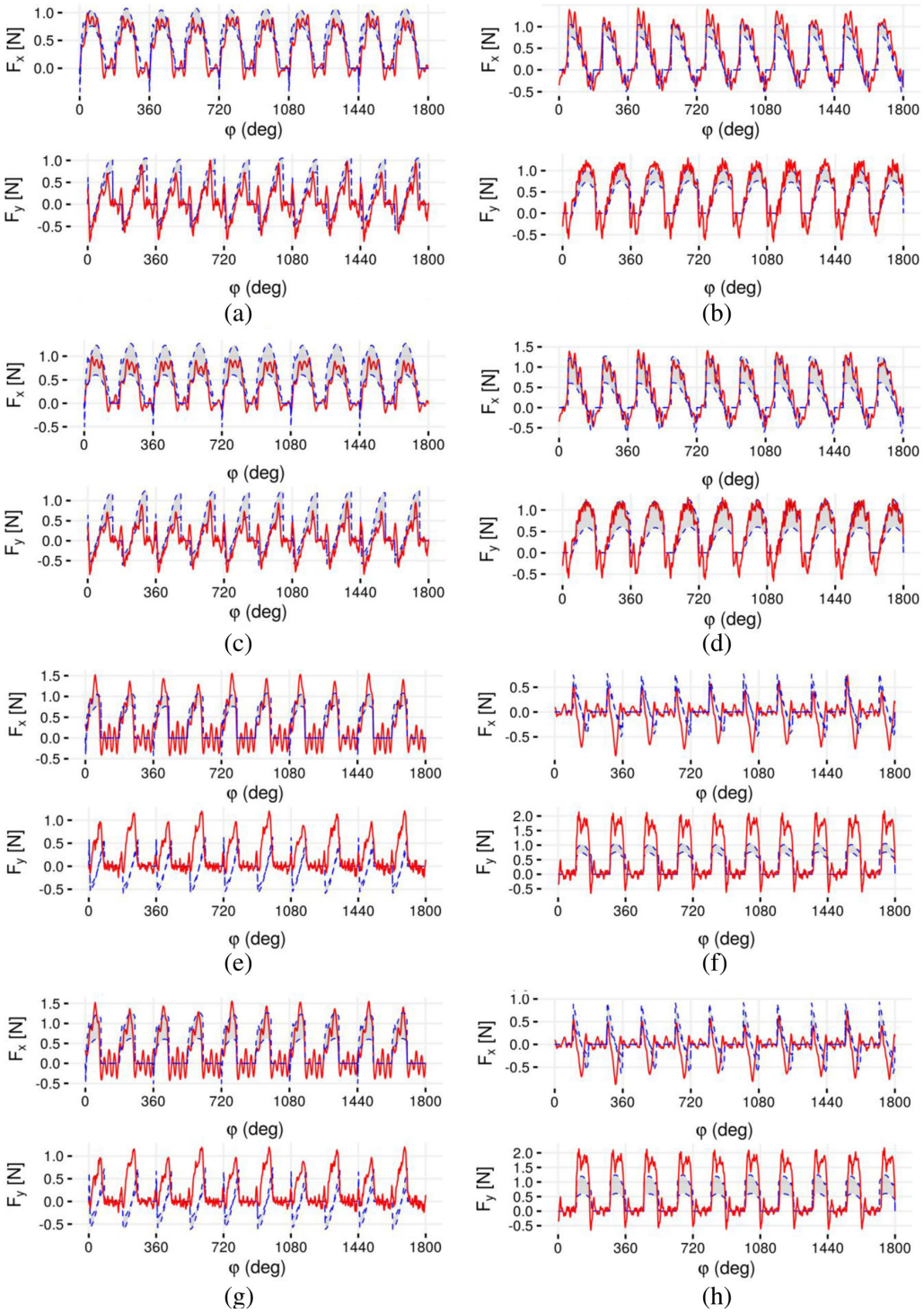

Figure 3.6: Comparison of simulated and measured micromilling forces: 60% RI (*a.* upmilling-normal, *b.* downmilling-normal, *c.* upmilling-uniform, *d.* upmilling-uniform), 25% RI (*e.* upmilling-normal, *f.* downmilling-normal, *g.* upmilling-uniform, *h.* downmilling-uniform)

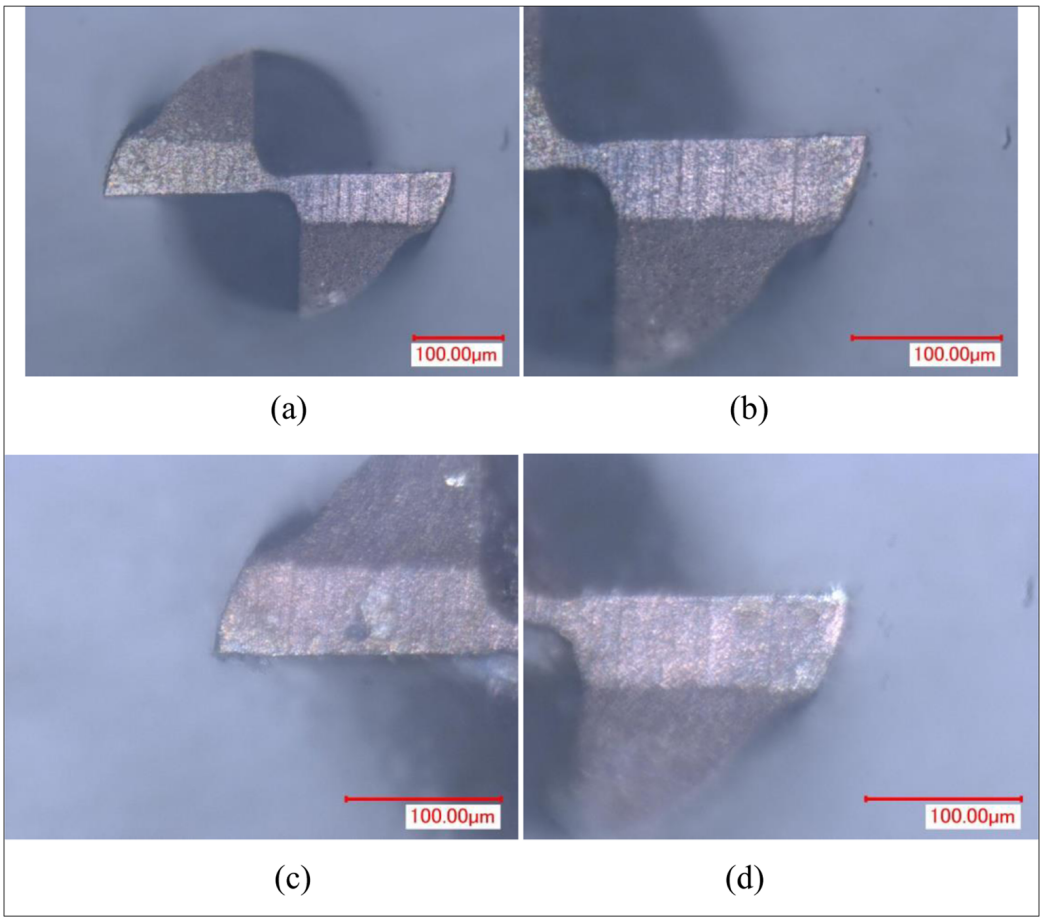

Figure 3.7: Tool edge condition. *a.* New micro end mill. *b.* Cutting edge of the new micro end mill. *c.* After radial immersion tests right edge. *d.* After radial immersion tests left edge

Chapter 4

Bayesian Inference with FEM Simulation Outputs

In the previous chapters, uncertainties associated with cutting, edge and ploughing force coefficients were characterized via Bayesian inference. Experimentally measured force data were used to update our initial beliefs regarding force coefficients; which are assumed to have uniform and normal distributions. Although Bayesian inference reduces the amount of tests needed to achieve a high level of confidence, slot milling experiments are still needed to be performed in order to update our prior knowledge. Therefore, it is important to develop physics-based machining models capable of predicting process outputs without conducting time-consuming and costly experiments [46]. 2D finite element simulations allows simulating 3D micro milling process [32] and can be useful when prior knowledge about force coefficients and experimental data are not available.

This chapter illustrates the application of finite element simulation on machining processes as an intermediate tool to update our prior knowledge on cutting force coefficients. First, 2D finite element simulation of titanium alloy Ti6AL4V is employed under hybrid friction conditions. BUE formation has taken into consideration and cutting edge was modified in the machining model. Cutting force

coefficients of mechanistic modeling are estimated and compared with the experimental data which were published in [47] and [48]. Second, these estimated force coefficients are used to update non-informative uniform distributions and the distributions of cutting force coefficients are obtained. Third, these probability distributions are updated via experimental measurements and further improvement is done. Finally, convergence of the cutting force coefficients during MCMC simulations is investigated in detail. Training data under different conditions with various sizes are used to update our initial distributions and the performance of the fits and their convergence are examined.

4.1 Finite Element Simulation With Hybrid-Friction Conditions

A material model developed by Karpat [49] is employed to simulate micromachining of titanium alloy Ti6AL4V. This material model was validated in a previous study for its ability to predict macroscale machining forces under various machining conditions. Simulations were run on commercial software DEFORM.

In Section 2.4, the lowest surface roughness value of 0.06 µm was identified at 1.5-2 µm/tooth corresponding to the experimental setup given in Table 2.1. Thus, 1, 1.5 and 3 µm uncut chip thickness and 35 m/min cutting speed are selected for the simulation runs. The cutting edge geometry is modified according to the previous study of Oliaei and Karpat [50]. BUE edge radius is selected to be 2.5 µm and clearance angle is assumed to be 1°. Figure 4.1a illustrates the modified geometry of the cutting edge and 4.1b shows the hybrid-friction model [50]. Shear friction was selected between 0.7 and 0.95 and Coulomb friction was selected between 0.1 and 0.3. Table 4.1 shows the friction combinations used in the simulation runs and Table 4.2 presents the cutting force coefficients determined under these friction conditions. Figure 4.2 illustrates chip formation at 3 µm uncut chip thickness under the friction conditions μ= 0.1 and m = 0.95.

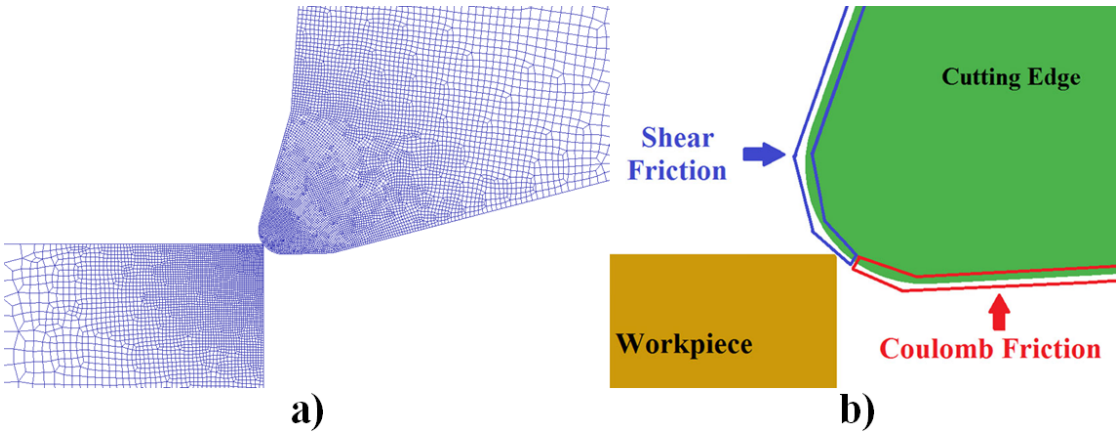

Figure 4.1: *a)* Modified cutting edge geometry used in finite element simulation. BUE edge radius is selected to be 2.5 µm. *b)* Hybrid friction model used in the finite element simulations.

The cutting force coefficients obtained from finite element simulations are compared with the experimental data which were published in [47] and [48]. The experimental conditions of these micromilling experiments are given in Table 4.3 and the corresponding cutting force coefficients are given in Table 4.4. It is seen that K_{rc} and K_{te} values obtained with the tool having 0.6 mm diameter under 120 µm depth of cut condition are compatible with the finite element simulations. As the tool diameter and depth of cut reduces, the discrepancy between the simulations and the measurements increases. It should be noted that K_{tc} and K_{re} values are underestimated for all conditions.

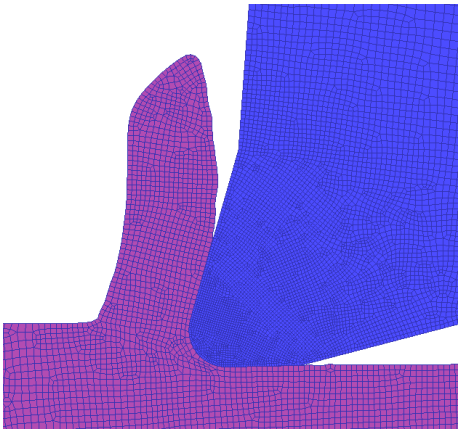

Figure 4.2: Chip formation for the finite element simulation for hybrid friction model under the conditions μ= 0.1 and m = 0.95.

Table 4.1: Friction conditions in the hybrid-friction model

Model	**Friction definitions**	
1	μ= 0.1	m = 0.70
2	μ= 0.1	m = 0.80
3	μ= 0.1	m = 0.95
4	μ= 0.2	m = 0.70
5	μ= 0.2	m = 0.80
6	μ= 0.2	m = 0.95
7	μ= 0.3	m = 0.70
8	μ= 0.3	m = 0.80
9	μ= 0.3	m = 0.95

Table 4.2: Cutting force coefficients obtained from finite element simulations corresponding to the friction conditions in Table 4.1, at a cutting speed of 35 m/min and uncut chip thickness values of 1, 1.5 and 3 µm.

	K_{te} (N/mm)	K_{tc} (N/mm^2)	K_{re} (N/mm)	K_{rc} (N/mm^2)
1	6.8	775	5.1	1417
2	6.3	980	5.5	1336
3	8.0	485	5.3	1490
4	8.1	97	5.2	1488
5	8.5	-105	5.5	1467
6	7.4	477	5.4	1501
7	6.0	465	5.6	1423
8	6.7	306	6.3	1237
9	8.0	101	5.8	1514
Avg.	7.3	398	5.5	1430

4.2 Bayesian Inference Combined With FEM Outputs

In this section, FEM simulation outputs are used to update non-informative uniform priors in Table 3.1. As the friction condition is unknown, the average of the cutting force coefficients obtained by 2D finite element simulations is taken into consideration. Micromilling force averages are predicted under the experimental conditions given in Table 4.3 and used in accordance with Bayesian inference.

Table 4.3: Experimental conditions of the experiments which is given in previous studies.

	Tool diameter (mm)	**Cutting speed (m/min)**	**Axial depth of cut (μm)**	**Feed per tooth (μm/rev)**
1	0.6	32	120	2, 4, 6, 8
2	0.4	32	80	1.5, 2, 3, 4, 6
3	0.4	35	40	0.4, 0.6, 0.8, 1, 1.2, 1.5, 2, 3, 4

Table 4.4: Cutting and edge force coefficients for Ti6Al4V in previous studies

	K_{te} (N/mm)	K_{tc} (N/mm^2)	K_{re} (N/mm)	K_{rc} (N/mm^2)
1	9.1	2820	14.9	1523
2	7.1	2729	8.5	1990
3	9.1	4475	13.2	2854

Likelihood function is assumed so that experimental mean force values are distributed normally with a standard deviation of 0.3 N. Since natures of the cutting processes differ, a discrepancy between experimental micromilling forces and the outputs of 2D orthogonal machining simulations is expected. The errors caused by transition from 2D orthogonal machining simulations to micromilling can be compensated by manipulating likelihood function in Bayesian inference.

Metropolis-Hastings algorithm was applied for 10^4 iterations to obtain samples from the joint target densities of force coefficients and first 1000 samples were discarded. The obtained posterior distributions of the force coefficients are given in Appendix B and the simulated forces are given in the first figures of appendices E, F and G.

Figures E.1, F.1 and G.1 suggest that, although the limits of the predicted forces are quite wide, measured forces are within the limits for all experimental conditions and expectations of the force predictions are close to the experimental measurements. The outputs of the computer experiments can be used for updating non-informative uniform distributions and the intervals of the cutting forces can be estimated. This approach provides a cheaper way of estimating probability distributions and modeling randomness in micromilling forces, according to the information retrieved from computer simulations. On the other hand, the

ranges of obtained force coefficients are considerably wide compared to the results obtained from Bayesian updatings with experimental data. The obtained probability distributions can be considered as initial knowledge and further refinement can be done in light of a new observation, e.g. experimental data or data obtained from literature.

4.3 Analysis of the Learning Process

It was seen that the information obtained from computer simulations can be useful for obtaining rough estimates of force coefficients without performing time-consuming and costly experiments. In order to improve the information coming from Bayesian updatings with FEM outputs, cutting force measurements can be used to improve these initial models. Since performing machining experiments is an expensive way of obtaining information, the number of data points in the training set and the experimental conditions during the collection of data are two main considerations in model development phase. In this section, training data under different conditions with various sizes are used to update our initial distributions and the effect of them on the convergence and the quality of the fits are presented.

The distributions obtained by the outputs of FEM simulations are considered as prior knowledge and experimental force measurements are used to update these probability distributions. In order to analyze the effect of machining conditions on convergence, the sequence the of experimental measurements in the training set is determined in three settings; starting from lowest feed per tooth to the highest, highest feed per tooth to the lowest and shuffled order. First n data points are used for Bayesian updating where n can have a range from one to the size of the total number of data points available. For instance, the first experimental setup in Table 4.3 has four sets of experimental measurements available for updating, corresponding to the feed per tooth values.

Similarly, Metropolis-Hastings algorithm was applied for 10^4 iterations for all settings. First 1000 samples were discarded. Since the level of confidence in the experimental data are usually stronger compared to simulation outputs, a narrower standard deviation can be selected for the likelihood function, e.g. 0.1N. Tool run-out magnitude and angle can also be identified from the measurements by using genetic algorithm. For simplification, tool run-out magnitude and angle values are assumed to be the same for all feed values.

First, in order to analyze the effect of the order of data points corresponding to various machining conditions and the size of the training data on convergence, ranges of the estimated cutting force coefficients are examined. The figures in Appendix D shows the ranges of force coefficients obtained for various training data sets. In usual case, a rapid decrease in the first updates is expected and it stabilizes as the model converges. It is seen that, the ranges of edge force coefficients reduced faster in the first updates, compared to cutting coefficients. Estimated coefficients indicated the importance of edge force coefficients on the micromilling force predictions. Edge forces are directly related to the conditions of the tool edge. The condition of the cutting edge affects the cutting force calculations. In the following updates, the ranges of edge coefficients are stabilized and the larger improvements in the ranges of cutting coefficients are done, for all training data sets. It should also be highlighted that the amount of decrease on the ranges of force coefficients are done regardless of the order of data points.

Second, to analyze the quality of fits, the estimated intervals of peak values are compared with the actual measurements. With the estimated cutting force coefficients, the intervals of peak values are estimated. Figures in Appendix C shows the 95 % confidence intervals of peak values and the average peak force value measurements for all settings of training set. The ranges of the intervals decrease since a new data point is introduced, expectedly. However, as the number points in the training set exceeds a value, a well-known problem "over-fitting" is much harder to avoid, which the model overreacts to the minor fluctuations in the training data, and leads poor generalization and predictive performance on unseen data. The last updates in the third experimental setup indicate over-fitting since the improvements in the ranges of force coefficients in Figures D.3

are minor and and figures C.1, C.2 and C.3 suggest, the ranges of peak forces are too narrow to represent cutting force data for all machining combinations.

The results show, after the first 3-4 updates, the intervals become narrower and some of the peak forces ruins the confidence intervals; which indicates over-fitting. The peak forces are affected by various machininig conditions such as tool run-out, tool wear, BUE formation and ploughing effect. In order to generalize the cutting force coefficients for a given tool-workpiece pair and improve the predictive performance on unseen data, this research suggests at most 3-4 pairs of cutting force measurements to avoid over-fitting.

In this Chapter, physics based machining models are employed and their outputs are substituted with the experimental micromilling forces. First, 2D finite element simulations were performed and machining forces were predicted; which are then used to calculate cutting force coefficients of mechanistic modeling. These coefficients are compared with the previous studies of Gözü et al. [48] and Kanli [47]. It was seen that, as the tool diameter and depth of cut reduces, the discrepancy between the simulations and the measurements increases. By using these force coefficients, milling force averages are predicted under different conditions and fused into Bayesian updating procedure. Although the limits of the predicted forces are quite wide, this approach provides a cheaper way of estimating probability distributions and modeling randomness in micromilling forces. In order to improve the information coming from Bayesian updatings with FEM outputs, cutting force measurements are used. The effect of the number of data points and the experimental conditions during the collection of data on model development are analyzed and reported.

Chapter 5

Conclusion

A micromilling force model based on Bayesian inference has been developed in this study. Experimental observations of micromilling of titanium alloy were used to analyze the condition of the cutting edge and its influence on the surface texture of the micromilled surface.

Controlling the dimensional tolerances and surface quality of microcomponents is one of the major challenges in machining. The processes micro-hot embossing and micro-injection molding for the mass production of polymer micro-parts require micro-molds having precisely milled surface texture. In the first chapter, micromilling experiments were performed to investigate the influence of micromilling process parameters on machining forces, tool edge condition, and surface texture.

Under the experimental conditions used in this study, built-up edge (BUE) formation has been observed for all slot milling cases. In some cases, BUE is known to protect the cutting edge from rapid wear, but it has a detrimental effect on the surface finish, which is quite important in micromachining [18]. The size and stability of BUE depend on the machining conditions; thus BUE formation was investigated in detail and considered as an important source of uncertainty.

The findings of the first chapter can be summarized as follows:

- BUE formation significantly affects the surface texture at feed values lower than 1 µm/tooth by leaving smeared particles on the machined surface. Surface skewness (Ssk) and kurtosis (Sku) along with areal surface roughness (Sa) reveal important characteristics of surface texture in micromilling. The lowest surface roughness value of 0.06 µm was identified at 1.5-2 µm/tooth corresponding to the experimental setup given in Table 2.1.
- Peak-to-valley force variation together with surface texture analysis produced reliable results for identifying shearing-dominated, transition, and ploughing dominated machining regions for the machining of Ti6Al4V. Based on these results, feed above 1 µm/tooth can be identified as the shearing dominated zone, feed between 0.6 and 1 µm/tooth can be identified as the transition zone, and feed less than 0.6 µm/tooth can be identified as the ploughing-dominated zone.

In the second chapter, Bayesian inference is applied to model micromilling force prediction. Modeling micromilling forces is not a straightforward task due to work material size effects, tool run-out, tool wear, built-up edge, and difficulties in identifying structural dynamic parameters. It is difficult to deal with the stochastic behavior of the micromilling process and uncertainties introduced by these factors using deterministic predictive process models. Bayesian inference to milling force modeling provides a rational way to model randomness in micromilling forces.

Uncertainties about the micromilling process forces were estimated with this method. Force predictions are validated with the experimental measurements and the effectiveness of established models under special machining cases is discussed. Low-immersion milling experiments with micro end mills were performed. It is seen that, while 60% RI results are acceptable, as the predictions are within the limits, model predictions at 25% RI are poor. It should be noted that, BUE was not observed for the low-radial-immersion micromilling cases, indicating

a significant change in the process mechanics. With decreasing axial depth of cut, due to inhomogeneities in the work material microstructure, uncertainties are expected to increase. In order to improve low-radial-immersion predictions, additional tests at different feed levels can be conducted and force coefficients can be recalculated based on the new experimental measurements.

It is shown that the Markov chain Monte Carlo (MCMC) method with the Metropolis-Hastings (MH) updating algorithm can be successfully applied to calculate force coefficients of mechanistic machining models. The amount of experimental effort in micromilling studies can be reduced with this approach. Bayesian inference scheme allows for predicting the upper and lower limits of micromilling forces, providing useful information about stability boundary calculations and robust process optimization. Estimated coefficients indicated the importance of edge force coefficients on the micromilling force predictions. Edge forces are directly related to the conditions of the tool edge. The condition of the cutting edge affects the cutting force calculations.

In the third part of this research, finite element simulation of titanium alloy Ti6AL4V is employed to predict micromilling forces. Physics-based machining models allow simulating 3D micro milling process and useful since experimental knowledge is not available. BUE formation has taken into consideration and cutting edge was modified in the machining model according to the previous study of Oliaei and Karpat [50]. It was seen that, as the tool diameter and depth of cut reduces, the discrepancy between the simulations and the measurements increases. Finite element simulation of machining processes were used as an intermediate tool to update our prior knowledge on specific cutting force coefficients.

Finite element simulations provide a cheaper way of obtaining information and modeling randomness in micromilling forces. However, experimental data are usually much more reliable and the models trained by these data offer stronger predictive power. Bayesian inference method can be used to combine data coming from simulation results and the experiments. In order to improve models learned by simulation outputs, experimental data were fused into learning process and probability distributions were updated.

Since performing machining experiments are costly and time-consuming, the number of data points in the training set and the experimental conditions during the collection of data are two main considerations in model development phase. In this research, training data under different conditions with various sizes are used and the effect of them on the convergence and the quality of the fits are reported.

Bibliography

[1] D. Dornfeld, S. Min, and Y. Takeuchi, "Recent advances in mechanical micromachining," *CIRP Annals-Manufacturing Technology*, vol. 55, no. 2, pp. 745–768, 2006.

[2] J. Chae, S. Park, and T. Freiheit, "Investigation of micro-cutting operations," *International Journal of Machine Tools and Manufacture*, vol. 46, no. 3, pp. 313–332, 2006.

[3] P. Abgrall and A. Gue, "Lab-on-chip technologies: making a microfluidic network and coupling it into a complete microsystema review," *Journal of Micromechanics and Microengineering*, vol. 17, no. 5, p. R15, 2007.

[4] Y.-C. Kim, J.-H. Park, and M. R. Prausnitz, "Microneedles for drug and vaccine delivery," *Advanced drug delivery reviews*, vol. 64, no. 14, pp. 1547–1568, 2012.

[5] E. Vázquez, A. Amaro, J. Ciurana, and C. A. Rodríguez, "Process planning considerations for micromilling of mould cavities used in ultrasonic moulding technology," *Precision Engineering*, vol. 39, pp. 252–260, 2015.

[6] M. Malekian, S. S. Park, and M. B. Jun, "Modeling of dynamic micro-milling cutting forces," *International Journal of Machine Tools and Manufacture*, vol. 49, no. 7, pp. 586–598, 2009.

[7] X. Zhang, K. F. Ehmann, T. Yu, and W. Wang, "Cutting forces in micro-end-milling processes," *International Journal of Machine Tools and Manufacture*, vol. 107, pp. 21–40, 2016.

[8] Y. Srinivasa and M. Shunmugam, "Mechanistic model for prediction of cutting forces in micro end-milling and experimental comparison," *International Journal of Machine Tools and Manufacture*, vol. 67, pp. 18–27, 2013.

[9] X. Jin and Y. Altintas, "Prediction of micro-milling forces with finite element method," *Journal of Materials Processing Technology*, vol. 212, no. 3, pp. 542–552, 2012.

[10] J. M. Karandikar, T. L. Schmitz, and A. E. Abbas, "Application of bayesian inference to milling force modeling," *Journal of Manufacturing Science and Engineering*, vol. 136, no. 2, p. 021017, 2014.

[11] J. M. Karandikar, A. E. Abbas, and T. L. Schmitz, "Tool life prediction using bayesian updating. part 1: Milling tool life model using a discrete grid method," *Precision Engineering*, vol. 38, no. 1, pp. 9–17, 2014.

[12] J. M. Karandikar, A. E. Abbas, and T. L. Schmitz, "Tool life prediction using bayesian updating. part 2: Turning tool life using a markov chain monte carlo approach," *Precision Engineering*, vol. 38, no. 1, pp. 18–27, 2014.

[13] F. A. Niaki, D. Ulutan, and L. Mears, "Parameter inference under uncertainty in end-milling γ-strengthened difficult-to-machine alloy," *Journal of Manufacturing Science and Engineering*, vol. 138, no. 6, p. 061014, 2016.

[14] P. Mehta, M. Kuttolamadom, and L. Mears, "Mechanistic force model for machining processtheory and application of bayesian inference," *The International Journal of Advanced Manufacturing Technology*, pp. 1–10, 2017.

[15] Z. Cao and H. Li, "Investigation of machining stability in micro milling considering the parameter uncertainty," *Advances in Mechanical Engineering*, vol. 7, no. 3, p. 1687814015575982, 2015.

[16] S. H. I. Jaffery, M. Khan, L. Ali, and P. T. Mativenga, "Statistical analysis of process parameters in micromachining of ti-6al-4v alloy," *Proceedings of the Institution of Mechanical Engineers, Part B: Journal of Engineering Manufacture*, vol. 230, no. 6, pp. 1017–1034, 2016.

[17] S. Jaffery, N. Driver, and P. Mativenga, "Analysis of process parameters in the micromachining of ti-6al-4v alloy," in *Proceedings of the 36th International MATADOR Conference*, pp. 239–242, Springer, 2010.

[18] J. Chae and S. Park, "High frequency bandwidth measurements of micro cutting forces," *International Journal of Machine Tools and Manufacture*, vol. 47, no. 9, pp. 1433–1441, 2007.

[19] T. L. Schmitz, J. Couey, E. Marsh, N. Mauntler, and D. Hughes, "Runout effects in milling: Surface finish, surface location error, and stability," *International Journal of Machine Tools and Manufacture*, vol. 47, no. 5, pp. 841–851, 2007.

[20] S. Afazov, S. Ratchev, J. Segal, and A. Popov, "Chatter modelling in micro-milling by considering process nonlinearities," *International Journal of Machine Tools and Manufacture*, vol. 56, pp. 28–38, 2012.

[21] E. Budak, Y. Altintas, and E. Armarego, "Prediction of milling force coefficients from orthogonal cutting data," *Journal of Manufacturing Science and Engineering*, vol. 118, no. 2, pp. 216–224, 1996.

[22] Y. Altintas, *Manufacturing automation: metal cutting mechanics, machine tool vibrations, and CNC design*. Cambridge university press, 2012.

[23] J. P. Davim, *Machining of complex sculptured surfaces*. Springer, 2012.

[24] H.-J. Fu, R. DeVor, and S. Kapoor, "A mechanistic model for the prediction of the force system in face milling operations," *Journal of engineering for industry*, vol. 106, no. 1, pp. 81–88, 1984.

[25] W. Endres, R. DeVor, and S. Kapoor, "A dual-mechanism approach to the prediction of machining forces, part 1: model development," *Journal of engineering for industry*, vol. 117, no. 4, pp. 526–533, 1995.

[26] S. Engin and Y. Altintas, "Mechanics and dynamics of general milling cutters.: Part i: helical end mills," *International Journal of Machine Tools and Manufacture*, vol. 41, no. 15, pp. 2195–2212, 2001.

[27] J. Gradišek, M. Kalveram, and K. Weinert, "Mechanistic identification of specific force coefficients for a general end mill," *International Journal of Machine Tools and Manufacture*, vol. 44, no. 4, pp. 401–414, 2004.

[28] M. Yang and H. Park, "The prediction of cutting force in ball-end milling," *International Journal of Machine Tools and Manufacture*, vol. 31, no. 1, pp. 45–54, 1991.

[29] P. Lee and Y. Altintaş, "Prediction of ball-end milling forces from orthogonal cutting data," *International Journal of Machine Tools and Manufacture*, vol. 36, no. 9, pp. 1059–1072, 1996.

[30] M. Bäker, "Finite element simulation of high-speed cutting forces," *Journal of Materials Processing Technology*, vol. 176, no. 1, pp. 117–126, 2006.

[31] S. Afazov, S. Ratchev, and J. Segal, "Modelling and simulation of micro-milling cutting forces," *Journal of Materials Processing Technology*, vol. 210, no. 15, pp. 2154–2162, 2010.

[32] I. Lazoglu and A. Mamedov, "Deformation of thin parts in micromilling," *CIRP Annals-Manufacturing Technology*, vol. 65, no. 1, pp. 117–120, 2016.

[33] Z. Fu, W. Yang, X. Wang, and J. Leopold, "Analytical modelling of milling forces for helical end milling based on a predictive machining theory," *Procedia CIRP*, vol. 31, pp. 258–263, 2015.

[34] M. E. Merchant, "Basic mechanics of the metal cutting process," *Journal of Applied Mechanics*, vol. 11, no. A, pp. 168–175, 1944.

[35] O. Gonzalo, J. Beristain, H. Jauregi, and C. Sanz, "A method for the identification of the specific force coefficients for mechanistic milling simulation," *International Journal of Machine Tools and Manufacture*, vol. 50, no. 9, pp. 765–774, 2010.

[36] G. Campatelli and A. Scippa, "Prediction of milling cutting force coefficients for aluminum 6082-t4," *Procedia CIRP*, vol. 1, pp. 563–568, 2012.

[37] M. A. Rubeo and T. L. Schmitz, "Mechanistic force model coefficients: A comparison of linear regression and nonlinear optimization," *Precision Engineering*, vol. 45, pp. 311–321, 2016.

[38] S. N. B. Oliaei and Y. Karpat, "Investigating the influence of built-up edge on forces and surface roughness in micro scale orthogonal machining of titanium alloy ti6al4v," *Journal of Materials Processing Technology*, vol. 235, pp. 28–40, 2016.

[39] R. Leach, *Characterisation of areal surface texture*. Springer, 2013.

[40] Z. Wang, V. Kovvuri, A. Araujo, M. Bacci, W. Hung, and S. Bukkapatnam, "Built-up-edge effects on surface deterioration in micromilling processes," *Journal of Manufacturing Processes*, vol. 24, pp. 321–327, 2016.

[41] D. B. Hitchcock, "A history of the metropolis–hastings algorithm," *The American Statistician*, 2012.

[42] C. Andrieu, N. De Freitas, A. Doucet, and M. I. Jordan, "An introduction to mcmc for machine learning," *Machine learning*, vol. 50, no. 1-2, pp. 5–43, 2003.

[43] P. D. Hoff, *A first course in Bayesian statistical methods*. Springer Science & Business Media, 2009.

[44] G. S. Duncan, M. Kurdi, T. Schmitz, and J. Snyder, "Uncertainty propagation for selected analytical milling stability limit analyses," *Trans. NAMRI/SME*, vol. 34, pp. 17–24, 2006.

[45] M. Davies, B. Dutterer, J. Pratt, A. Schaut, and J. Bryan, "On the dynamics of high-speed milling with long, slender endmills," *CIRP Annals-Manufacturing Technology*, vol. 47, no. 1, pp. 55–60, 1998.

[46] O. Gonzalo, H. Jauregi, L. Uriarte, and L. L. de Lacalle, "Prediction of specific force coefficients from a fem cutting model," *The International Journal of Advanced Manufacturing Technology*, vol. 43, no. 3-4, p. 348, 2009.

[47] M. Kanlı, *Modeling of cutting forces in micro milling including run-out*. PhD thesis, Bilkent University, 2014.

[48] E. Gözü and Y. Karpat, "Uncertainty analysis of force coefficients during micromilling of titanium alloy," *The International Journal of Advanced Manufacturing Technology*, pp. 1–17, 2017.

[49] Y. Karpat, "Temperature dependent flow softening of titanium alloy ti6al4v: An investigation using finite element simulation of machining," *Journal of Materials Processing Technology*, vol. 211, no. 4, pp. 737–749, 2011.

[50] S. N. B. Oliaei and Y. Karpat, "Investigating the influence of friction conditions on finite element simulation of microscale machining with the presence of built-up edge," *The International Journal of Advanced Manufacturing Technology*, vol. 90, no. 1-4, pp. 819–829, 2017.

Appendix A

Illustration of Metropolis-Hastings Algorithm

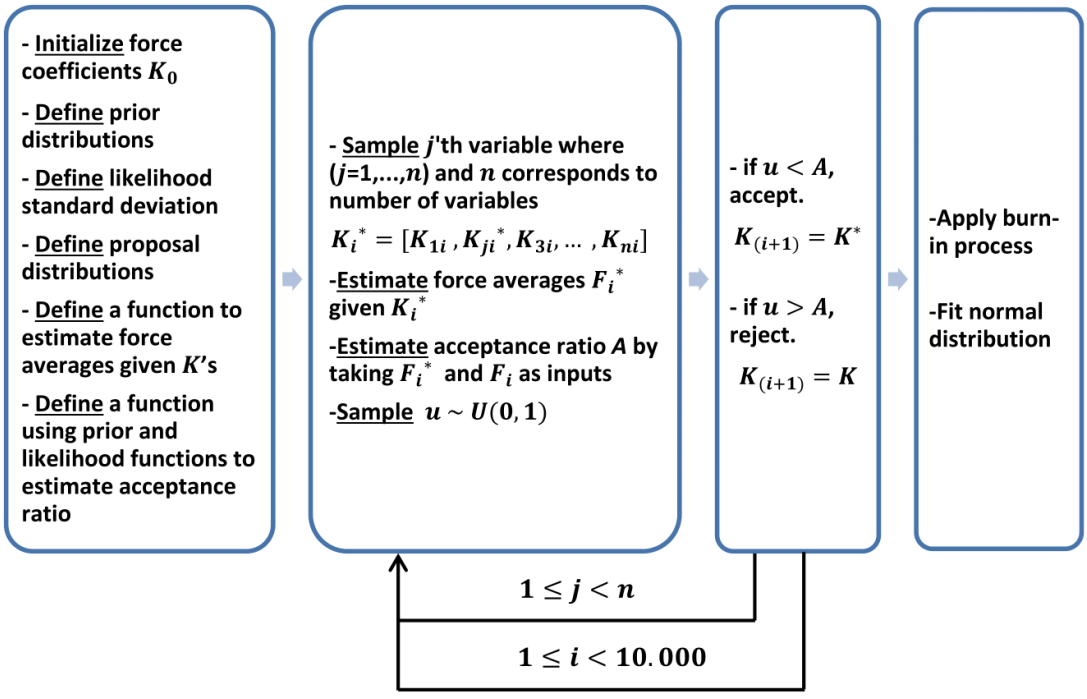

Figure A.1: Flowchart illustrating the application of MH algorithm to estimate force coefficients

Appendix B

Densities After Bayesian Updating with FEM Outputs

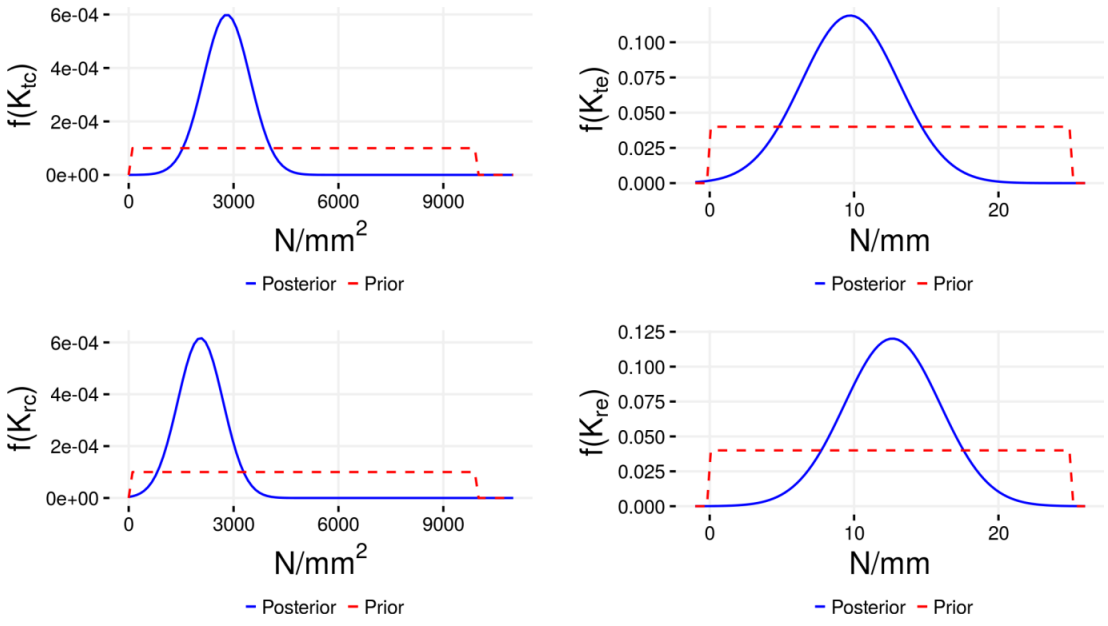

Figure B.1: Posterior *(blue lines)* and prior *(red dashed lines)* distributions of the force coefficients for the tool having 0.6 mm diameter and 120 µm depth of cut.

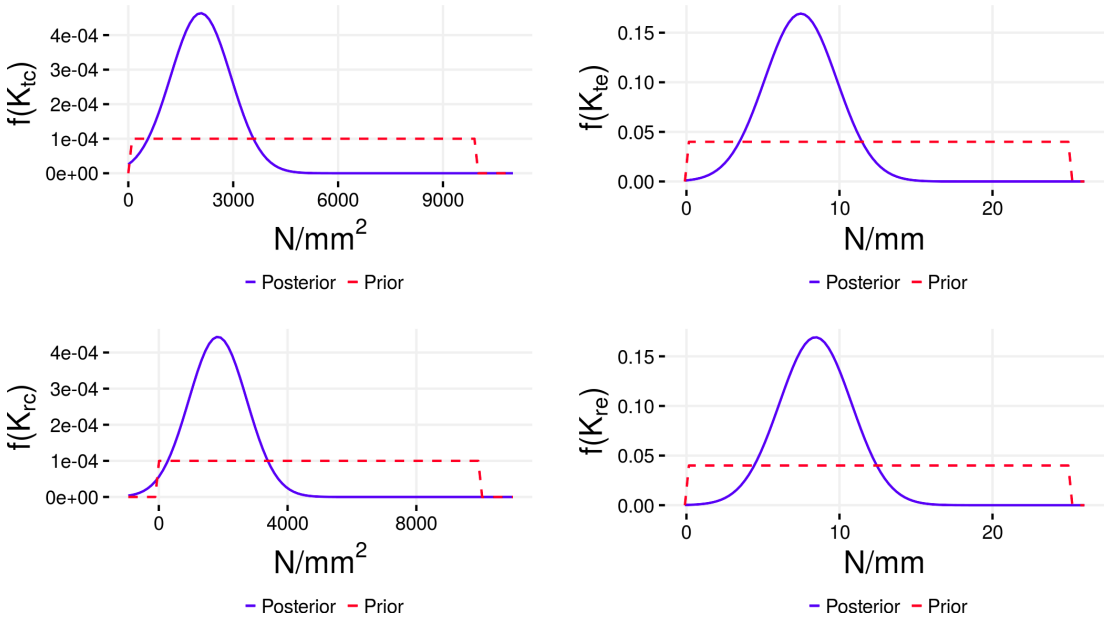

Figure B.2: Posterior *(blue lines)* and prior *(red dashed lines)* distributions of the force coefficients for the tool having 0.4 mm diameter and 80 µm depth of cut.

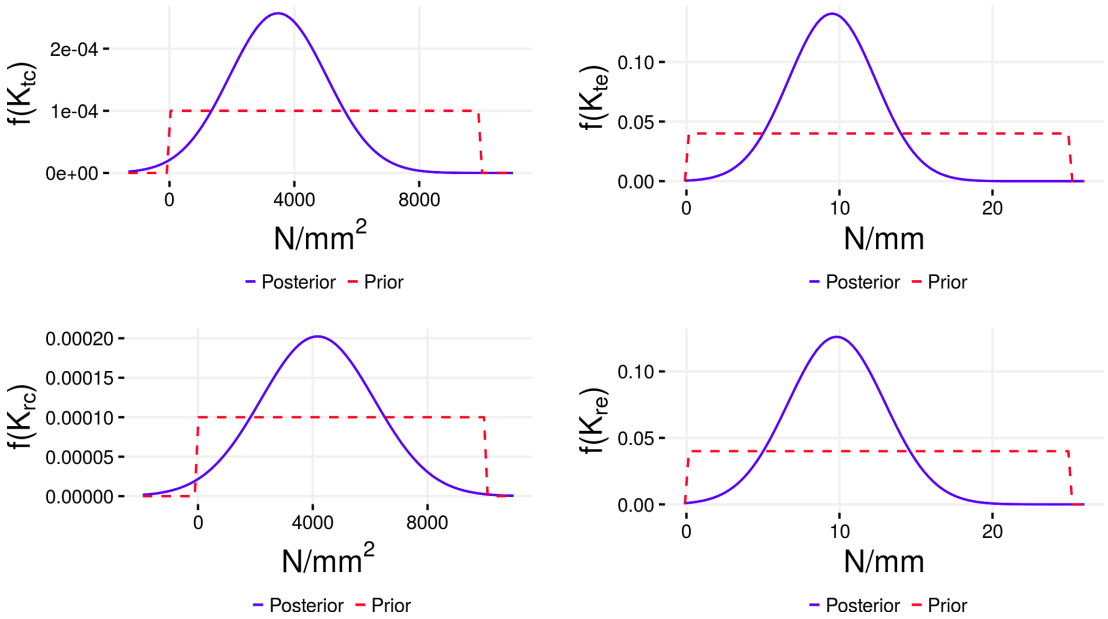

Figure B.3: Posterior *(blue lines)* and prior *(red dashed lines)* distributions of the force coefficients for the tool having 0.4 mm diameter and 40 µm depth of cut.

Appendix C

Predicted Peak Force Intervals

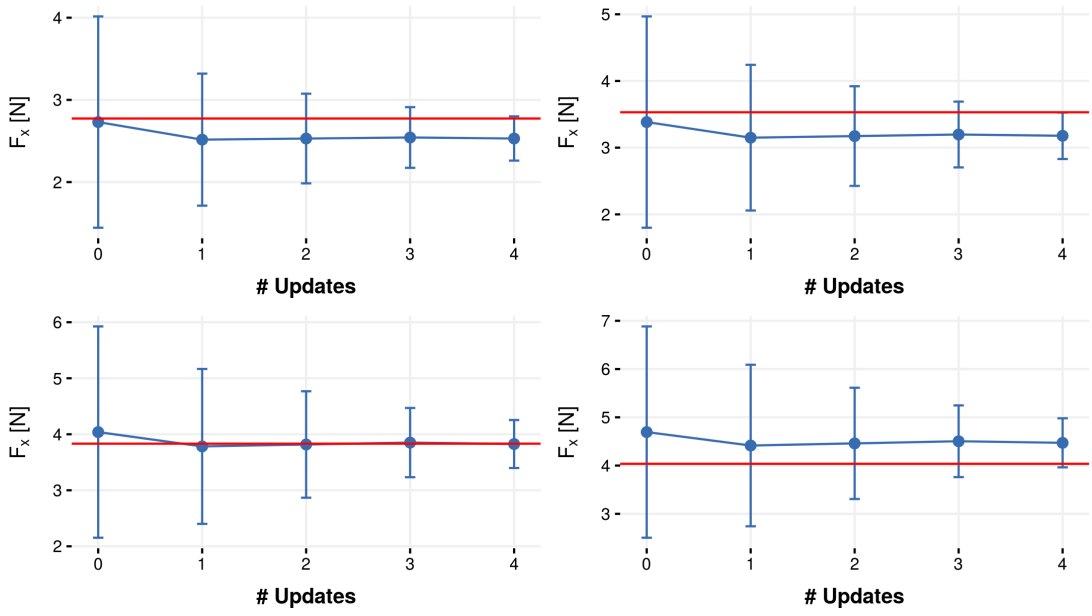

(a) $x - direction$

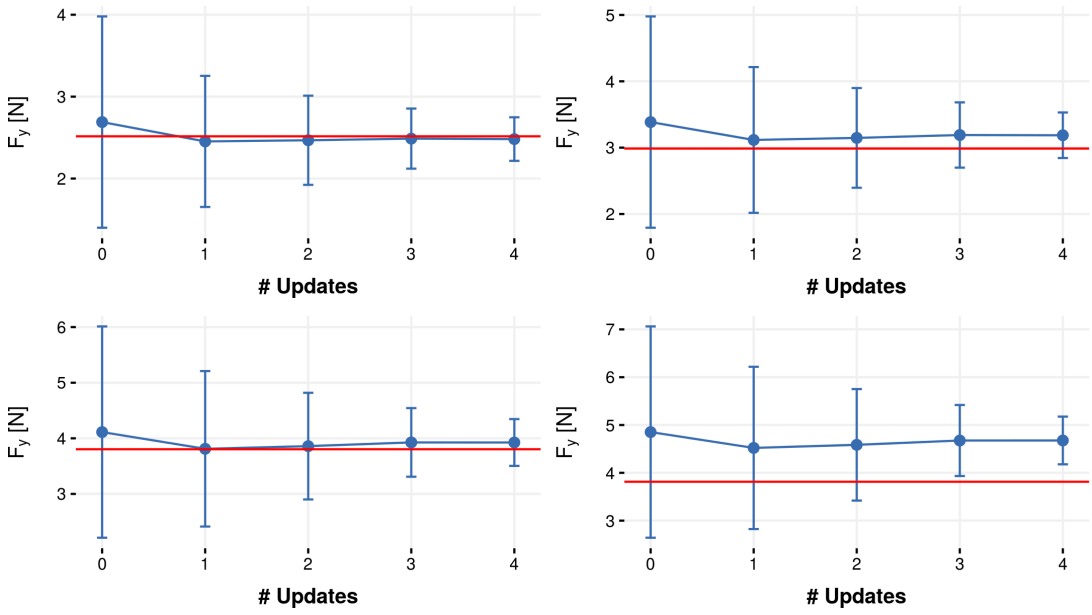

(b) $y - direction$

Figure C.1: Intervals of the peak forces for the experimental setup #1 in Table 4.4, updated from lowest feed per tooth value to the highest.

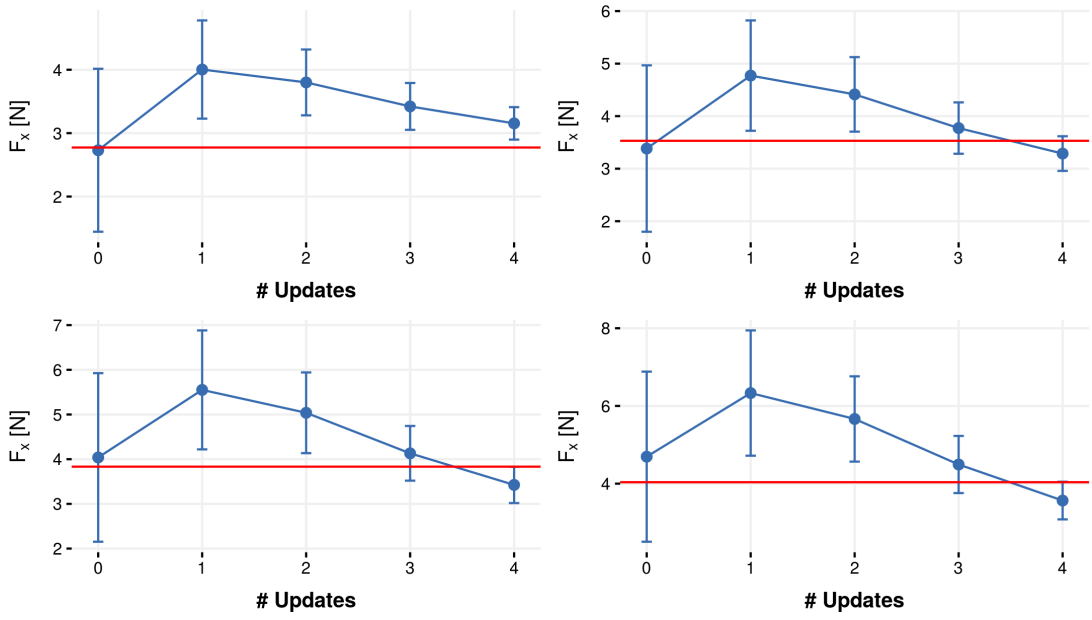

(a) $x - direction$

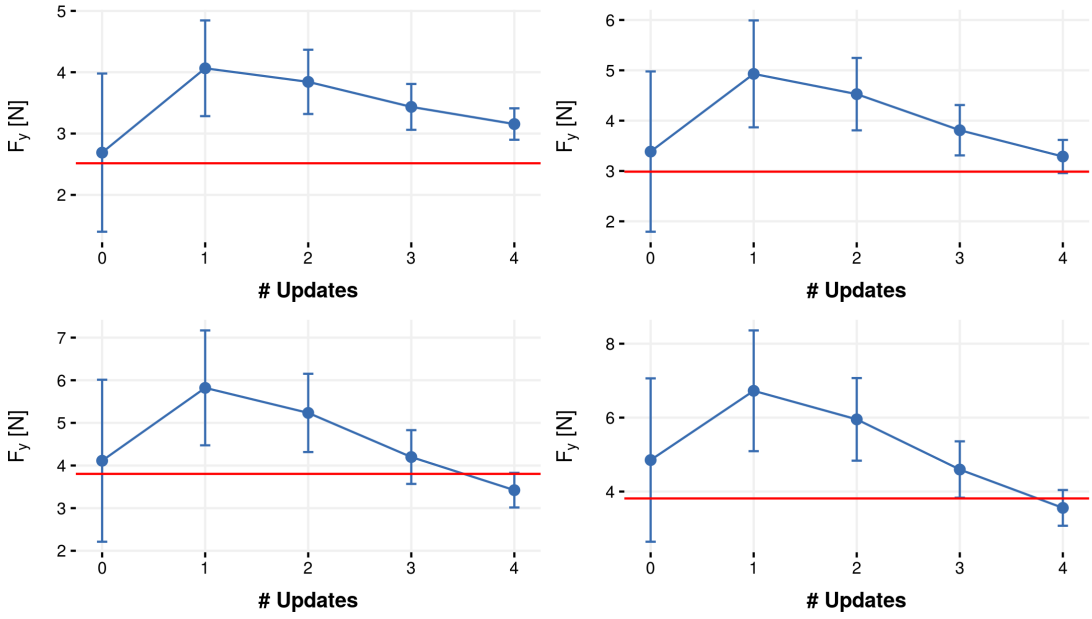

(b) $y - direction$

Figure C.2: Intervals of the peak forces for the experimental setup #1 in Table 4.4, updated from highest feed per tooth value to the lowest.

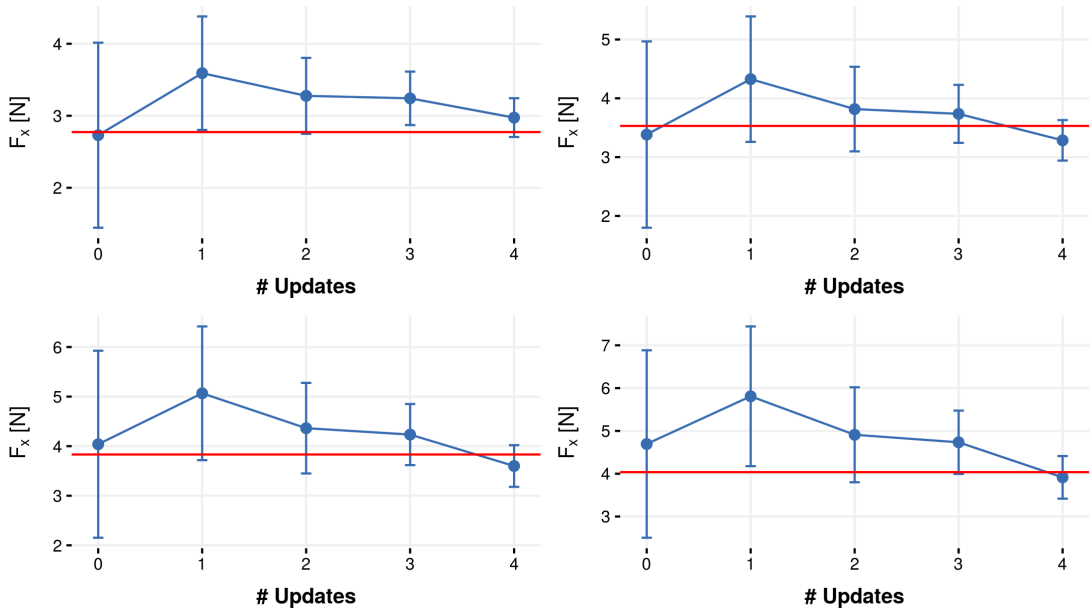

(a) $x - direction$

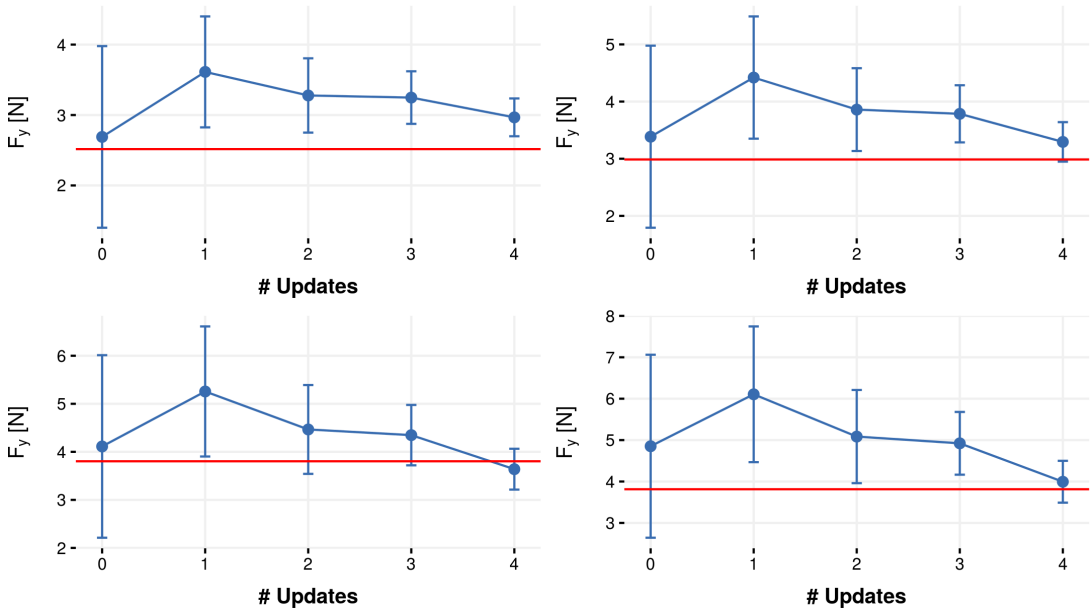

(b) $y - direction$

Figure C.3: Intervals of the peak forces for the experimental setup #1 in Table 4.4, updated by a random sequence of feed per tooth values (3-2-4-1).

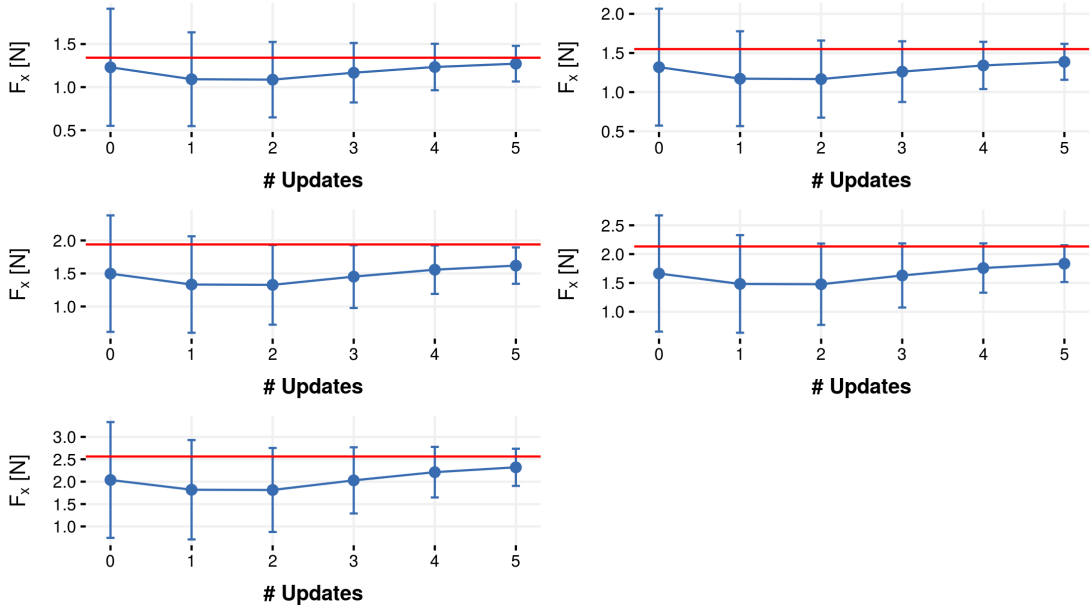

(a) $x - direction$

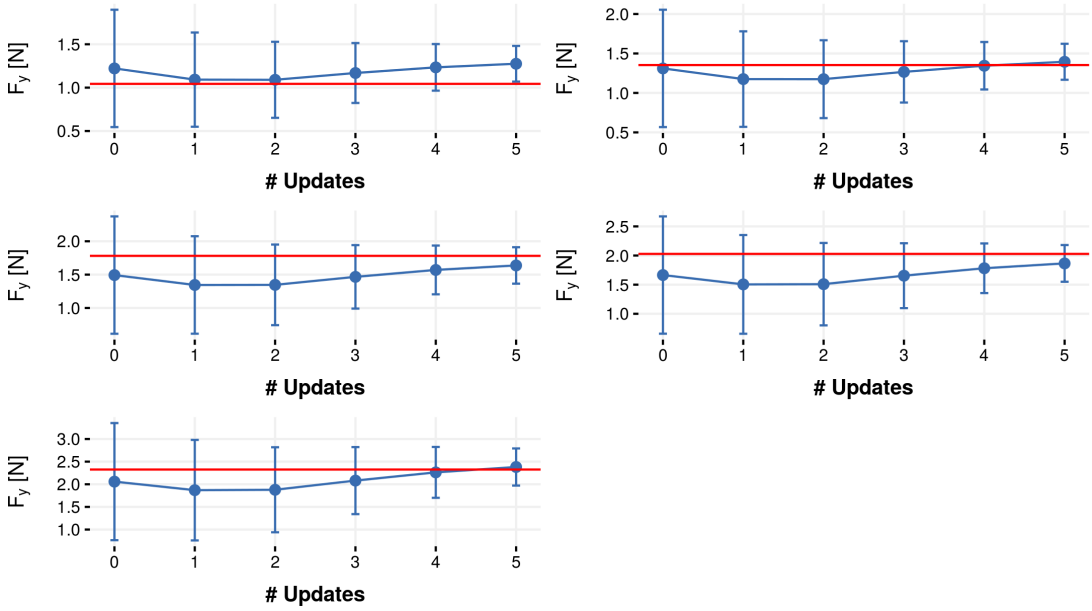

(b) $y - direction$

Figure C.4: Intervals of the peak forces for the experimental setup #2 in Table 4.4, updated from lowest feed per tooth value to the highest.

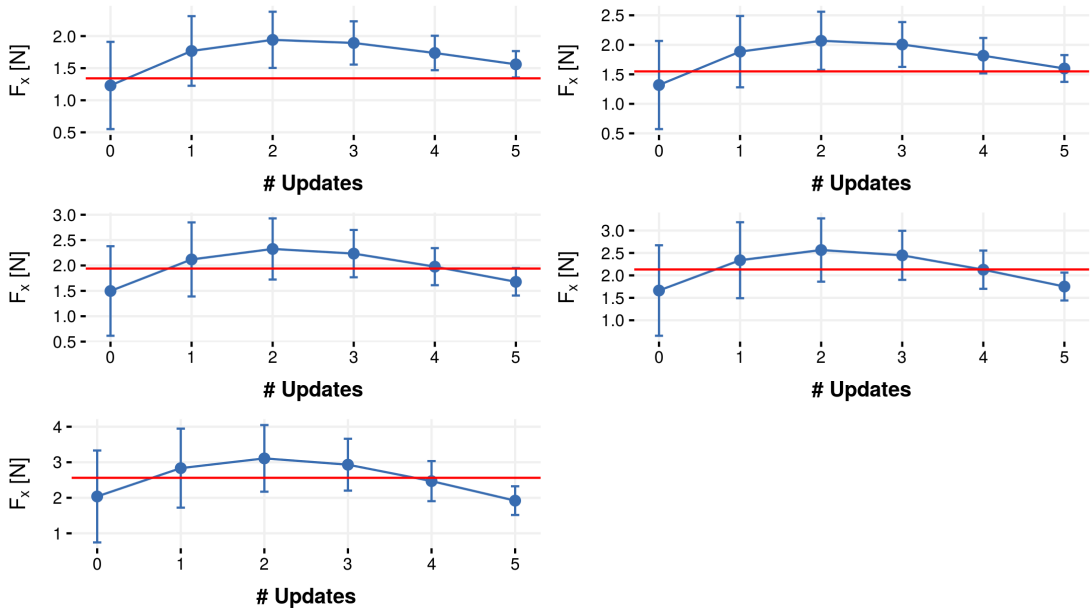

(a) $x - direction$

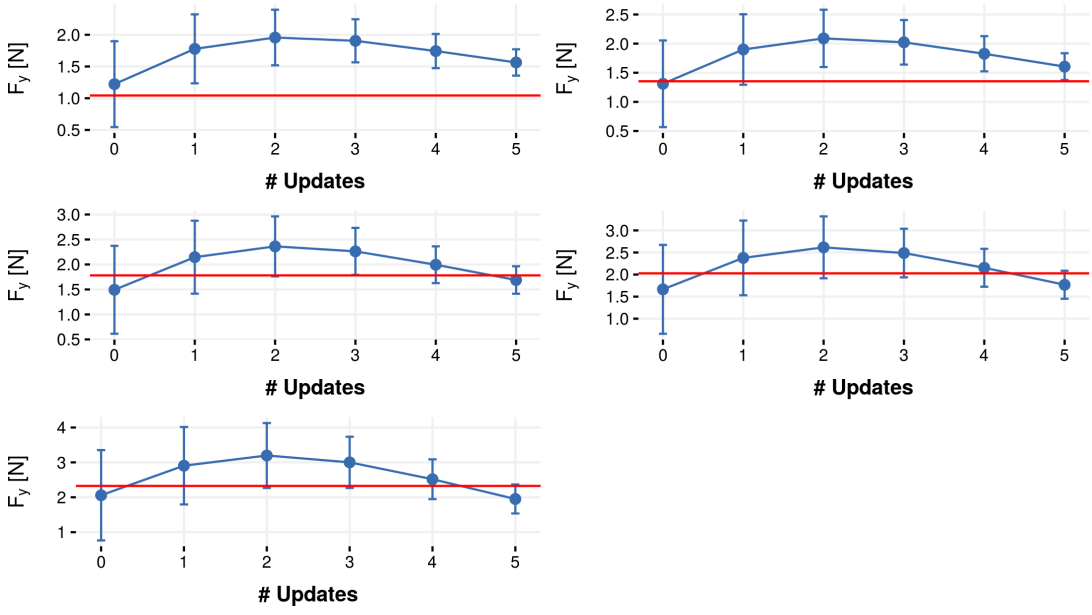

(b) $y - direction$

Figure C.5: Intervals of the peak forces for the experimental setup #2 in Table 4.4, updated from highest feed per tooth value to the lowest.

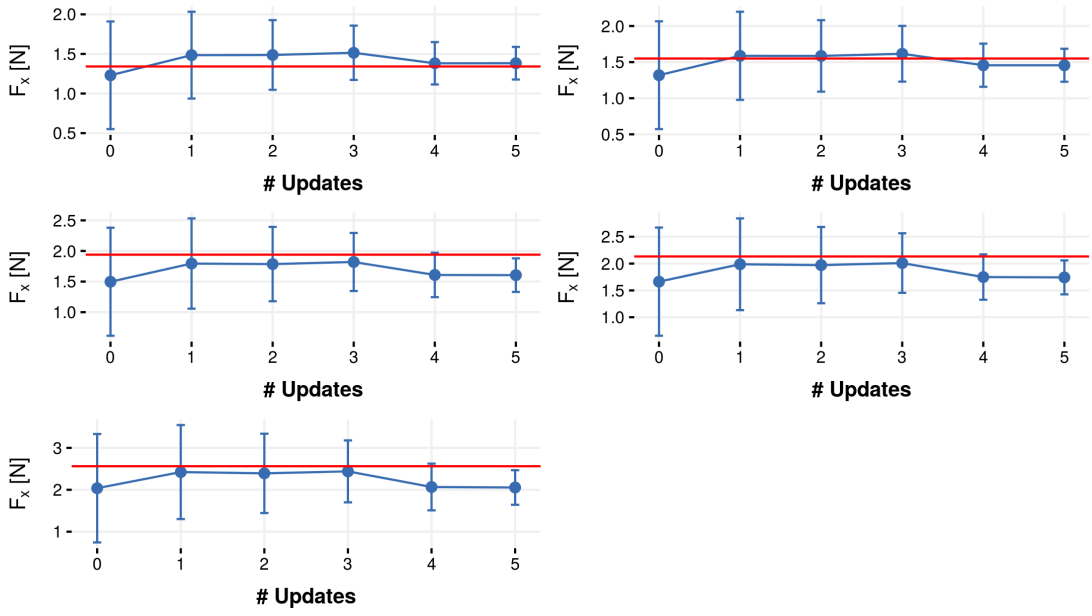

(a) $x - direction$

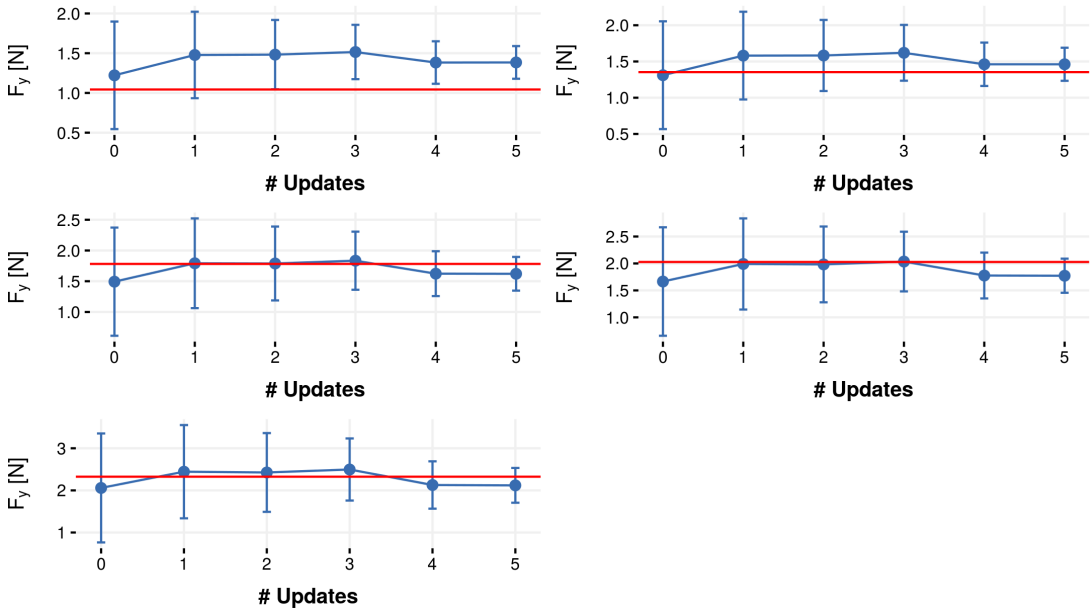

(b) $y - direction$

Figure C.6: Intervals of the peak forces for the experimental setup #2 in Table 4.4, updated by a random sequence of feed per tooth values (3-2-4-1-5).

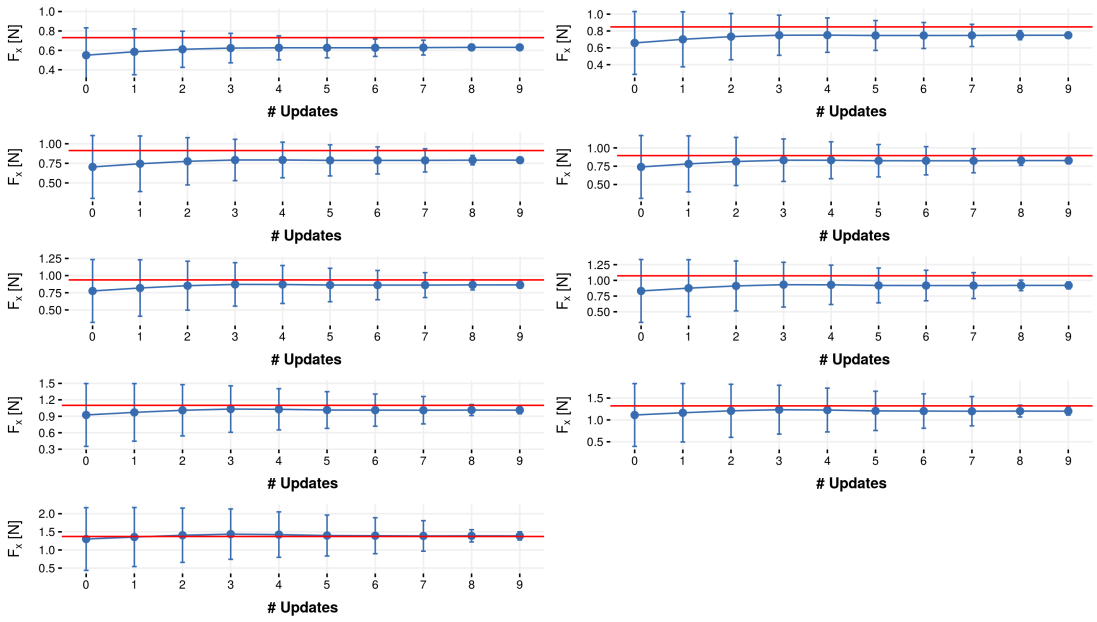

(a) $x - direction$

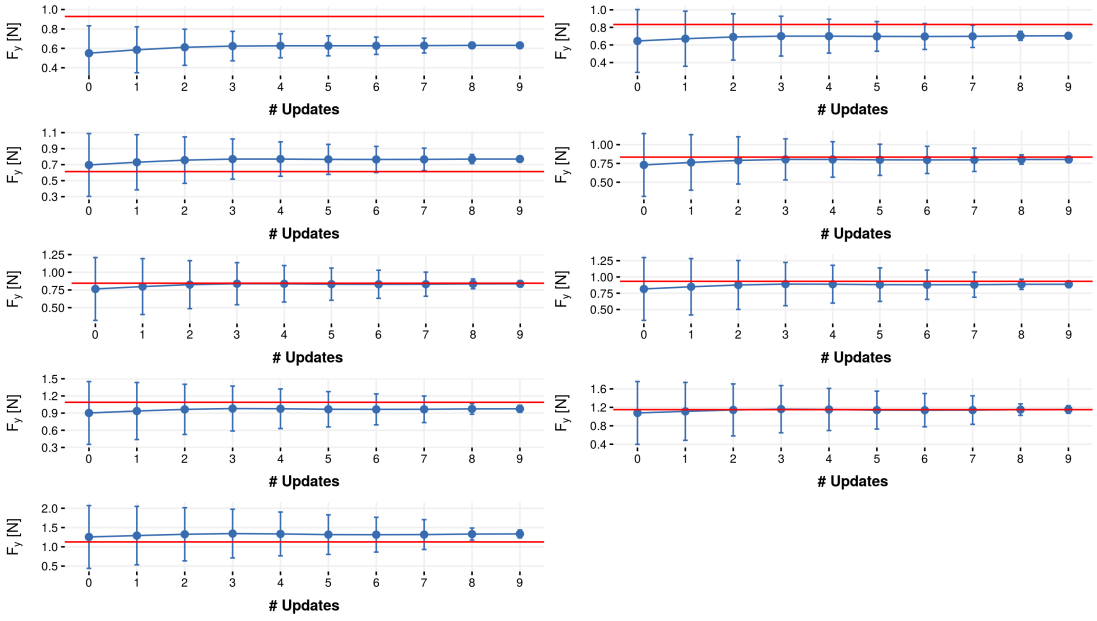

(b) $y - direction$

Figure C.7: Intervals of the peak forces for the experimental setup #3 in Table 4.4, updated from lowest feed per tooth value to the highest.

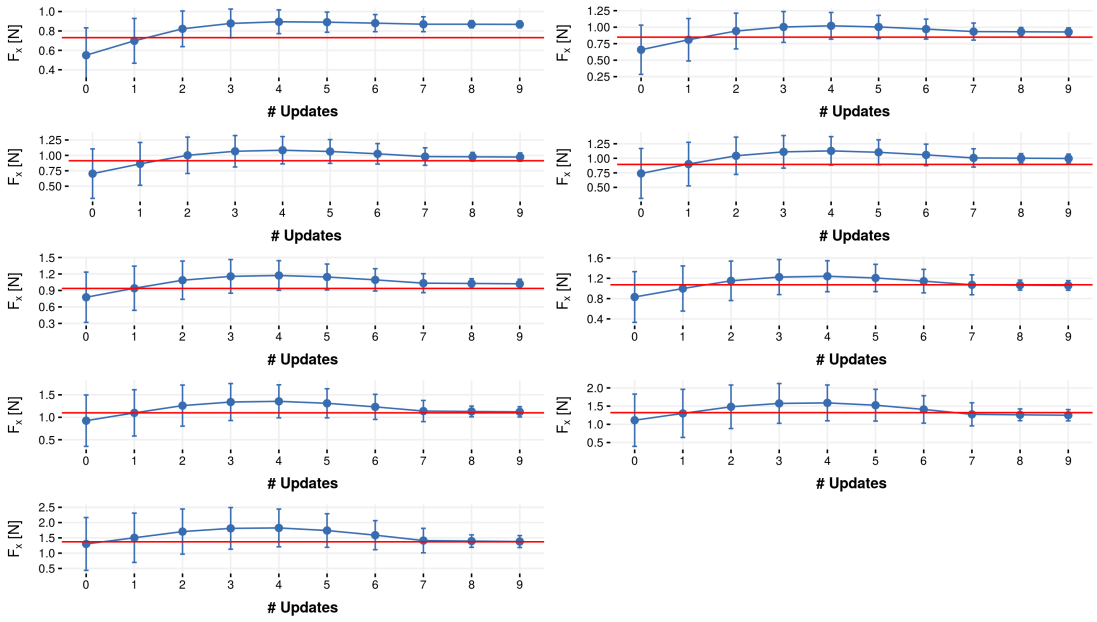

(a) $x - direction$

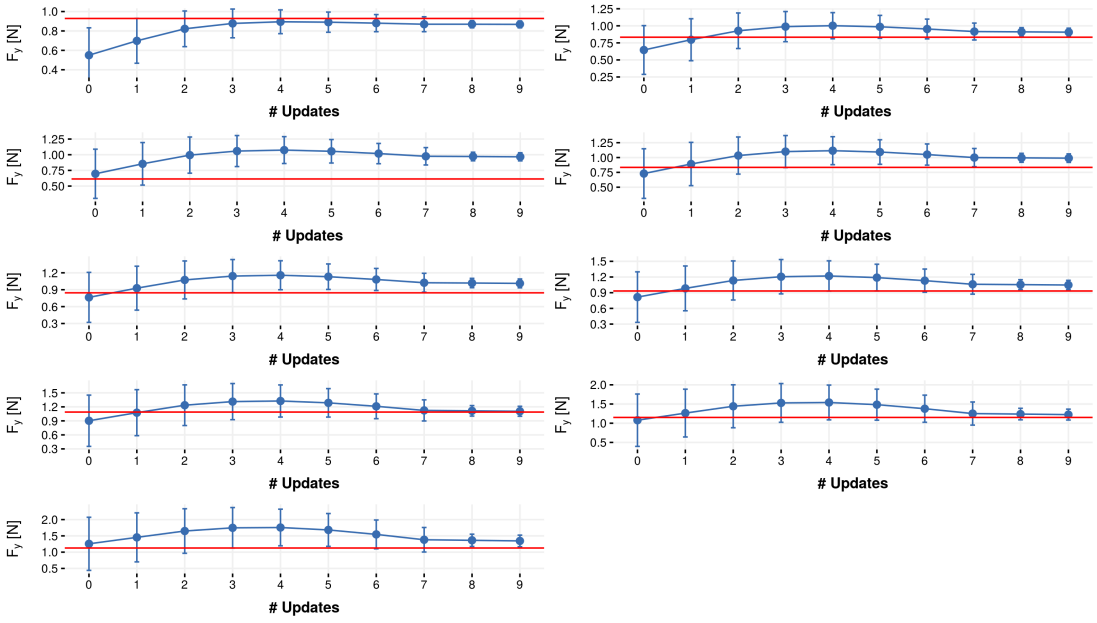

(b) $y - direction$

Figure C.8: Intervals of the peak forces for the experimental setup #3 in Table 4.4, updated from highest feed per tooth value to the lowest.

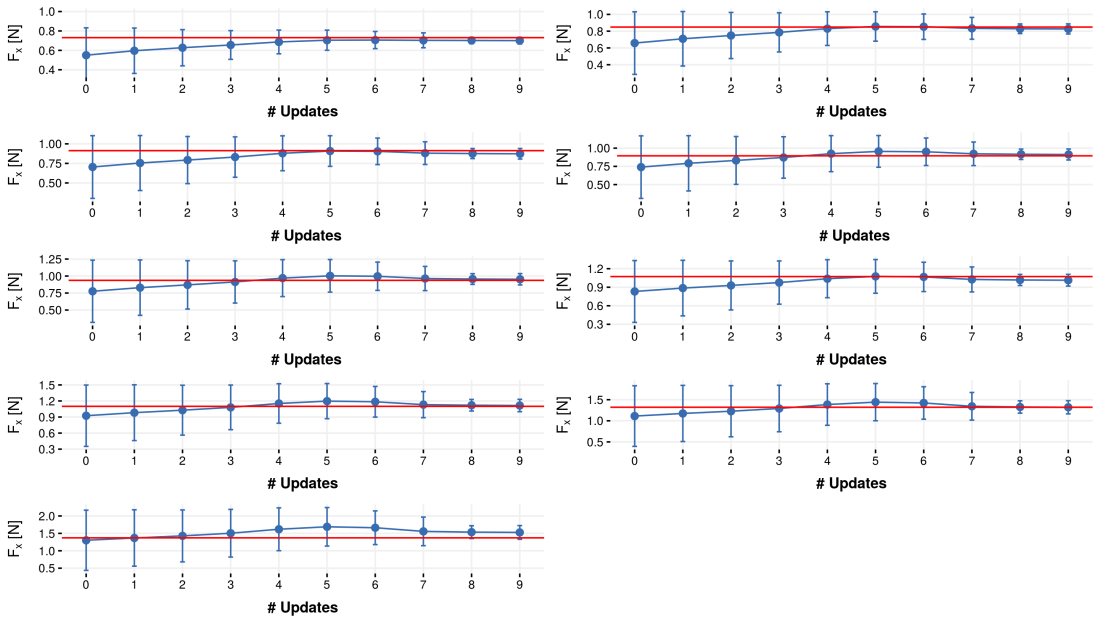

(a) $x - direction$

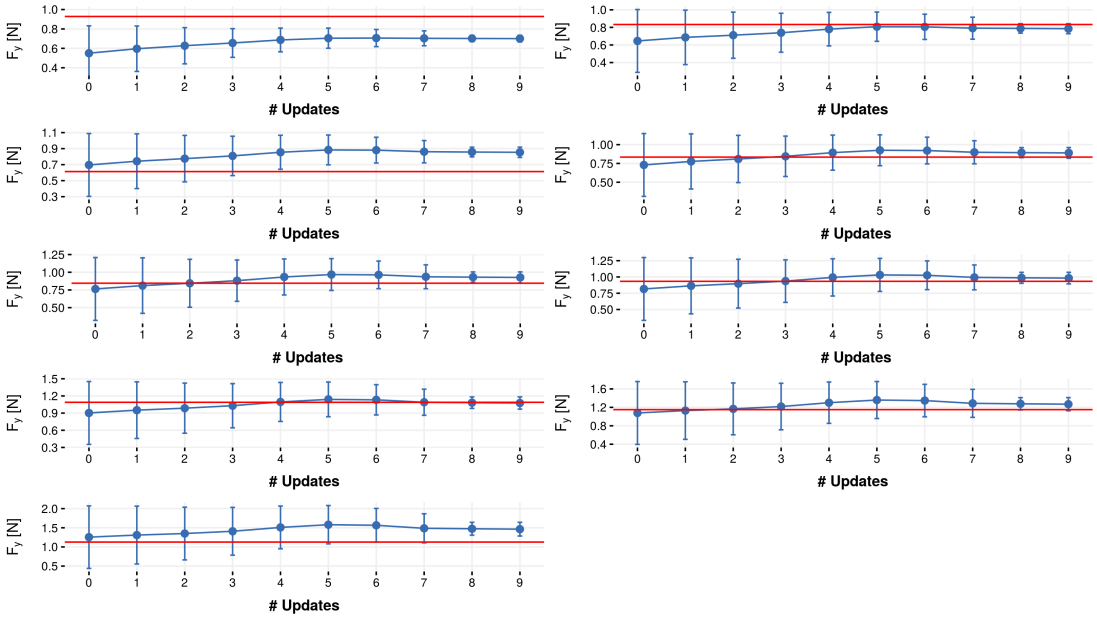

(b) $y - direction$

Figure C.9: Intervals of the peak forces for the experimental setup #3 in Table 4.4, updated by a random sequence of feed per tooth values (5-1-6-8-7-3-2-9-4).

Appendix D

Ranges of Force Coefficients with Respect to Updates

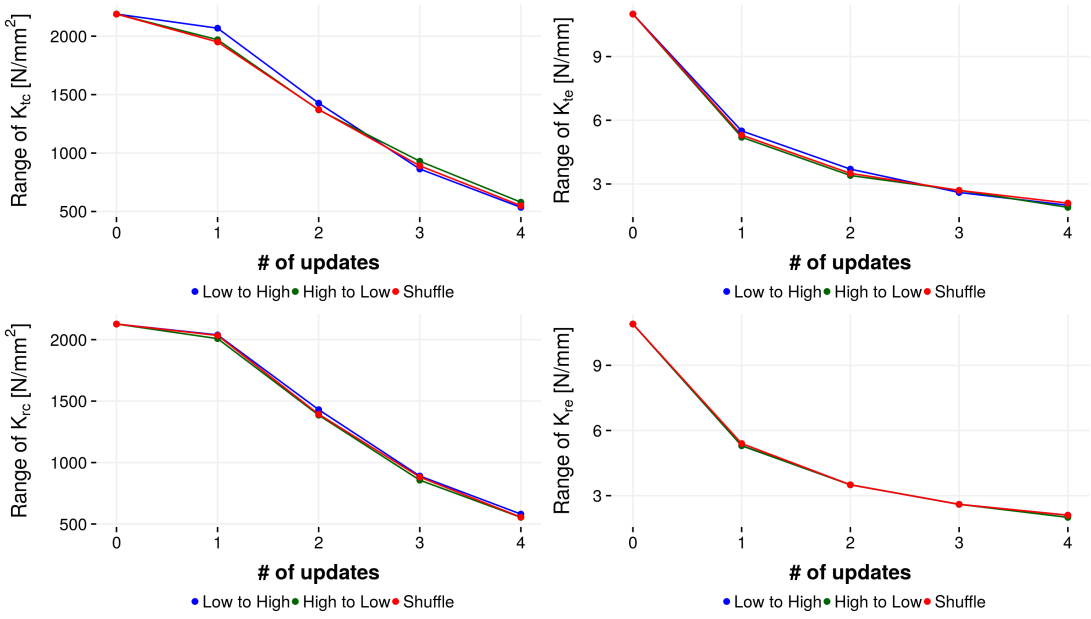

Figure D.1: Ranges of cutting force coefficients with respect to updates for experiment #1 in Table 4.4.

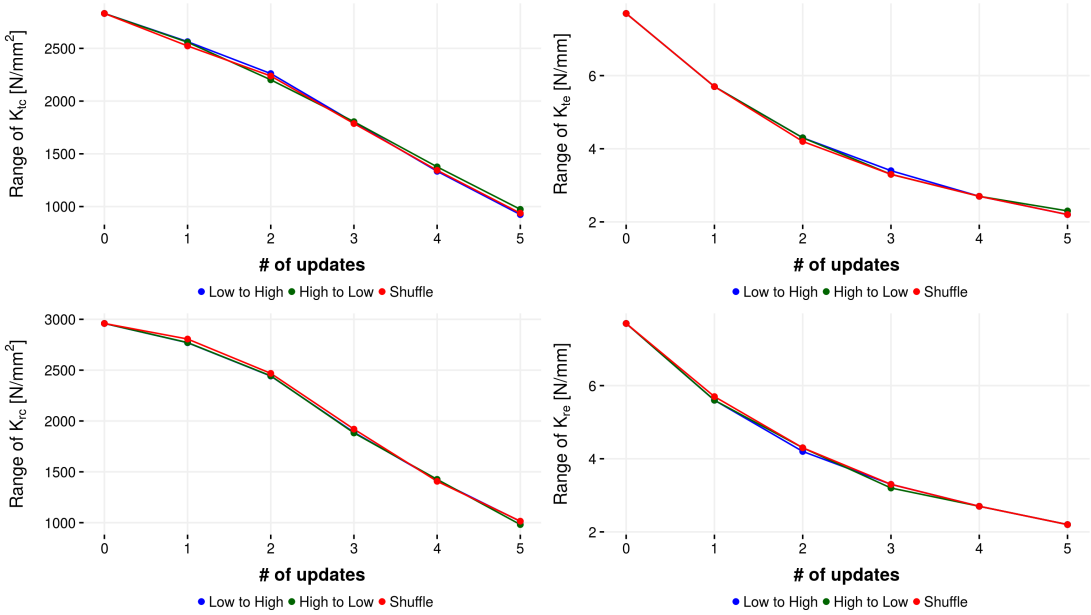

Figure D.2: Ranges of cutting force coefficients with respect to updates for experiment #2 in Table 4.4.

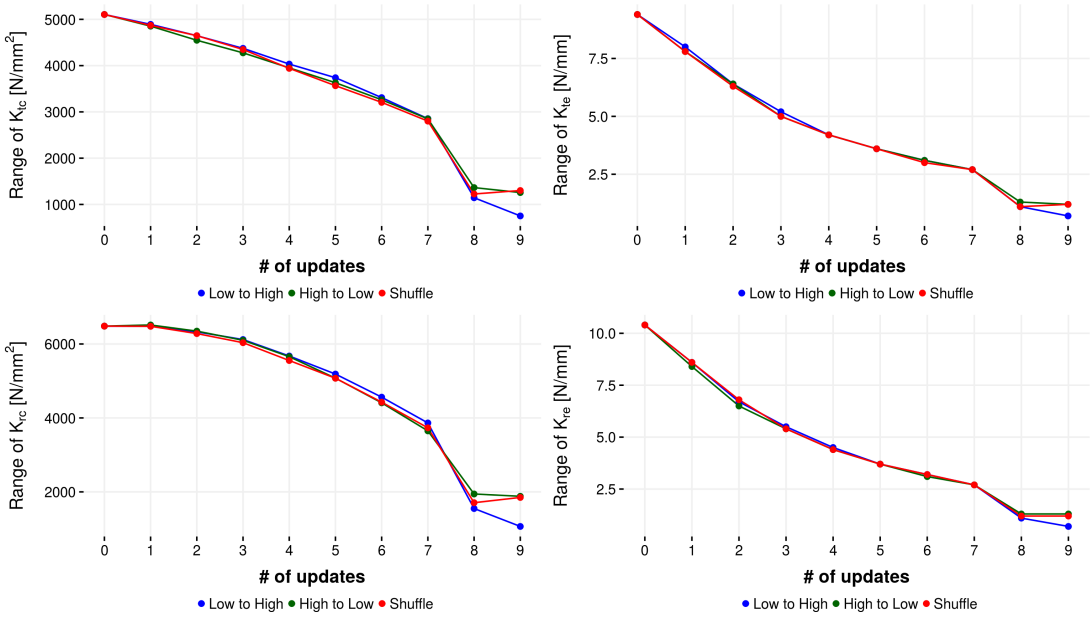

Figure D.3: Ranges of cutting force coefficients with respect to updates for experiment #3 in Table 4.4.

Appendix E

Force Predictions After Bayesian Updatings for Exp. #1

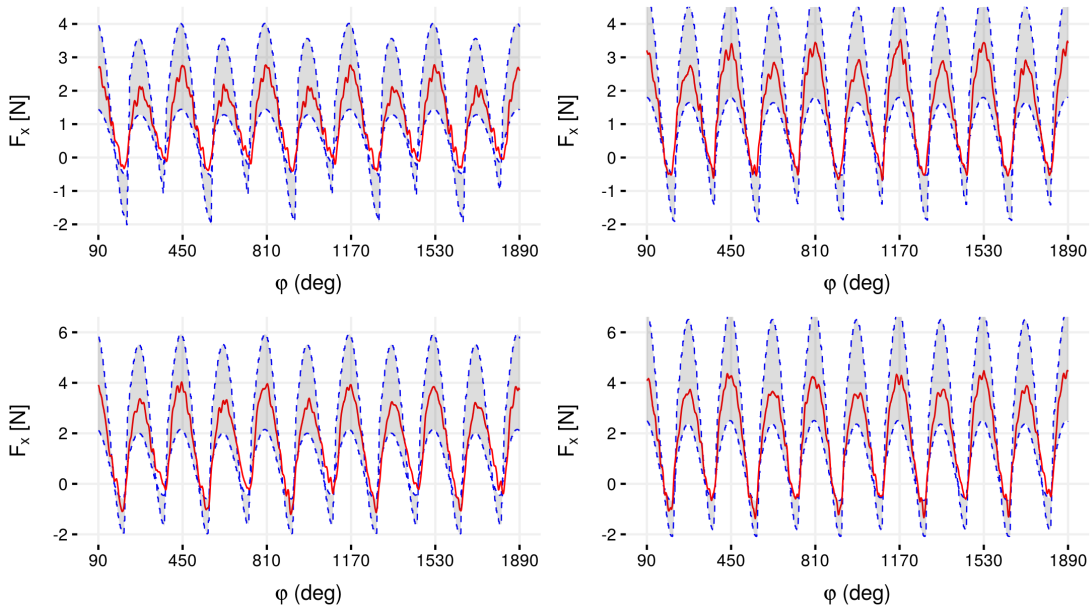

(a) $x - direction$

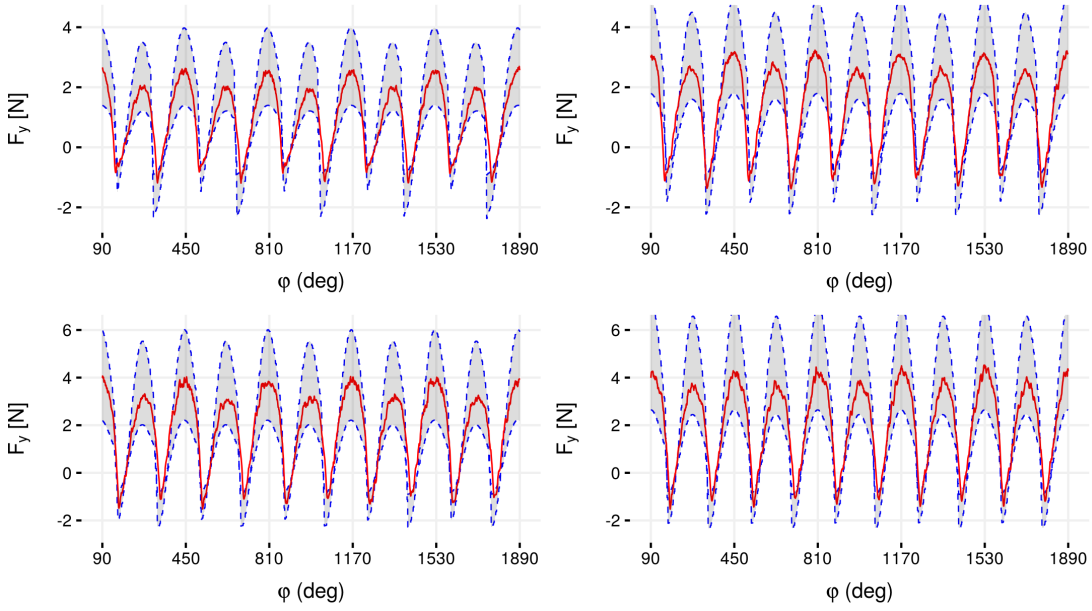

(b) $y - direction$

Figure E.1: Simulated and measured force predictions with cutting tool having 0.6 mm diameter at 32 m/min cutting speed, 120 µm/depth of cut and 2, 4, 6, 8 µm/tooth, *a.* in direction x and *b.* in direction y, after Bayesian updating with FEM outputs.

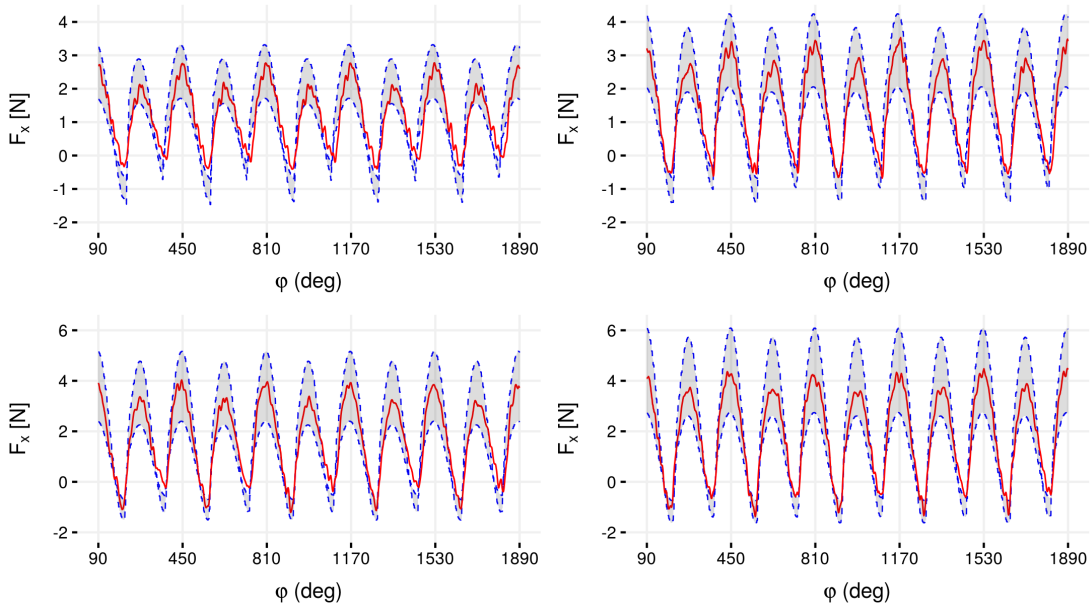

(a) $x - direction$

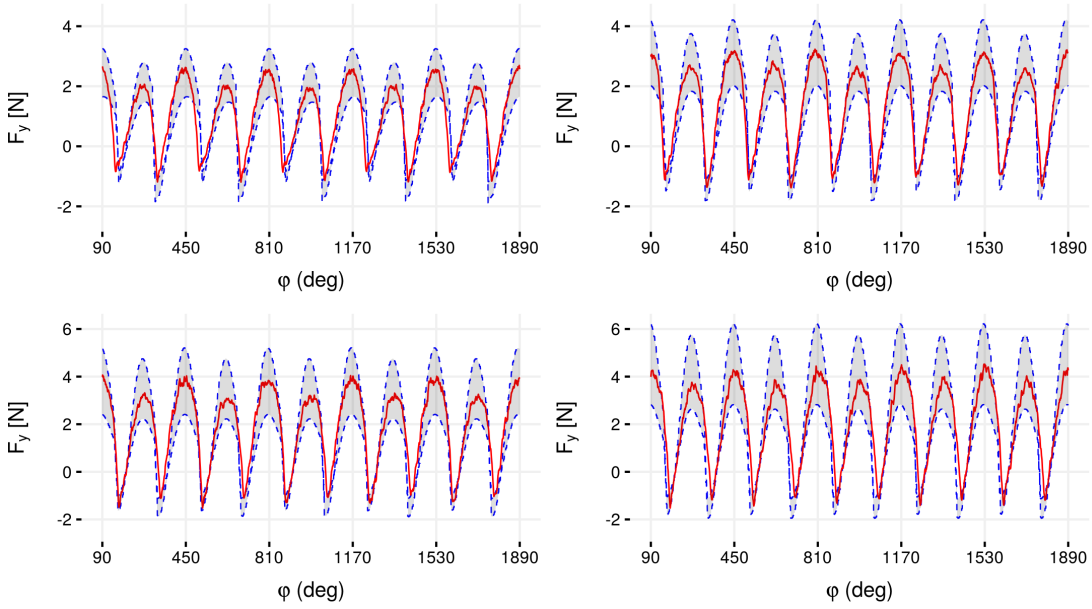

(b) $y - direction$

Figure E.2: Simulated and measured force predictions with cutting tool having 0.6 mm diameter at 32 m/min cutting speed, 120 µm/depth of cut and 2, 4, 6, 8 µm/tooth, *a.* in direction x and *b.* in direction y, after first update (update sequence is from lowest feed per tooth value to the highest).

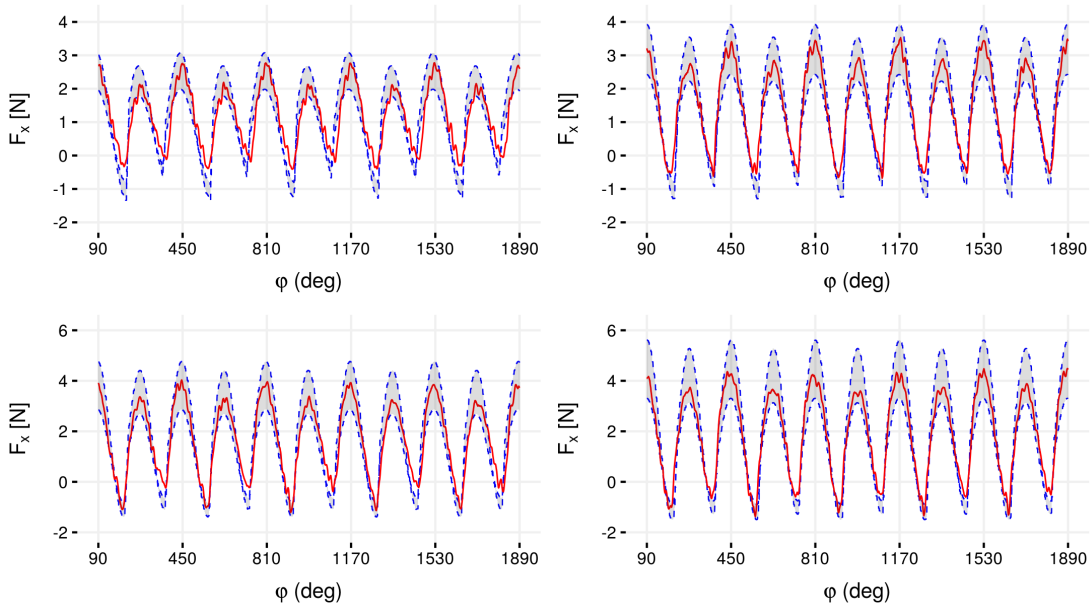

(a) $x - direction$

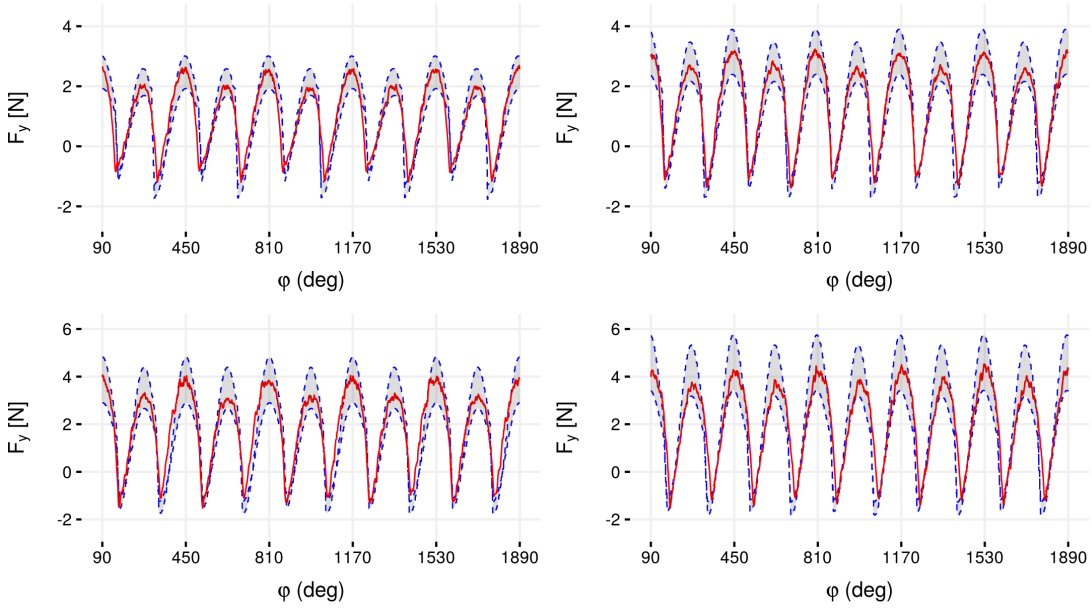

(b) $y - direction$

Figure E.3: Simulated and measured force predictions with cutting tool having 0.6 mm diameter at 32 m/min cutting speed, 120 µm/depth of cut and 2, 4, 6, 8 µm/tooth, *a.* in direction x and *b.* in direction y, after second update (update sequence is from lowest feed per tooth value to the highest).

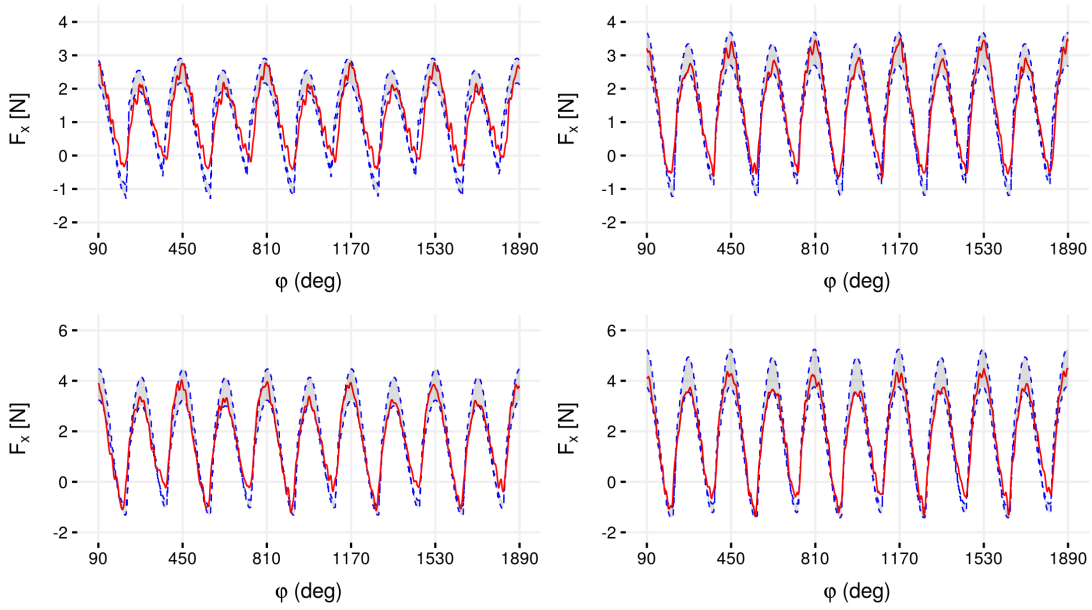

(a) $x - direction$

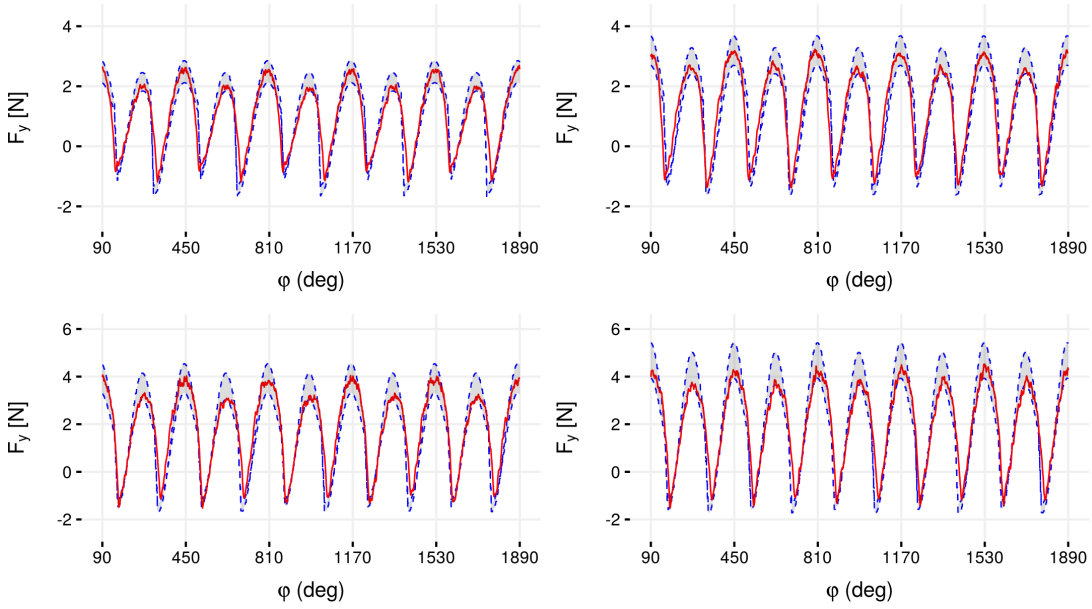

(b) $y - direction$

Figure E.4: Simulated and measured force predictions with cutting tool having 0.6 mm diameter at 32 m/min cutting speed, 120 µm/depth of cut and 2, 4, 6, 8 µm/tooth, *a.* in direction x and *b.* in direction y, after third update (update sequence is from lowest feed per tooth value to the highest).

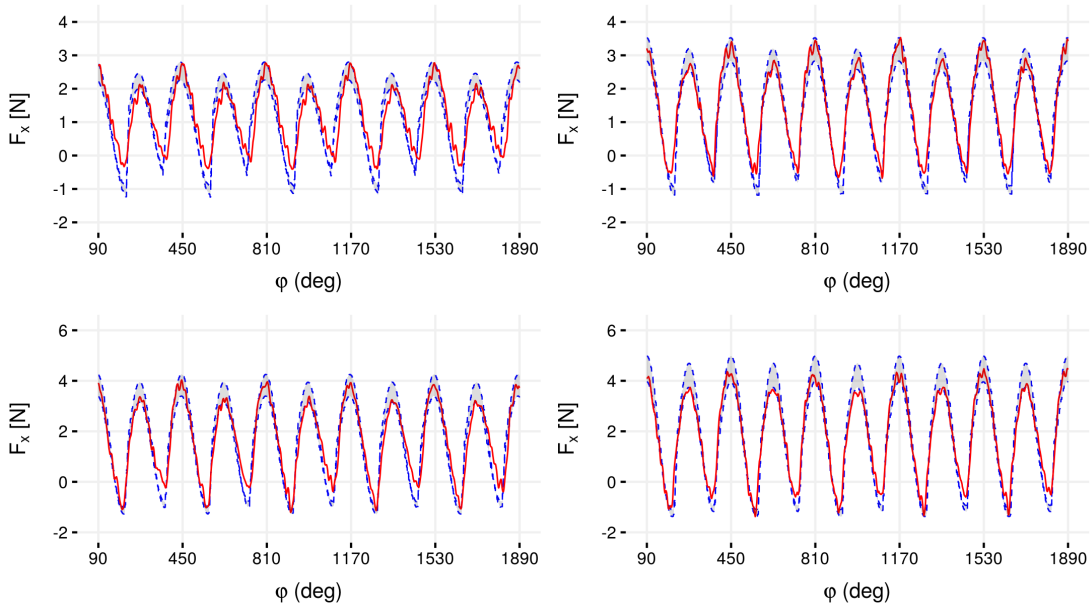

(a) $x - direction$

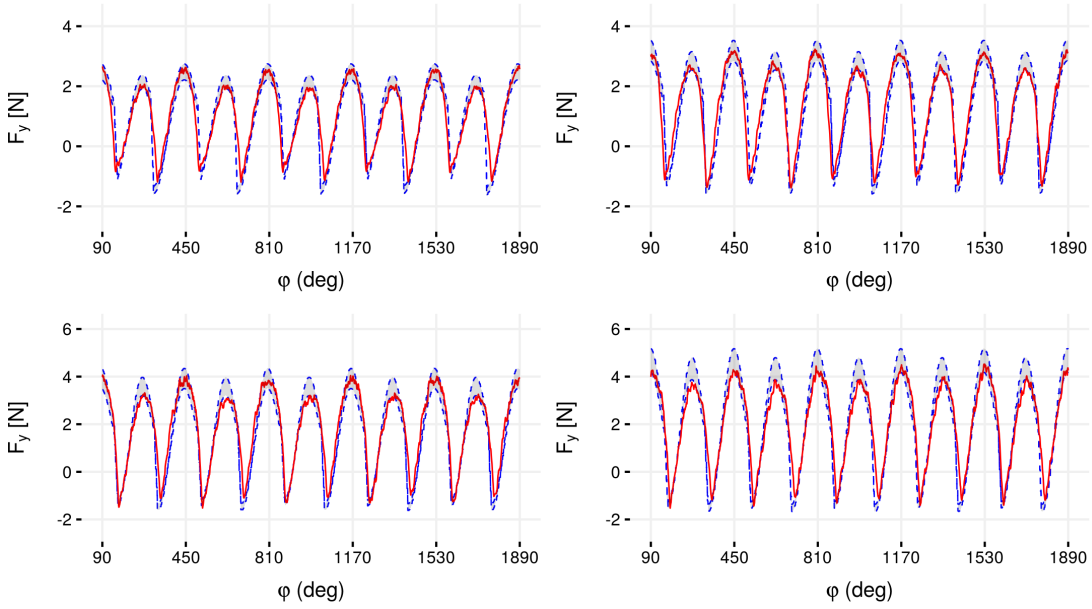

(b) $y - direction$

Figure E.5: Simulated and measured force predictions with cutting tool having 0.6 mm diameter at 32 m/min cutting speed, 120 µm/depth of cut and 2, 4, 6, 8 µm/tooth, *a.* in direction x and *b.* in direction y, after fourth update (update sequence is from lowest feed per tooth value to the highest).

Appendix F

Force Predictions After Bayesian Updatings for Exp. #2

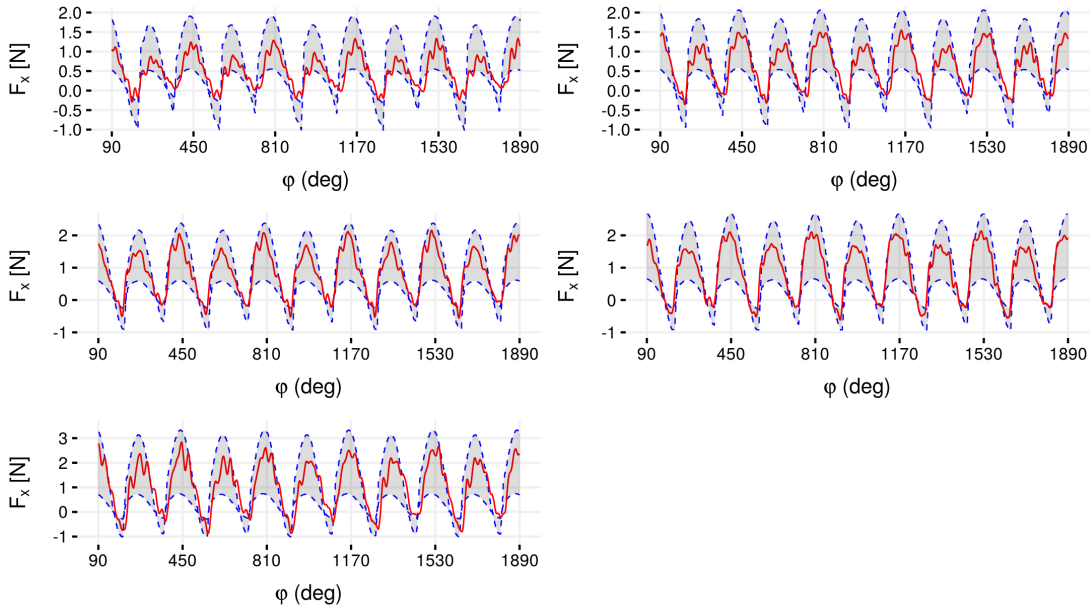

(a) $x-direction$

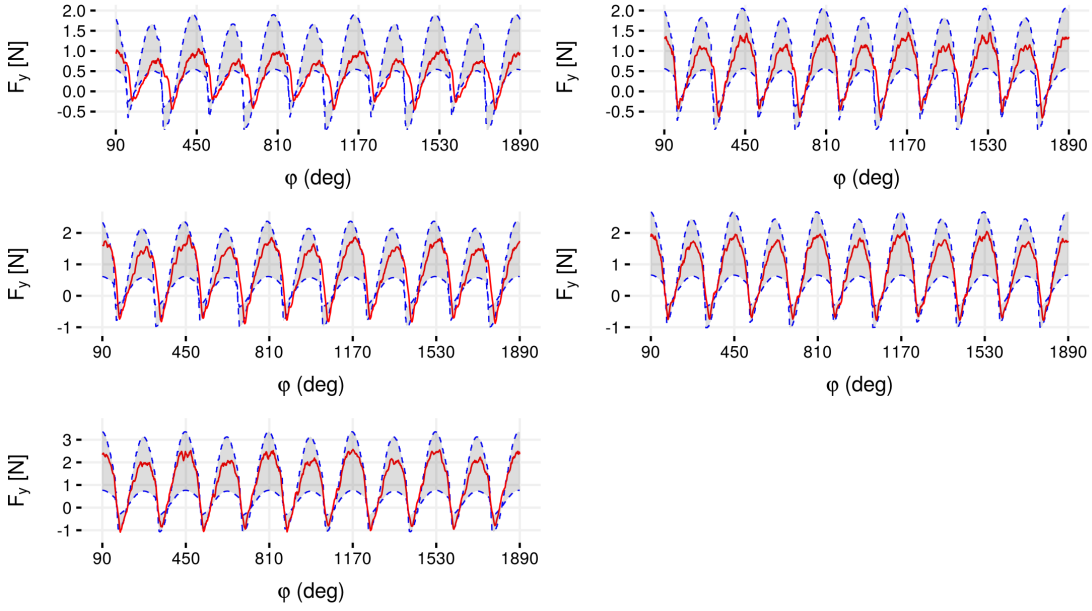

(b) $y-direction$

Figure F.1: Simulated and measured force predictions with cutting tool having 0.4 mm diameter at 32 m/min cutting speed, 80 µm/ depth of cut and 1.5, 2, 3, 4, 6 µm/tooth, a. in $x-direction$ and b. in $y-direction$, after Bayesian updating with FEM outputs.

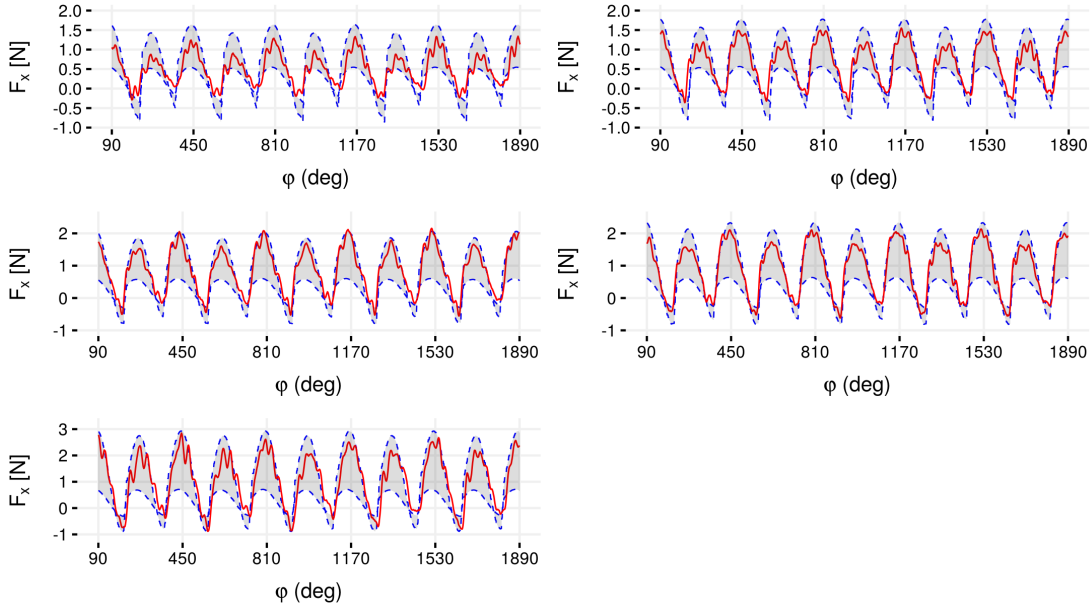

(a) $x - direction$

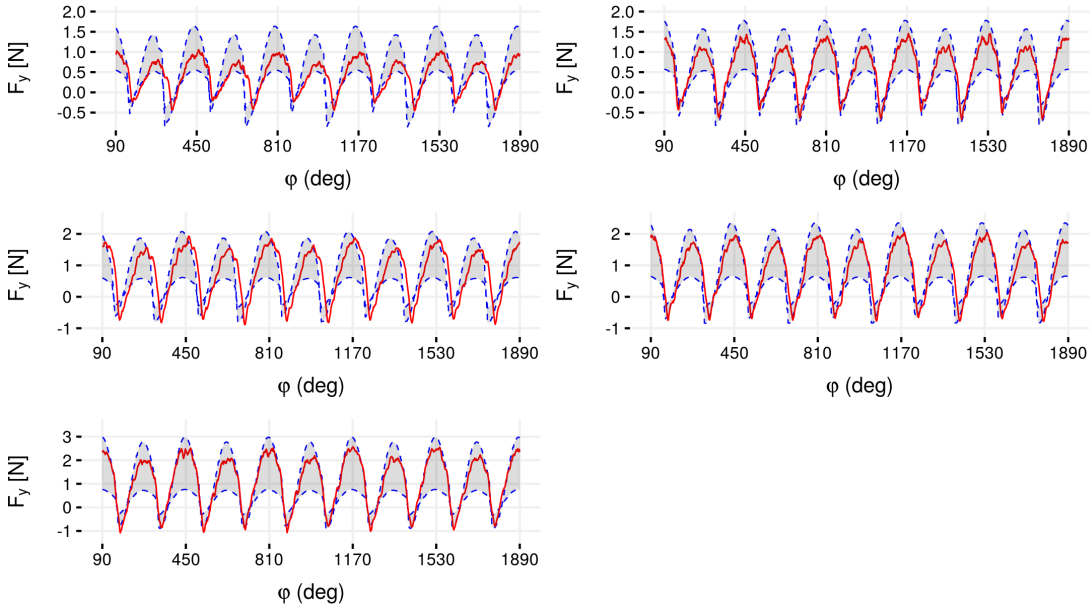

(b) $y - direction$

Figure F.2: Simulated and measured force predictions with cutting tool having 0.4 mm diameter at 32 m/min cutting speed, 80 µm/ depth of cut and 1.5, 2, 3, 4, 6 µm/tooth, a. in $x - direction$ and b. in $y - direction$, after first update (update sequence is from lowest feed per tooth value to the highest).

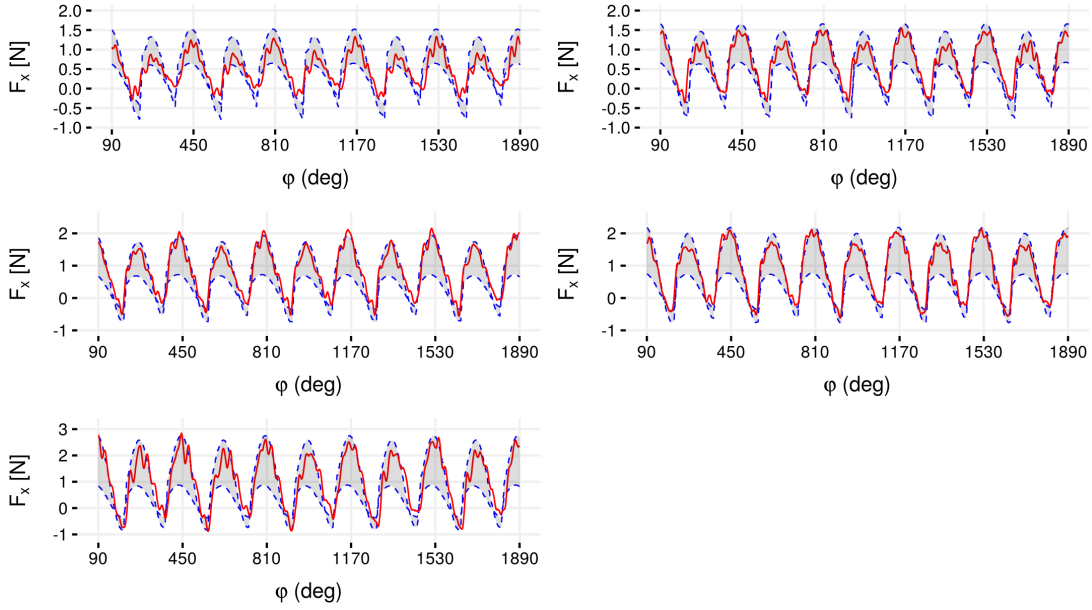

(a) $x - direction$

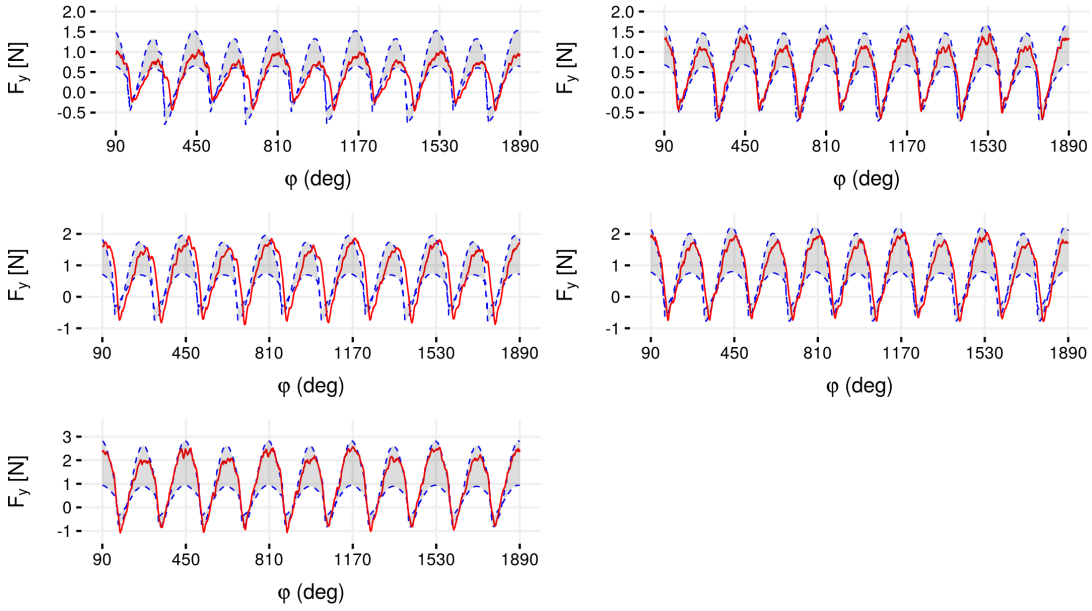

(b) $y - direction$

Figure F.3: Simulated and measured force predictions with cutting tool having 0.4 mm diameter at 32 m/min cutting speed, 80 µm/ depth of cut and 1.5, 2, 3, 4, 6 µm/tooth, a. in $x - direction$ and b. in $y - direction$, after second update (update sequence is from lowest feed per tooth value to the highest).

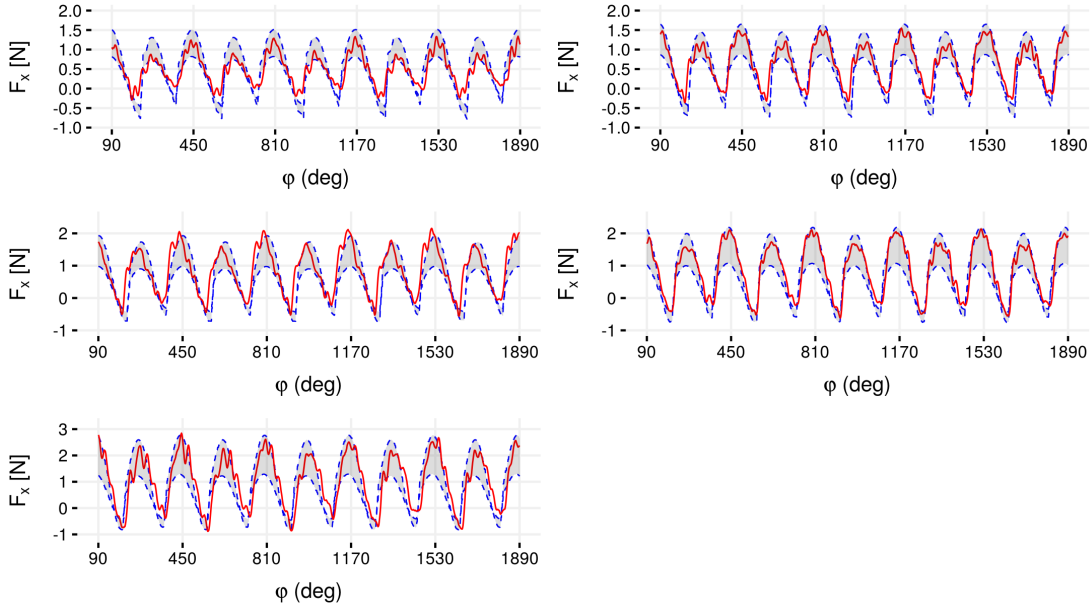

(a) $x - direction$

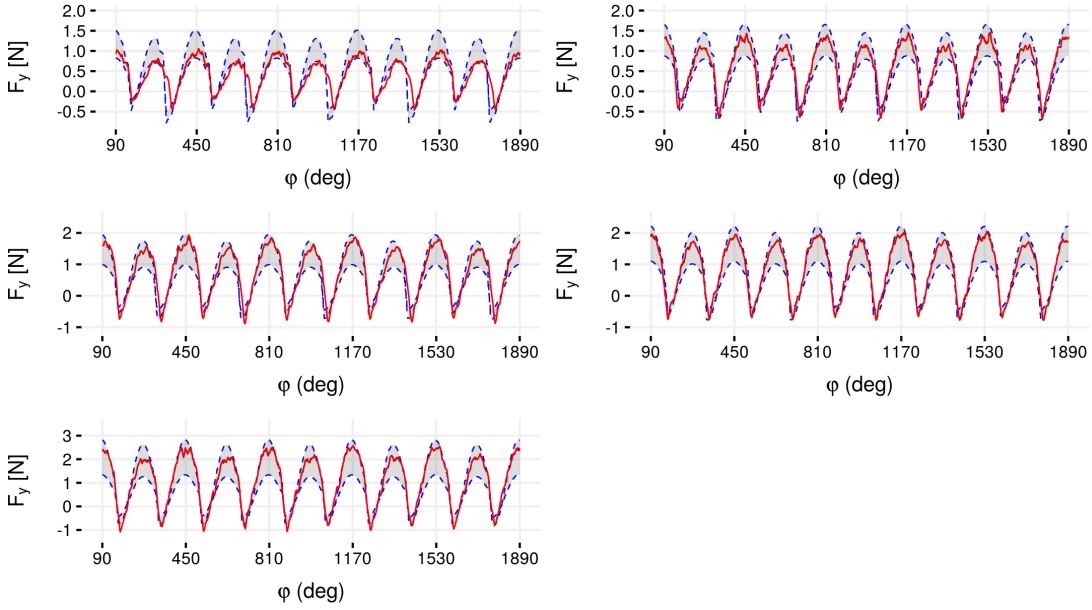

(b) $y - direction$

Figure F.4: Simulated and measured force predictions with cutting tool having 0.4 mm diameter at 32 m/min cutting speed, 80 µm/ depth of cut and 1.5, 2, 3, 4, 6 µm/tooth, a. in $x - direction$ and b. in $y - direction$, after third update (update sequence is from lowest feed per tooth value to the highest).

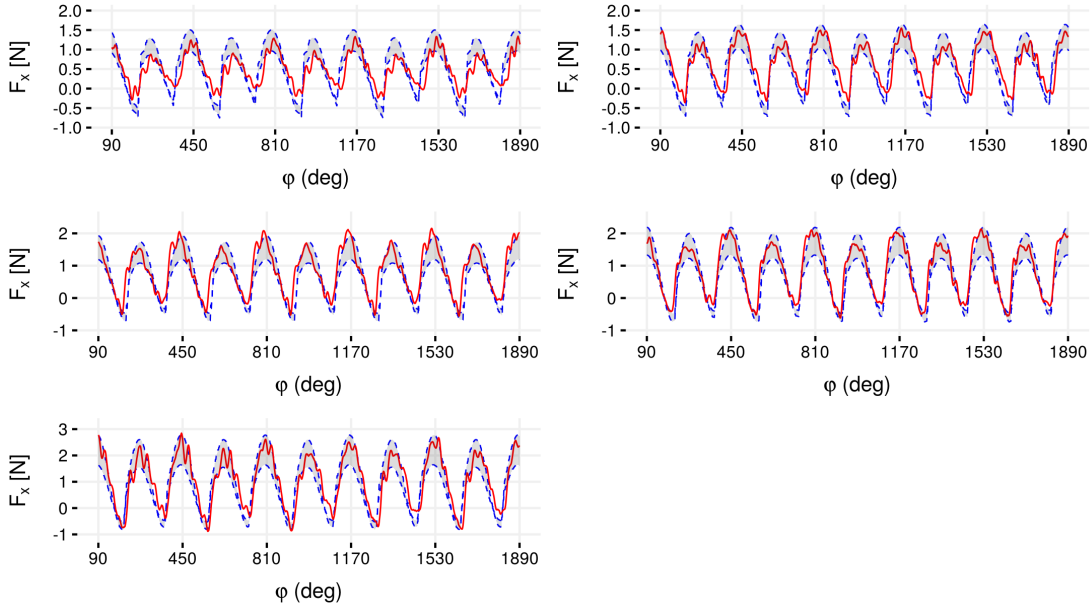

(a) $x - direction$

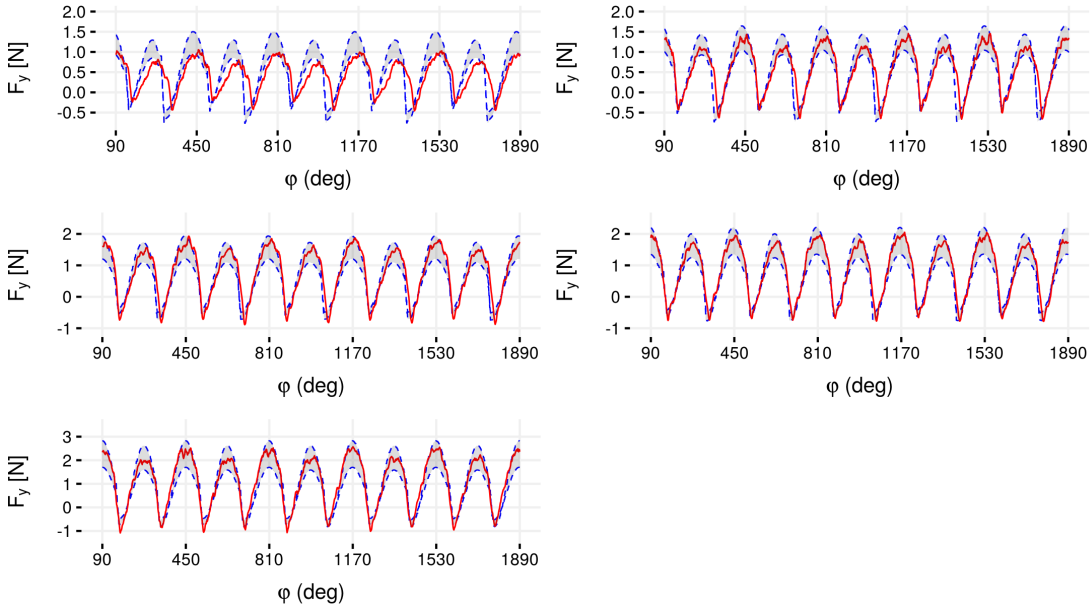

(b) $y - direction$

Figure F.5: Simulated and measured force predictions with cutting tool having 0.4 mm diameter at 32 m/min cutting speed, 80 µm/ depth of cut and 1.5, 2, 3, 4, 6 µm/tooth, a. in $x - direction$ and b. in $y - direction$, after fourth update (update sequence is from lowest feed per tooth value to the highest).

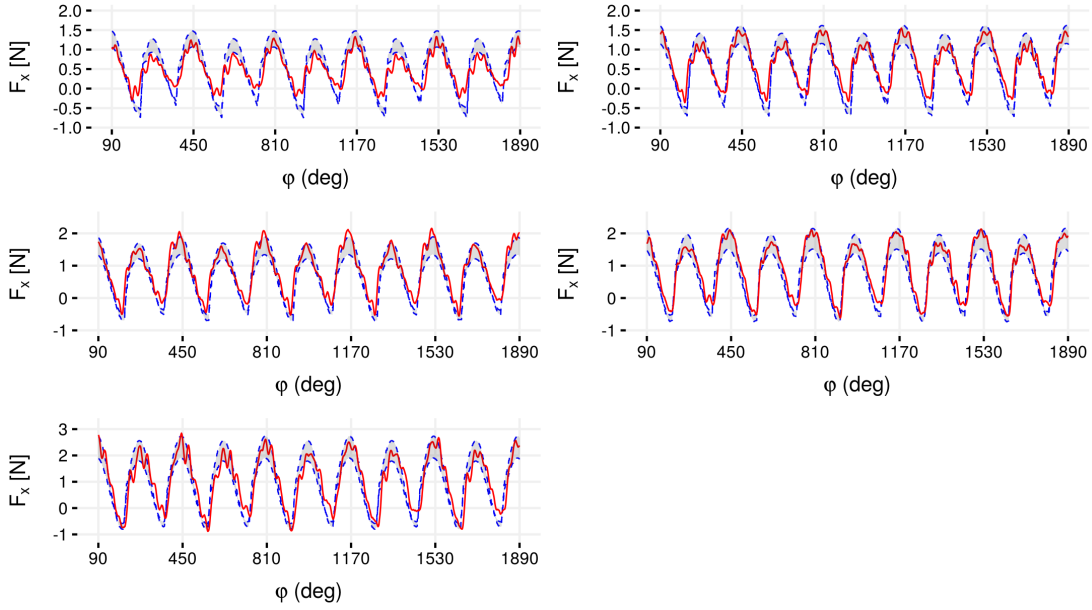

(a) $x - direction$

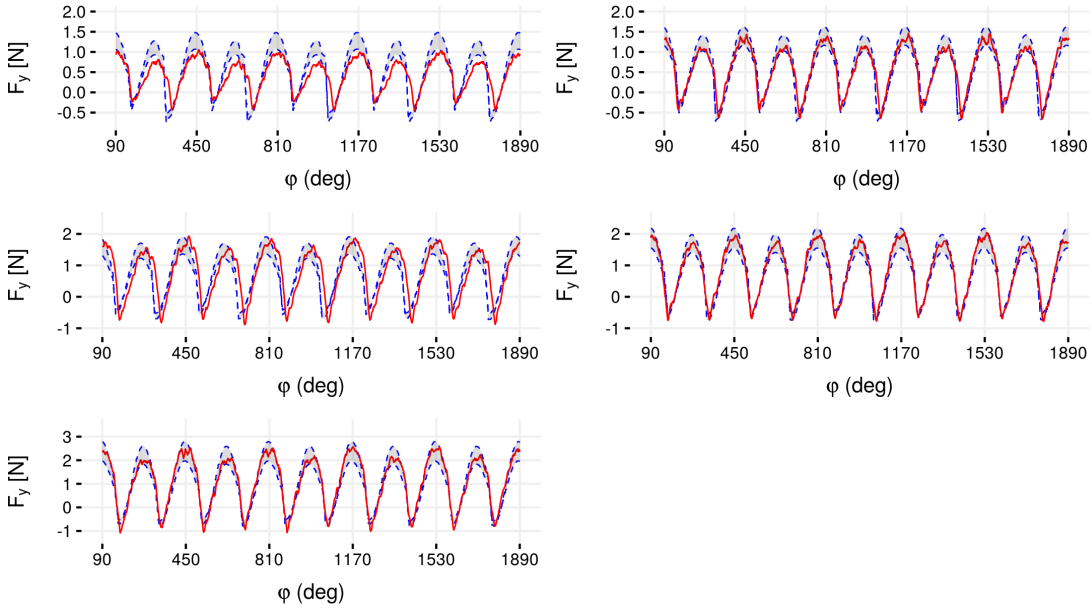

(b) $y - direction$

Figure F.6: Simulated and measured force predictions with cutting tool having 0.4 mm diameter at 32 m/min cutting speed, 80 µm/ depth of cut and 1.5, 2, 3, 4, 6 µm/tooth, a. in $x - direction$ and b. in $y - direction$, after fifth update (update sequence is from lowest feed per tooth value to the highest).

Appendix G

Force Predictions After Bayesian Updatings for Exp. #3

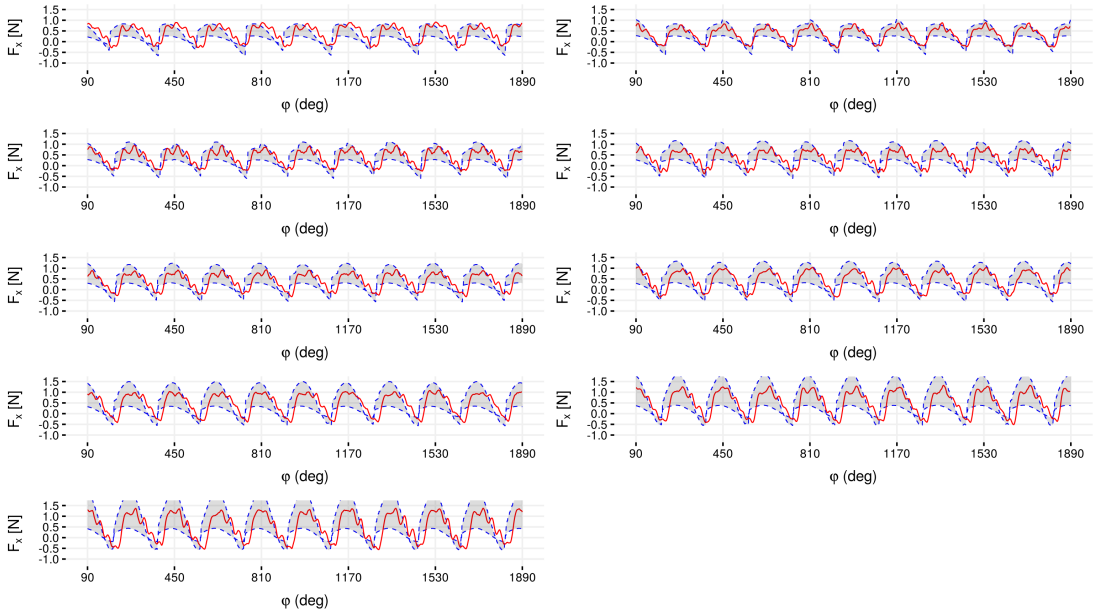

(a) $x - direction$

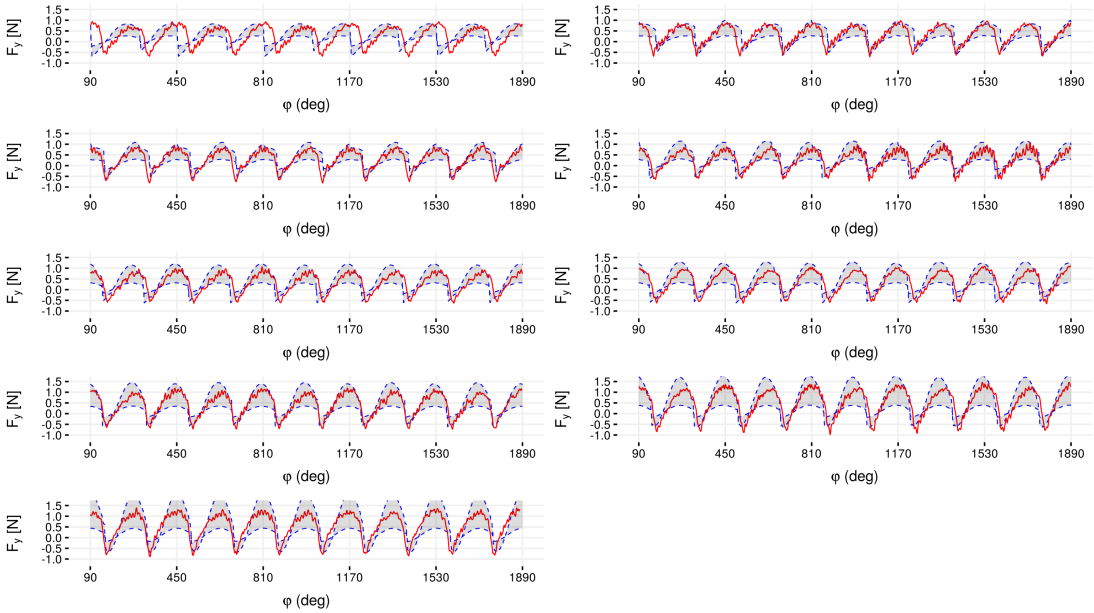

(b) $y - direction$

Figure G.1: Simulated and measured force predictions with cutting tool having 0.4 mm diameter at 35 m/min cutting speed, 40 µm/ depth of cut and 0.4, 0.6, 0.8, 1, 1.2, 1.5, 2, 3, 4 µm/tooth, a. in $x - direction$ and b. in $y - direction$, after Bayesian updating with FEM outputs.

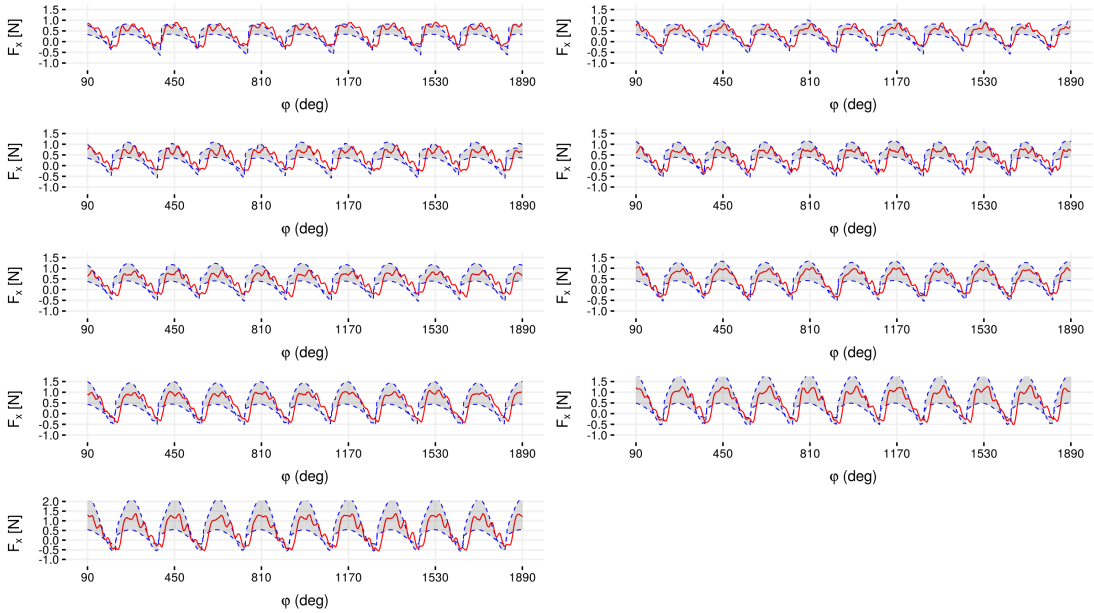

(a) $x - direction$

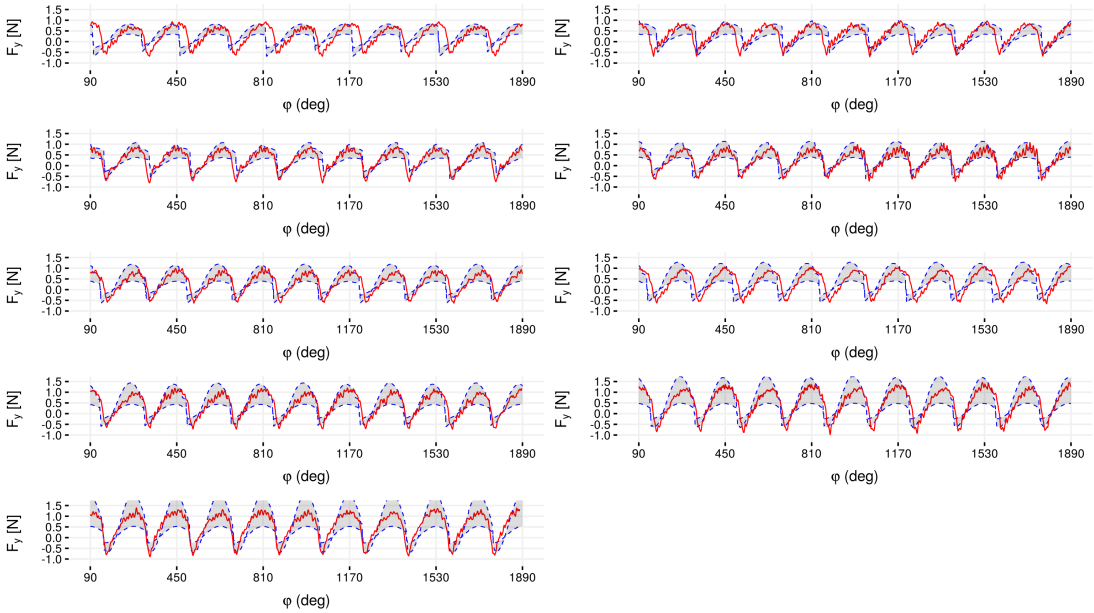

(b) $y - direction$

Figure G.2: Simulated and measured force predictions with cutting tool having 0.4 mm diameter at 35 m/min cutting speed, 40 µm/ depth of cut and 0.4, 0.6, 0.8, 1, 1.2, 1.5, 2, 3, 4 µm/tooth, a. in $x - direction$ and b. in $y - direction$, after first update (update sequence is from lowest feed per tooth value to the highest).

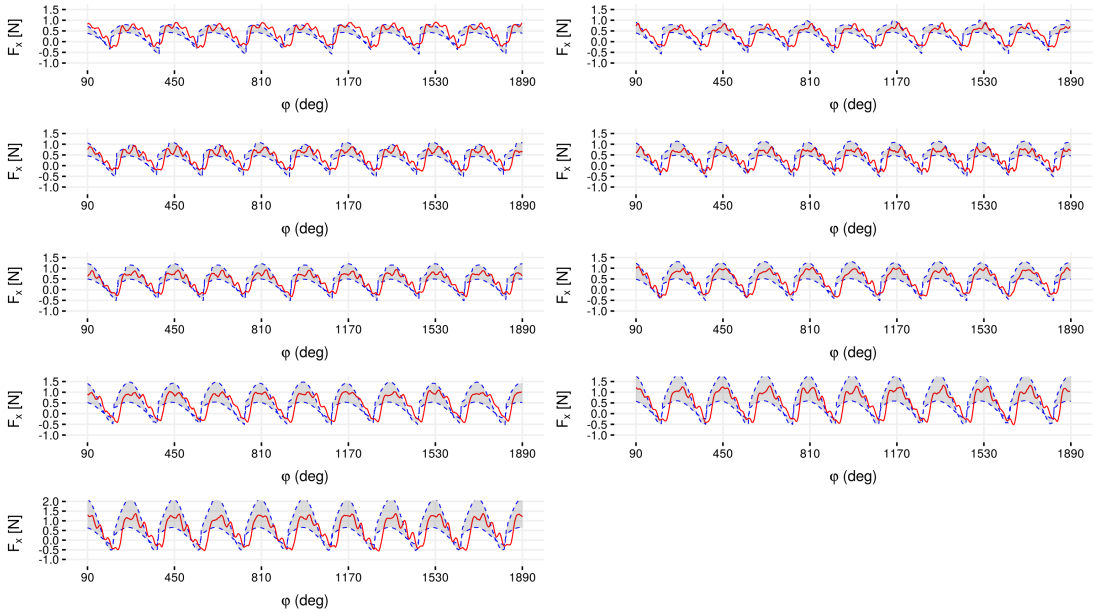

(a) $x - direction$

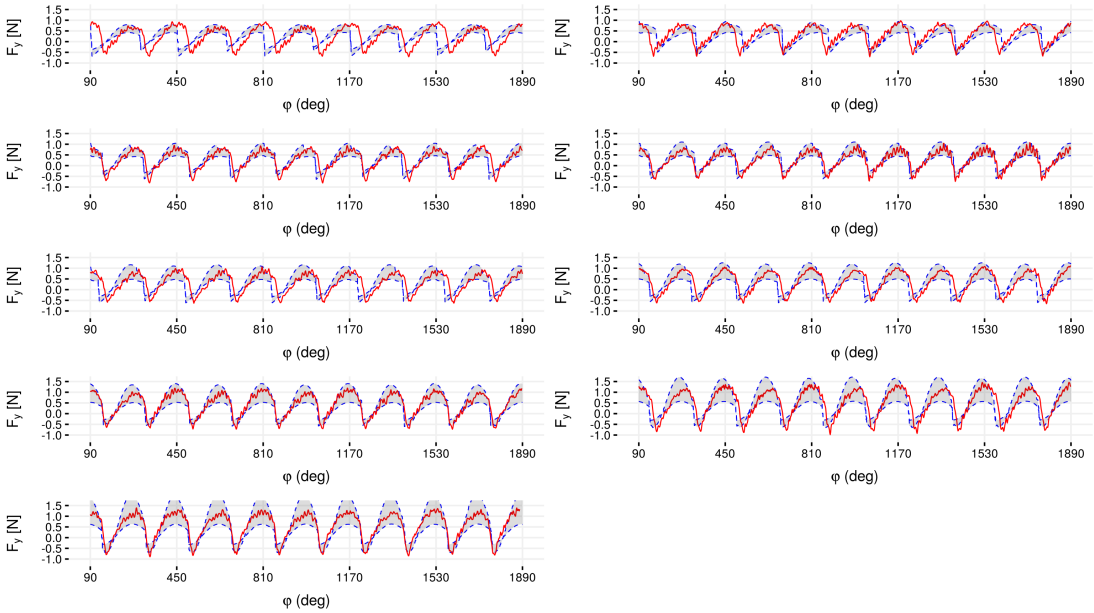

(b) $y - direction$

Figure G.3: Simulated and measured force predictions with cutting tool having 0.4 mm diameter at 35 m/min cutting speed, 40 µm/ depth of cut and 0.4, 0.6, 0.8, 1, 1.2, 1.5, 2, 3, 4 µm/tooth, a. in $x - direction$ and b. in $y - direction$, after second update (update sequence is from lowest feed per tooth value to the highest).

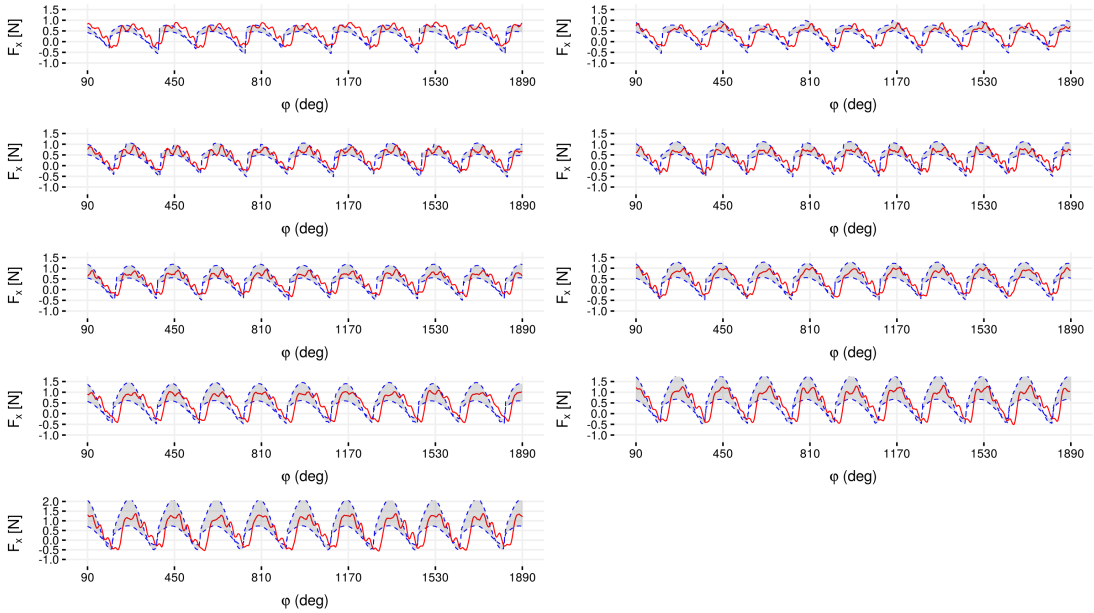

(a) $x - direction$

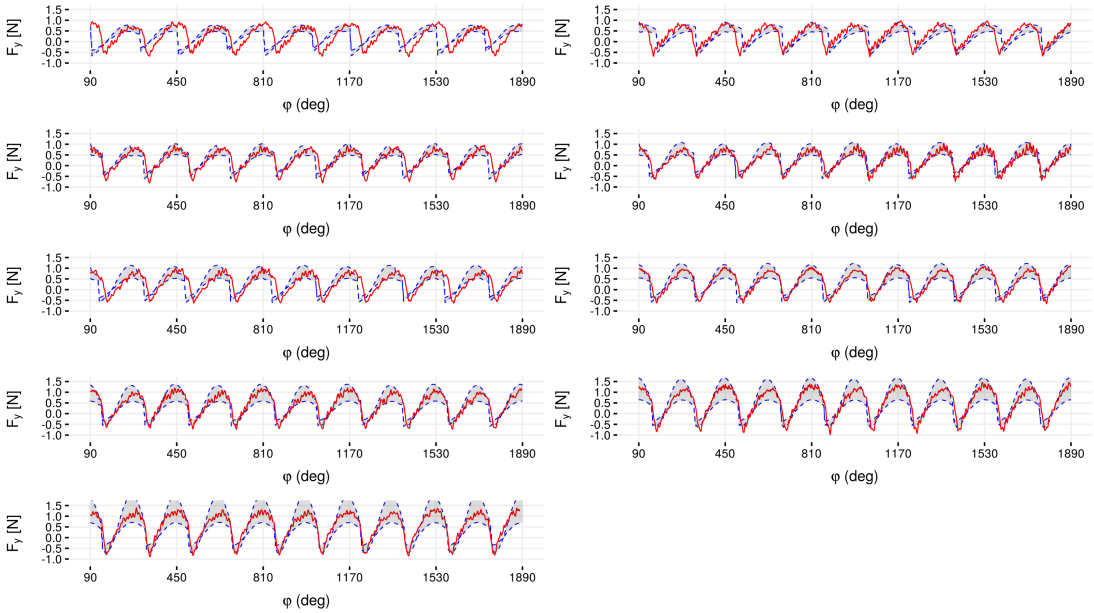

(b) $y - direction$

Figure G.4: Simulated and measured force predictions with cutting tool having 0.4 mm diameter at 35 m/min cutting speed, 40 µm/ depth of cut and 0.4, 0.6, 0.8, 1, 1.2, 1.5, 2, 3, 4 µm/tooth, a. in $x - direction$ and b. in $y - direction$, after third update (update sequence is from lowest feed per tooth value to the highest).

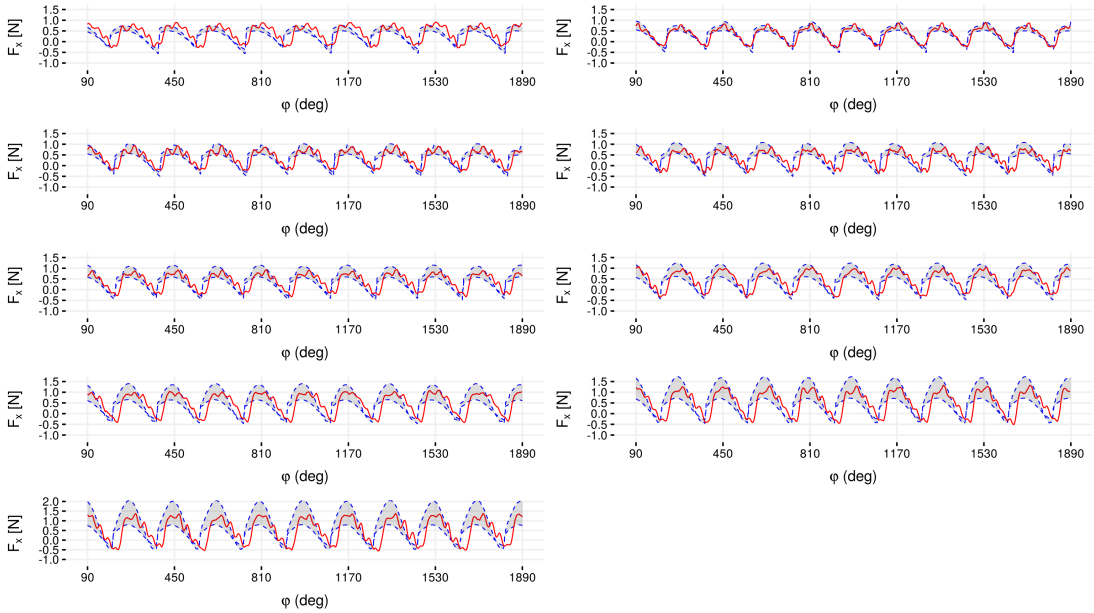

(a) $x - direction$

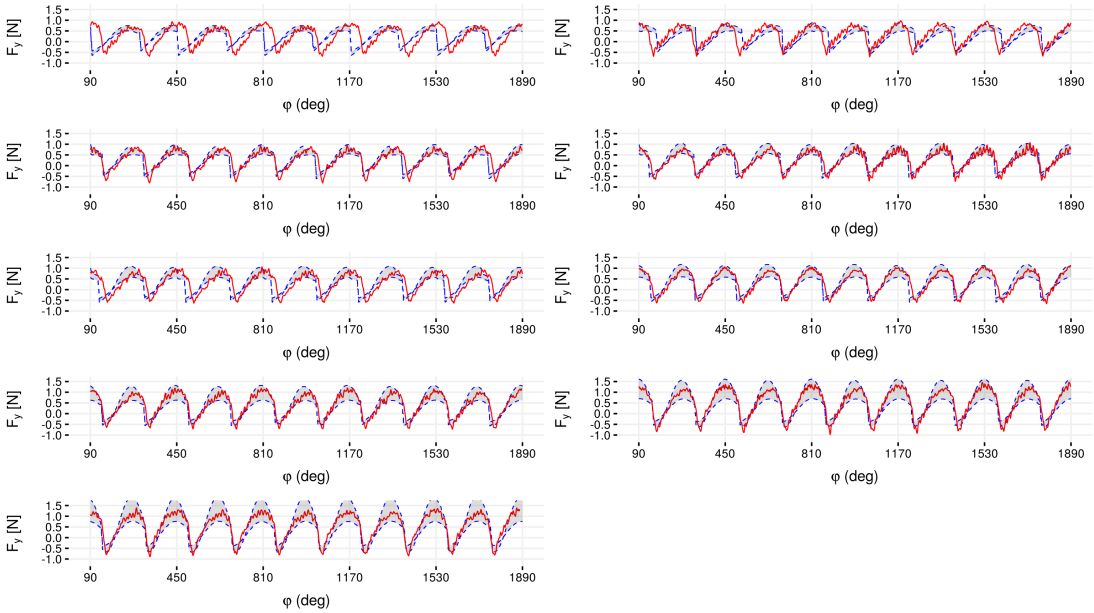

(b) $y - direction$

Figure G.5: Simulated and measured force predictions with cutting tool having 0.4 mm diameter at 35 m/min cutting speed, 40 µm/ depth of cut and 0.4, 0.6, 0.8, 1, 1.2, 1.5, 2, 3, 4 µm/tooth, a. in $x - direction$ and b. in $y - direction$, after fourth update (update sequence is from lowest feed per tooth value to the highest).

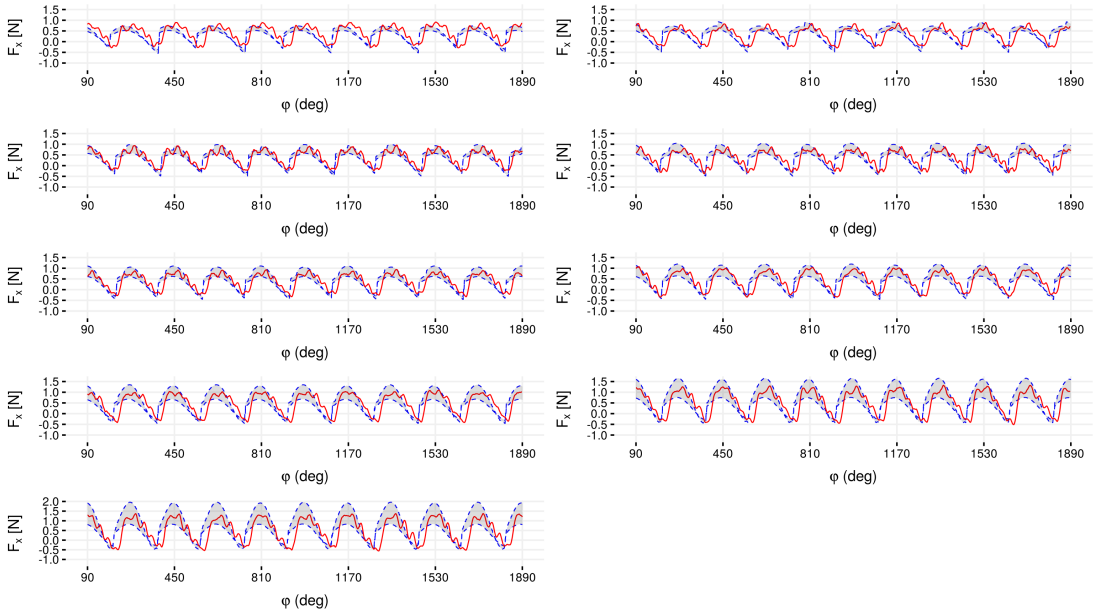

(a) $x - direction$

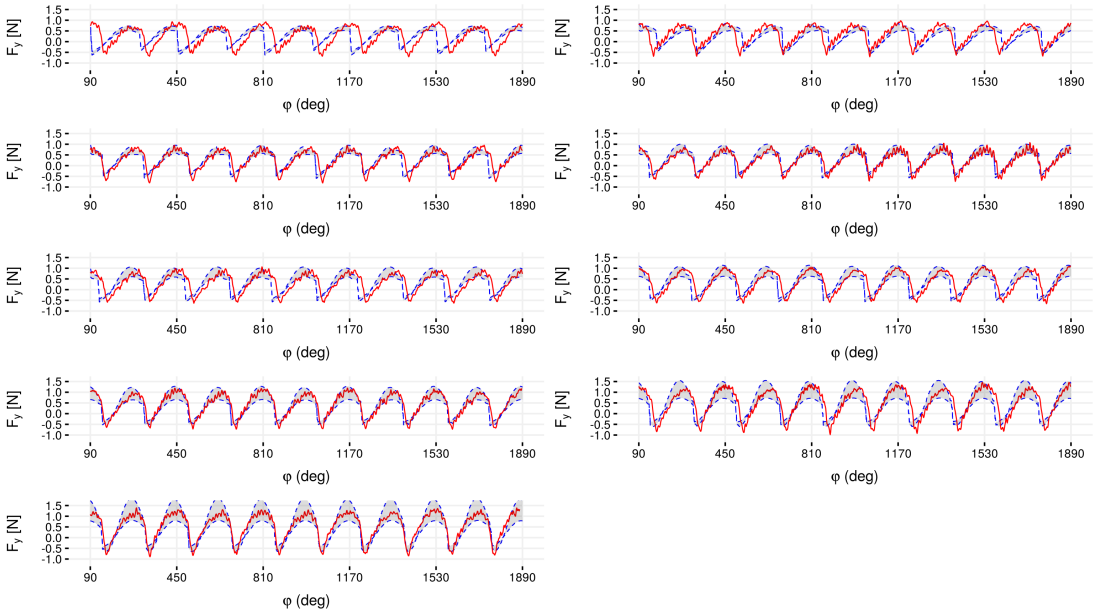

(b) $y - direction$

Figure G.6: Simulated and measured force predictions with cutting tool having 0.4 mm diameter at 35 m/min cutting speed, 40 µm/ depth of cut and 0.4, 0.6, 0.8, 1, 1.2, 1.5, 2, 3, 4 µm/tooth, a. in $x - direction$ and b. in $y - direction$, after fifth update (update sequence is from lowest feed per tooth value to the highest).

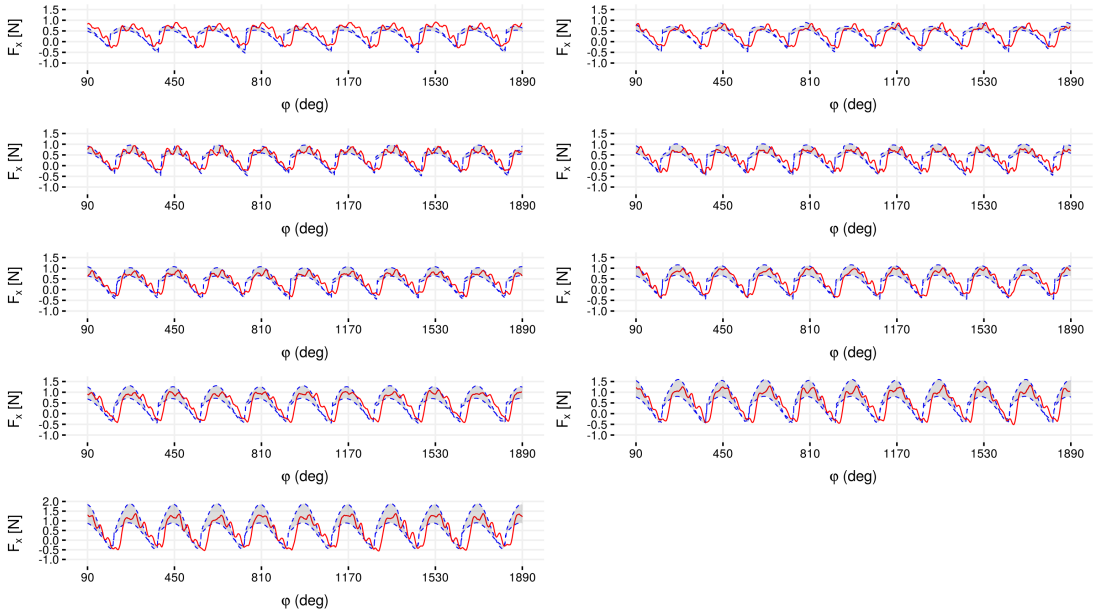

(a) $x - direction$

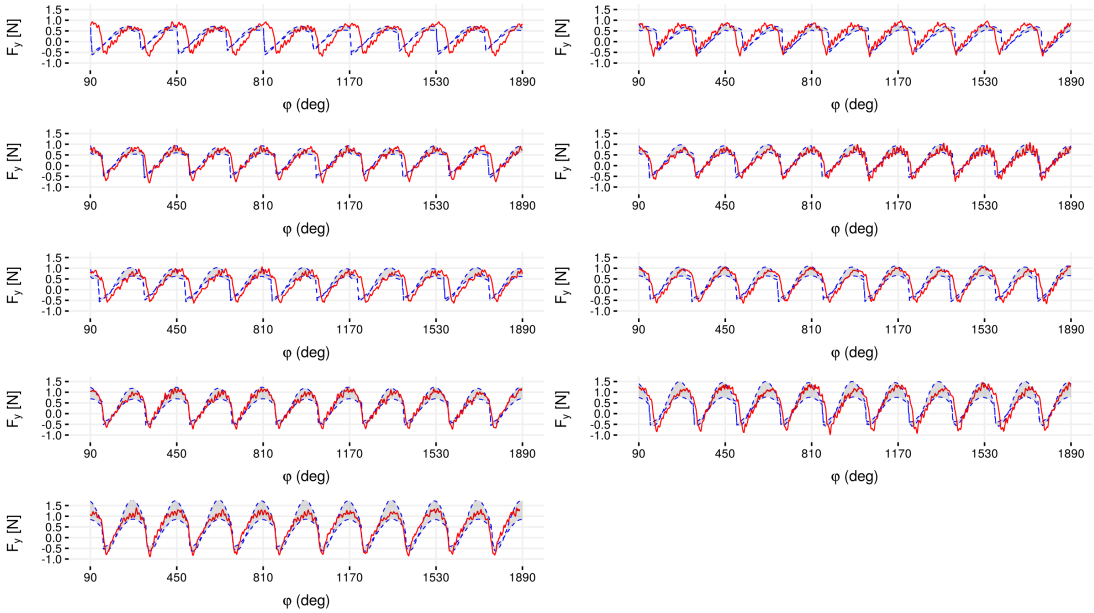

(b) $y - direction$

Figure G.7: Simulated and measured force predictions with cutting tool having 0.4 mm diameter at 35 m/min cutting speed, 40 µm/ depth of cut and 0.4, 0.6, 0.8, 1, 1.2, 1.5, 2, 3, 4 µm/tooth, a. in $x - direction$ and b. in $y - direction$, after sixth update (update sequence is from lowest feed per tooth value to the highest).

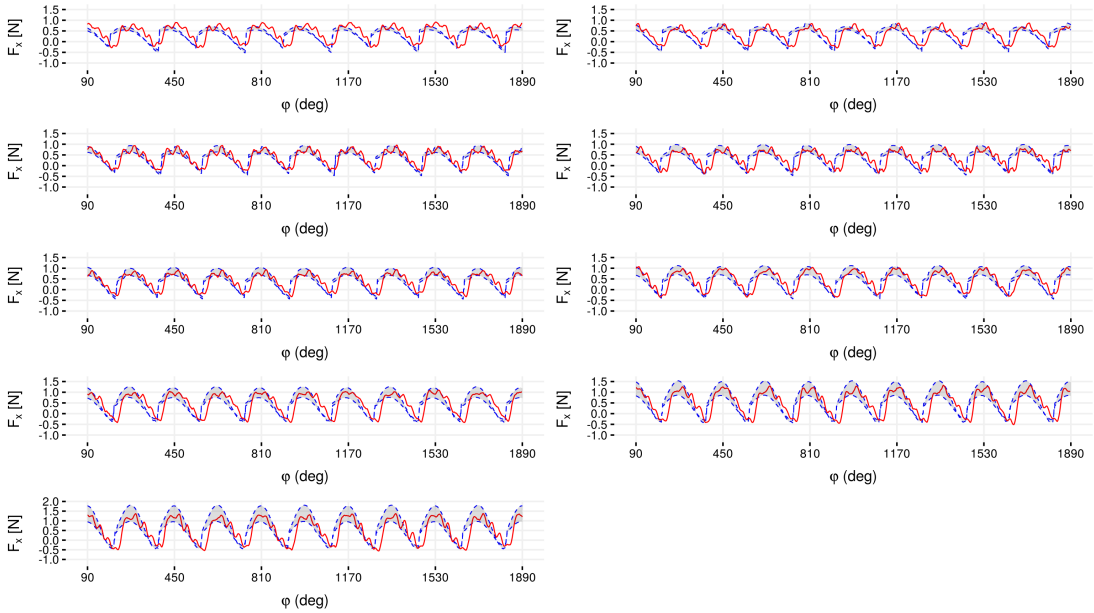

(a) $x - direction$

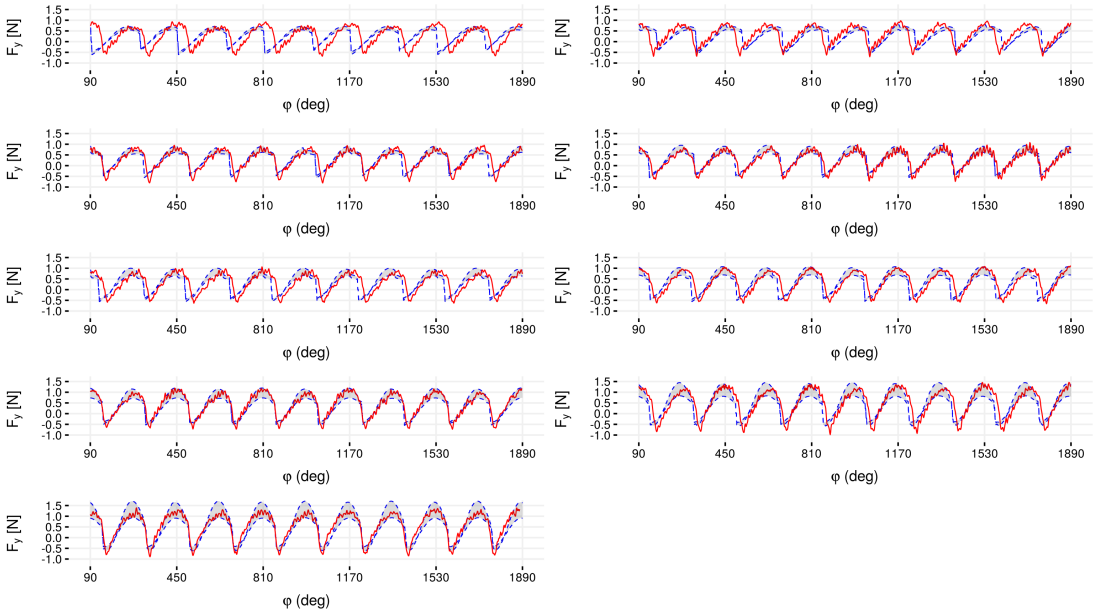

(b) $y - direction$

Figure G.8: Simulated and measured force predictions with cutting tool having 0.4 mm diameter at 35 m/min cutting speed, 40 µm/ depth of cut and 0.4, 0.6, 0.8, 1, 1.2, 1.5, 2, 3, 4 µm/tooth, a. in $x - direction$ and b. in $y - direction$, after seventh update (update sequence is from lowest feed per tooth value to the highest).

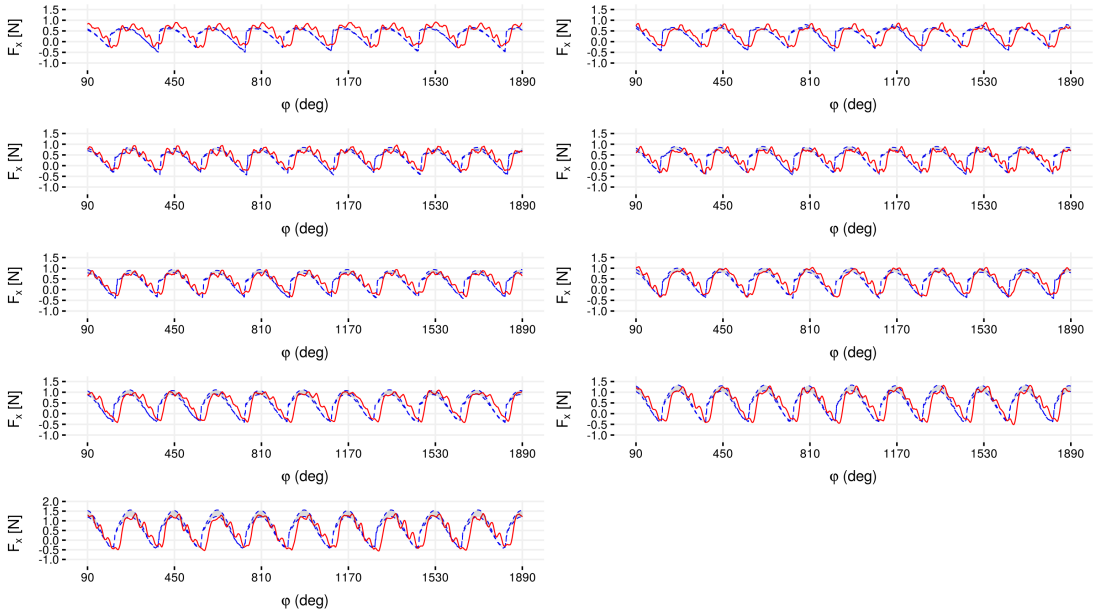

(a) $x - direction$

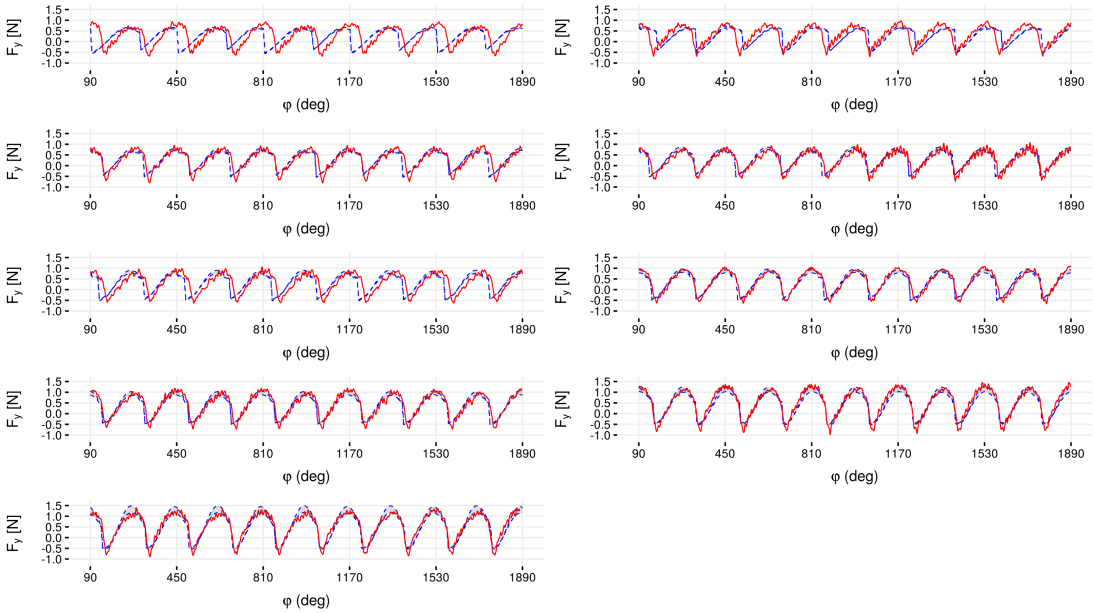

(b) $y - direction$

Figure G.9: Simulated and measured force predictions with cutting tool having 0.4 mm diameter at 35 m/min cutting speed, 40 µm/ depth of cut and 0.4, 0.6, 0.8, 1, 1.2, 1.5, 2, 3, 4 µm/tooth, a. in $x - direction$ and b. in $y - direction$, after eighth update (update sequence is from lowest feed per tooth value to the highest).

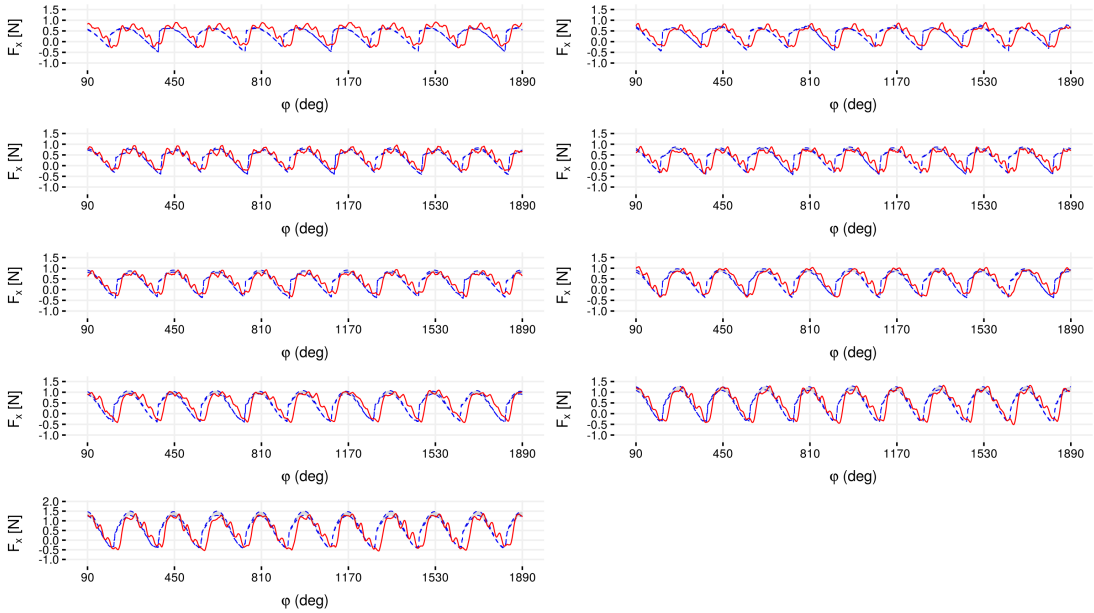

(a) $x - direction$

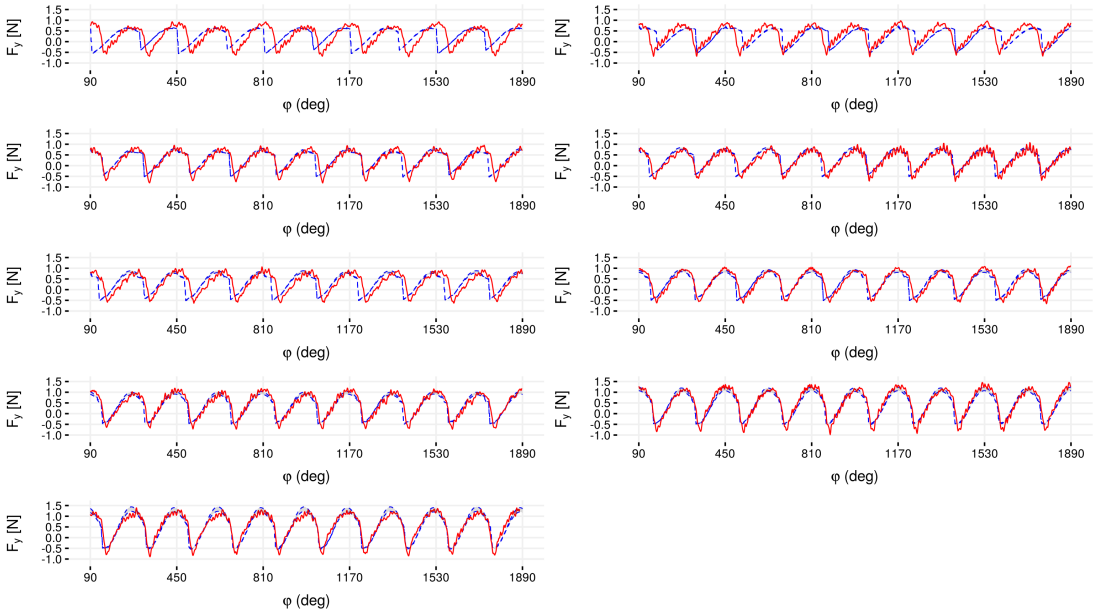

(b) $y - direction$

Figure G.10: Simulated and measured force predictions with cutting tool having 0.4 mm diameter at 35 m/min cutting speed, 40 µm/ depth of cut and 0.4, 0.6, 0.8, 1, 1.2, 1.5, 2, 3, 4 µm/tooth, a. in $x - direction$ and b. in $y - direction$, after ninth update (update sequence is from lowest feed per tooth value to the highest).